Optimization of Forged Magnesium Structural Automotive Components

by

Alexander W. Strong

A thesis
presented to the University of Waterloo
in fulfillment of the
thesis requirement for the degree of
Master of Applied Science
in
Mechanical Engineering

Waterloo, Ontario, Canada, 2016

Author's Declaration

I hereby declare that I am the sole author of this thesis. This is a true copy of the thesis, including any required final revisions, as accepted by my examiners.

I understand that my thesis may be made electronically available to the public.

Alexander W. Strong

Abstract

In an ongoing search for better vehicle fuel economy, the automotive industry has put significant emphasis on the reduction of vehicle weight while retaining stringent safety, quality and performance standards. With its high specific stiffness, strength, and fatigue performance under typical automotive service conditions, forged magnesium is a potential material to fill these requirements. Investigating an existing front lower control arm, engineering specifications were developed to evaluate the performance of a forged magnesium replacement. Combining a design volume derived from a kinematic CAD model and the produced engineering specifications, an optimization design space was created, and a component optimized within it using Altair Optistruct. Based on this optimized result an initial design was created in CAD, and design-analysis iterations conducted until it was structurally equivalent to the baseline design. This initial detail design produced a mass savings of 39% over the benchmark cast aluminum control arm, and only failed to challenge it in fatigue. It is expected that future designs will improve fatigue performance with little added mass, while continuing to integrate improving knowledge about the forging and mechanical performance of magnesium alloys.

Acknowledgements

I greatly appreciate the support I have had from my advisor, Dr. Steve Lambert, who has had patience with my work, even as I have encountered substantial challenges along the way. In addition, my research group partner, Yu Guo, was instrumental in my understanding of the forging process and very helpful in supporting my research work generally.

The useful insights generated by my fellow APC project researchers have been of great help in forming the ideas behind this paper, and I would like to thank them all for their active collaboration. Within the group, Behzad Behravesh and Andrew Gryguc are both responsible for a great deal of insight I have gained into the mechanical behaviour and fatigue performance of magnesium, and much of the data used in simulation here.

This project would not have been possible without direct support and guidance from Alex Duquette, Jim Prsa and Tom Sparrow of Multimatic. The support of Multimatic through an NSERC IPS grant was also very helpful in facilitating our collaboration. Additional assistance from Eric Gillund, Alex Posatskiy, Philippe Picchiottino, Jeff Mock, Alex Bond and Paul Charbonneau was very helpful along the way.

David Kirby and Ross Myher of Altair Canada also provided significant assistance in getting our optimization efforts kicked off in the right direction.

I must also extend my thanks to the other participant organizations in this research: Automotive Partnership Canada, Ford Motor Company, CanmetMATERIALS, and Centerline.

Lastly I would like to thank the staff of MME IT at Waterloo, especially Steve Hitchman and Martha Morales, for keeping our computational resources up and running.

Dedication

I thank God for his blessings and support in working through this project, and for the faith and perseverance that he has inspired in me.

This document would not exist without the incredible support of my wife Victoria, and so I must thank her for her patience, understanding and support. I also thank my family for their steadfast support, including my parents Tracey and Warren, my sister Shelby, and all of my grandparents, aunts, uncles and cousins.

Table of Contents

List of Figures

List of Tables

“ I hear you say “Why?” Always “Why?” You see things; and you say “Why?” But I dream of things that never were; and I say “Why not?” ”

-Back to Methuselah (1921), GB Shaw

Chapter 1
Introduction

1.1 Motivation

In a three-pronged approach towards vehicle lightweighting, designers have the option of decreasing fuel consumption at the expense of performance, creating more efficient powertrains, or reducing vehicle mass and size [1]. Reducing vehicle mass is a significant industry focus, as it often also results in improved vehicle performance. Automotive original equipment manufacturers (OEMs) have an interest in reducing the mass of vehicles to improve fuel economy in order to meet corporate average fuel economy (CAFE) standards, and are willing to invest in new technologies to meet these challenges [2].

Magnesium is a material well suited to lightweight design, with a density of only 1.7-1.8 g/cm^3. The strength and elastic modulus of magnesium are also in a viable range for many components typically made from other metals that may have not been easily converted to plastic. The use of cast magnesium alloys for internal vehicle structures is already commonplace, including instrument panel beams and steering components; however, their mechanical performance is a limiting factor in structural applications [3]. Forging has been shown to produce superior mechanical properties in magnesium, and has opened the door to implementation in more heavily stressed components that are currently dominated by aluminum and steel [4].

Topology optimization continues to become a part of automotive design practice, as it allows a designer to generate an optimal design shape that may be based on a novel distribution of material [5]. The combination of this technique with a low density material like magnesium is interesting, as the mass penalty for using unpredicted load paths will be reduced, potentially allowing for more efficient designs. The application of topology optimization to a forged magnesium part has great potential to challenge the mass efficiency of aluminum automotive components.

In 2014, a project supported by Automotive Partnership Canada (APC) began, with the objective of investigating the design of fatigue-critical automotive components forged from magnesium. The project team involves the University of Waterloo, Ford Motor Company, Multimatic Inc., CanmetMATERIALS, and Centerline Ltd. The work presented in this thesis was completed as part of the design task associated with this project, and focused on the design of a forged magnesium component based on the insights generated by the research team.

1.2 Objectives

The overall goal of the APC project is to create a forged magnesium component that is equivalent to the benchmark OEM design with at least a 20% mass reduction. For this research, the design of an optimum component was undertaken using available information, including the development of specifications, optimization of the component, and the dimensional design of the part.

Generation of an Engineering Specification

Specifications for a benchmark component were compiled and evaluated. Manufacturing specifications were developed through research, especially on the forging practices typically used in the aerospace industry. The specifications had to be verified through comparison with the analysis of the benchmark component geometry and material properties.

Optimization

With information on the geometry of surrounding parts and structural requirements, a design volume and optimization model could be created. An objective of this research is to develop and verify the robustness of this optimization model, and also to develop appropriate manufacturability parameters for the model. From the output, several viable design concepts will be extracted.

Preliminary Design and Verification

The final objective of this work is to produce a design that meets all specified requirements. With limited information available about the performance of wrought alloys at the outset of the project, it was expected that this verification would take the most accurate form available at the given time. Furthermore, as more information became available about the performance of magnesium as a material it was to be integrated into the design.

1.3 Overview

The presented thesis is composed of five main sections:

In Chapter 2, background information on magnesium, forging, and the optimization of structural components is detailed. Pertinent sources in literature are discussed, and the project objectives are put in the context of other successful projects in the forging of magnesium and structural optimization.

Chapter 3 first details the analysis of the benchmark component, and discusses why it is a relevant component to design using forged magnesium. Structural design specifications, and the related

analysis processes are then discussed. Finally, the chapter details requirements related to manufacturing, derived through the project's experience to date with forging magnesium, and aerospace industry guidelines.

Topology optimization for the design of the forged magnesium component is presented in Chapter 4. The model is first assessed for robustness through a sensitivity analysis procedure. Following confidence being established in the model, a number of trials were used to create design concepts and investigate the performance of different materials for the application. Lastly, a preliminary design was extracted from the optimization model and analyzed to determine if it complied with the engineering specifications.

Following optimization, Chapter 5 explores the design of a manufacturable component and the verification of most engineering specifications. First the final design is detailed, including discussion of the forging and machining processes involved, as well as the design work undertaken. The design is then verified against the engineering specifications. Lastly, engineering specifications that were not met are discussed.

Chapters 6 and 7 cover the conclusions and recommendations generated through the completion of this project.

Chapter 2
Background and Literature Review

The following section investigates current research progress and directions found in the literature, as well as relevant background information. Increasing focus on magnesium as an engineering material and its related characteristics are explored. The use of forging to form more structurally advantageous magnesium components is then investigated. Finally, state-of-the art strategies for structural optimization will be discussed, along with some successful applications in the automotive industry.

2.1 Magnesium Alloys

Magnesium has been implemented as a structural and non-structural material for over eighty years, including use in lightweight transport trucks, aircraft, electronics enclosures and automotive instrument panel beams [3] [6]. With 65% of aluminum's density (1.7-1.8 g/cm^3), magnesium is the lightest structural metal, while still demonstrating similar strength and fatigue properties to aluminum. Magnesium has the potential to provide superior specific stiffness and strength compared to most commonly used materials in many automotive applications. These characteristics suggest opportunities with regards to the use of magnesium in automotive lightweighting efforts [3].

Magnesium alloys have a hexagonal closed packed (HCP) crystal structure, with only two easily activated basal slip systems at room temperature. Since five active slip systems are required for uniform yielding, magnesium's behaviour is influenced by other deformation mechanics as well [7]. Mechanical twinning systems contribute alternative deformation mechanisms, allowing the material to deform in a ductile manner. Twins however contribute to asymmetric and anisotropic material properties, forming strong textures that make forming and mechanical behaviour complex [8]. Alloy development including the application of rare earth elements, heated processing, and grain refinement are all strategies that are being commonly applied in mitigating these formability challenges [7] [9].

From a sustainability point of view, magnesium is an environmentally available material and can be reduced from MgO or obtained through electrolysis of MgCl salts [10]. With abundance in sea water, this method offers a large supply without large mining operations. Additional work on recycling is still needed, although focus on recovery, especially of valuable secondary elements, is ongoing as magnesium becomes more commonly used [11]. Possibly the largest environmental benefit is in vehicle fuel economy, with overall mass savings of 100 kg contributing 0.3 to 0.4

L/100km of fuel savings [1]. The large scale implementation of structural magnesium in vehicles may significantly assist in meeting government fuel economy targets and reducing greenhouse gas emissions.

Alongside the difficulties with formability and mechanical behaviours, magnesium alloys also commonly suffer from relatively poor corrosion resistance, especially in galvanic couples, due to their high electrochemical activity [3]. For use in moderate environments, conversion coatings and the application of paints or sealants is typically required [12]. There are also concerns with flammability in processing, however they can generally be overcome by process control, effective chip clearing during machining, and the presence of appropriate emergency extinguishing equipment [10] [13].

Magnesium has been utilized in the automotive industry dominantly in the form of cast components. Instrument panel beams, steering components, and seat structures commonly use magnesium alloys, as they are internal parts not susceptible to aggressively corrosive environments. Magnesium has also been used in engine blocks, intake manifolds, wheels, transmission cases, brackets, and engine cradles on a more limited basis [3] [10]. Overall, there is an interest in applying wrought alloys within the automotive industry to achieve further lightweighting performance on parts with more demanding mechanical property requirements.

2.2 Forging

Forging is a metalworking process in which compressive loading is used to form a metal using a die or other tooling. This family of processes has been in use since at least 5000 BC, however traditional blacksmithing methods have mostly given way to specialized dies and industrial scale presses and hammers [14]. Magnesium forging found its first significant uses with the second world war, in which it was used to replace aluminum in aerospace applications, partly due to aluminum shortages [10]. With the first flight of the B-36 ‘Peacemaker’ in 1946, aerospace magnesium forgings had reached maturity with 680kg of them on the plane, helping enable the first intercontinental range bomber [3] [15]. Since then, renewed interest in the process has arisen due to the potential of challenging aluminum in terms of strength and fatigue properties for automotive applications [4].

An exemplar I-beam section forging is shown in Figure 1 with important features labelled [14]. With high specific bending strength and stiffness, the I-section is likely to be a component of a structural forging, and the nomenclature will be used in the description of design features going forward. The labelled features all have relevance to component forgeability. If the web is too thin,

defects may occur as metal flows through the rib to the flash, breaking the grain flow and initiating cracks in a cold shut. The fillet radius is critical to filling the rib, and must be sufficient to allow metal to flow around it without folding over itself. The flash is also crucial for impression die forgings, as it restricts flow outward and helps fill the rest of the die. Overall, it is the balanced consideration of these parameters that permit successful forging of components in any material [14] [16].

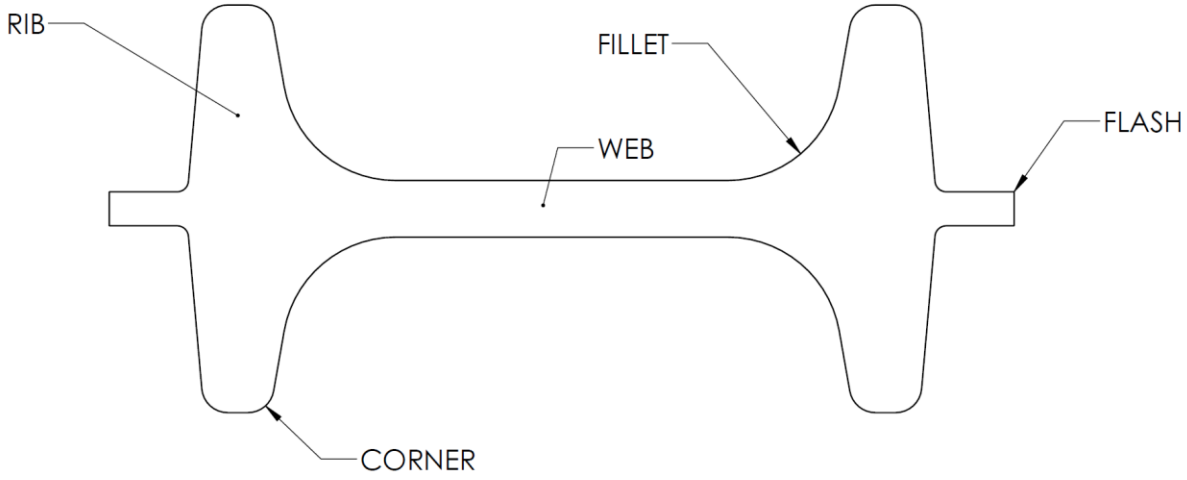

Figure 1: I-beam Forging Section

There are many available forging techniques and presses with which to accomplish forging operations. Mechanical screw presses, hydraulic presses and drop hammers have all been found in use producing magnesium forgings throughout the literature [16] [17]. Precision forging, in which a component is formed to tight tolerance and minimal draft has also been successfully used to produce parts from magnesium with minimal machining requirements [16] [18].

Forging process design has been greatly aided by the use of thermo-mechanical simulations with the finite element method. Vazquez and Altan developed first a predictive physical simulation using plasticine, then a refined finite element model in DEFORM 3D that informed the design of a near-flashless forging process for an engine connecting rod [19]. Preform design using structural optimization approaches was developed by Shao et al. and implemented to investigate the optimal preform topologies of a wheel and a turbine blade [20]. Furthermore, several projects involving the forging of magnesium components have utilized finite element forging models to effectively predict die filling, the presence of defects, and the final shape of completed forgings [17] [18] [21] [22]. The

use of these computational simulation techniques give confidence to the designer that design performance in manufacturing can be predicted and optimized prior to the manufacturing of tooling.

Although magnesium forgings have been produced in industry since the second world war, a number of more recent projects have successfully implemented magnesium forging and proved out various technologies. Gontarz et al. successfully simulated and forged a lever using a drop forging process without heated dies [17]. The component had flaws in locations predicted by simulation, but by using a larger number of lighter strikes the part was produced with good quality. Using a heated, multiple piece female die, Wang et al. simulated and forged a bracket and wheel from cast materials. The resultant forged AZ80 part had significantly improved ultimate strength (320-330MPa) and elongation of 10-12% [18]. Pepelnjak et al. forged a shock absorber head from AZ80 magnesium, and used collected anisotropic forming data to add anisotropy into the simulation [21]. There was significant variation between the topologies predicted from three different simulation software packages, but DEFORM 3D produced a fairly accurate result compared to the forged part. Near-net-shape precision forging has also been used to successfully produce pulley wheels and an aerospace door stop from magnesium alloys [4].

2.3 Structural Optimization

In the design of automotive components, structural optimization techniques have been implemented to achieve optimal designs for vehicle lightweighting. Three dominant methods exist: sizing optimization, shape optimization, and topology optimization. Sizing optimization selects the most appropriate feature size for a given location; for example, tubing sizes in a spaceframe might be selected this way. Shape optimization techniques use variations in external object shape or FEA nodal locations to produce optimal contours for the exterior of a part. Since shape optimization is unable to create holes in a component robustly, topology optimization was developed to generate a starting point for component design [23] [5]. Upon the completion of an optimization process, design engineers are required to translate an optimal structure into a viable part that meets all the imposed requirements.

The topology optimization process starts with a finite element mesh encompassing the space in which material can be placed. Each design element has an element density, and the compliance of the structure can be computed with this information. In practice, commercial programs can use a wide variety of design variables, objectives, and constraints; however, the method was pioneered to design

structures of minimum compliance with a given average density [23] [24]. In early studies the variation in element density and stiffness was computed by the modelling of microstructural composites via the homogenization method, but simpler methods use a penalization process for intermediate density elements driven by a power function known as the solid isotropic material with penalization model (SIMP). The power function is set based on empirical studies rather than physical composite models, but accomplishes the same function of avoiding designs with large areas of intermediate density [5] [25]. The optimization begins with the assignment of an initial element density for the set followed by solution of the finite element model. Using an optimization algorithm (many can be used), elements with high strain energy density see an increase in density, whereas those with low strain energy density have their density reduced. This solution and optimization process is then iterated until the change in compliance of the design reaches a convergence criterion [5]. The end result is a set of element densities for the design that suggest the distribution of material. Design interpretation is required to transform this into a viable part of non-intermediate density.

Manufacturability of designs generated via topology optimization is a concern due to the freedom inherent in the process. In order to constrain the design further, commercial codes such as Altair Optistruct have introduced penalization methods that model manufacturing requirements such as casting and forging draft, extrusion, patterning, symmetry and structural member size requirements [24] [26]. These methods have been directly applied to challenges in creating geometries suitable for forging, and are likely to be critical in the design interpretation process [27].

Topology optimization has been widely used in industry to design more efficient automotive components. Multimatic and General Motors collaborated to produce a series of topology-optimized control arm designs using different high strength steel-friendly processes. The best component concept was able to equal a benchmark aluminum component in mass at up to 34% savings in production costs [28]. Audi AG used two commercially available topology optimization packages to optimize the mass of an engine support, auxiliary bracket and a crankshaft bearing cap, all with significant reductions in mass over baseline designs. Design volumes were generated from clearance models and using the baseline parts, allowing the designer to approach the problem from a design refinement perspective with greater success for the given case [29]. Honda R&D used topology optimization to reduce the mass of a transmission housing with a very complex design volume. It was determined that the best design strategy revolved around the use of topology optimization for the

generation of an initial concept design when freedom of material placement was at its greatest, and for further trials making use of shape optimization to refine the design space [30].

Overall, the combination of magnesium forging and topology optimization seem likely to be an effective pairing. The optimization method is capable of capturing limitations of the manufacturing process, while still creating an optimal topology relevant to the design scenario. Additionally, the low density of magnesium may permit the exploitation of a large design space with novel load direction strategies.

Chapter 3
Engineering Specifications

In order to create a design capable of replacing an in service automotive component, it was necessary to generate an engineering specification. The benchmark component was analyzed for performance, and engineering requirements from Ford were evaluated. Manufacturing research was then incorporated to generate the completed specification. Some requirements were tentatively not included in this specification, including balljoint and bushing design integration, due to limitations in research scope.

3.1 Component Benchmarking

3.1.1 Description of Benchmark Component

The front lower control arm (FLCA) of the 2013 Ford Fusion was selected as the benchmark component for this project, as it is a substantial component in terms of mass, and structurally critical. The Ford Fusion front suspension is a typical Macpherson strut design as shown in Figure 2. Because of this, the FLCA reacts the majority of wheel loads in the x-y plane while loads in the z direction are passed almost directly into the strut as shown in Figure 3. Over the vehicles lifetime the FLCA must safely transmit all braking, cornering and acceleration loads back into the chassis, provide sufficient stiffness to support good vehicle handling, avoid excessive deformation in light overloading, and survive heavy overloading events without becoming a safety risk. In addition to these requirements, the control arm must be sufficiently corrosion resistant, durable, and of sufficient quality to integrate with the rest of the vehicle. The benchmark FLCA is made of cast A356-T6 aluminum and was calculated to weigh 2523 grams. To assess the performance of the benchmark, a finite element model was created and analyzed based on the requirements provided by Ford.

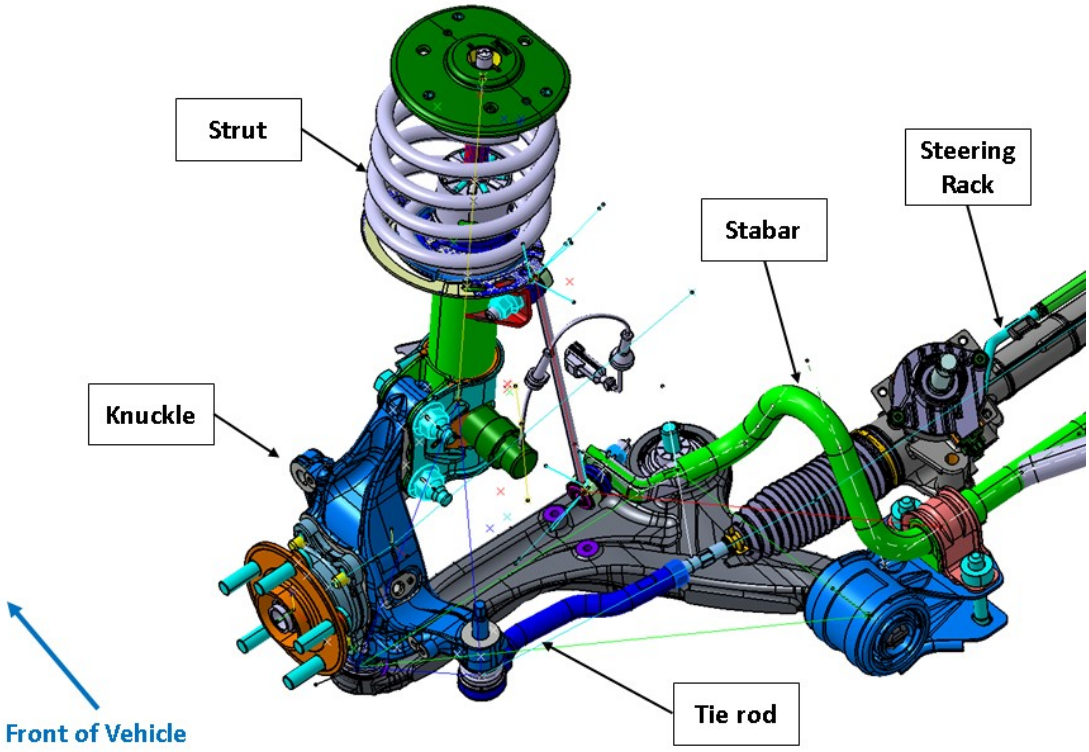

Figure 2: 2013 Ford Fusion Front Suspension Assembly

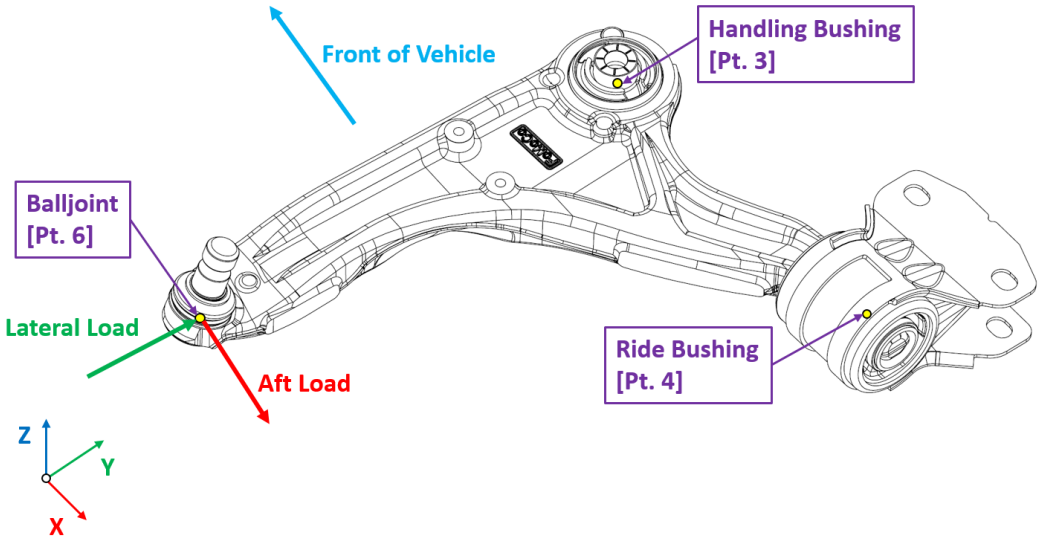

Figure 3: 2013 Ford Fusion Front Lower Control Arm

3.1.2 Finite Element Model

Using information provided by the OEM, a finite element model was generated for the benchmark FLCA. The results are captured in summary table form, and finite element contour plots. Finite element analysis was completed using Abaqus 6.13-4 and fatigue analysis was performed using nCode DesignLife v11.0.

Table 1 : Model Information

	Element Type	Count
Surface Mesh (2D Membrane)	Abaqus M3D6	21998
Solid Mesh (3D)	Abaqus C3D10M	74525

Selected Quality Parameters		
	Model Value	Target Value
Minimum Tet Collapse (3D)	0.21	> 0.3
Minimum Jacobian (3D)	0.15	> 0.2
Minimum Interior Angle (3D)	16.6°	> 20°

Table 1 above shows the element types and count used in the model, as well as three element quality measures that were referenced in building the FE model. The surface geometry of the part was simplified and de-featured, including the very complex cast parting line geometry. The part was then meshed with a uniform second order triangular surface mesh with a target size of 3 mm. Due to the complexity of the parting line geometry, it was difficult to reach the quality targets shown in Table 1; however, the majority of elements (99.8%) beat these quality guidelines. It was decided to go forward with the model, as all elements were above the software required quality measures and the model size was reasonable [31]. The 3D second order tetra mesh of C3D10M elements was surfaced with M3D6 membrane elements in order to provide more accurate stress results [32]. The final mesh is shown in Figure 4 below.

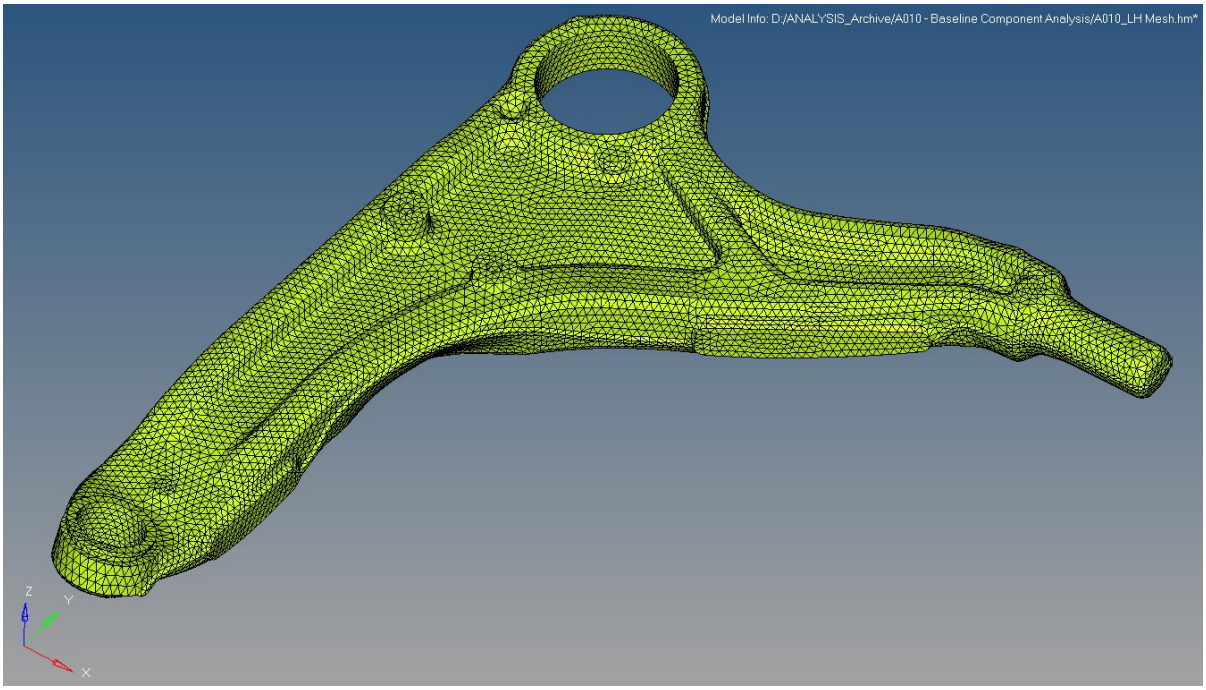

Figure 4: Baseline Component FE Mesh

3.1.3 Stiffness Analysis Results

The stiffness of the control arm was evaluated in the global x (Aft) and y (Lateral) directions of the model, which are shown in Figure 3. Loads were applied, and deflections measured at point 6 (the balljoint). The suspension hard points (3,4 and 6) were connected to the component via Abaqus DCOUP3D (RBE3) elements. Constraints were then applied to the hard points as shown in Table 2.

Table 2 : Model Constraints

Suspension Hard Point	Constrained Directions
3: Handling Bushing	1,2,3 (x, y, z)
4: Ride Bushing	2,3 (y, z)
6: Balljoint	3 (z)

When the model was set up, both Aft and Lateral stiffness analyses were run as linear perturbation steps. The results of this analysis are shown below in Table 3. Figure 5 and Figure 6 show contour plots for the analyses from which stiffness was computed. The RBE3 based stiffness method is presented here because it gives lower stiffness values than most other methods (and is thus conservative), is easy to set up for most cases, and non-proprietary.

Table 3 : Benchmark Component Stiffness Results

	Stiffness (RBE3)	
	Aft Pt 6	Lat Pt 6
	[kN/mm]	[kN/mm]
Benchmark FLCA	4.33	81.8

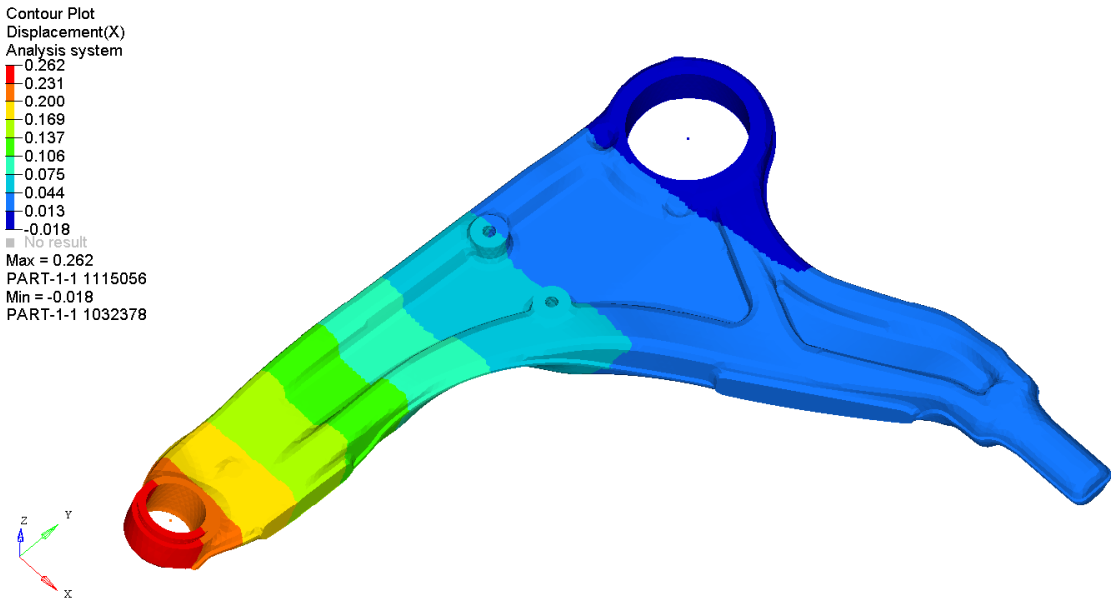

Figure 5: Benchmark aft deflection [mm] under 1 kN (+x) unit load

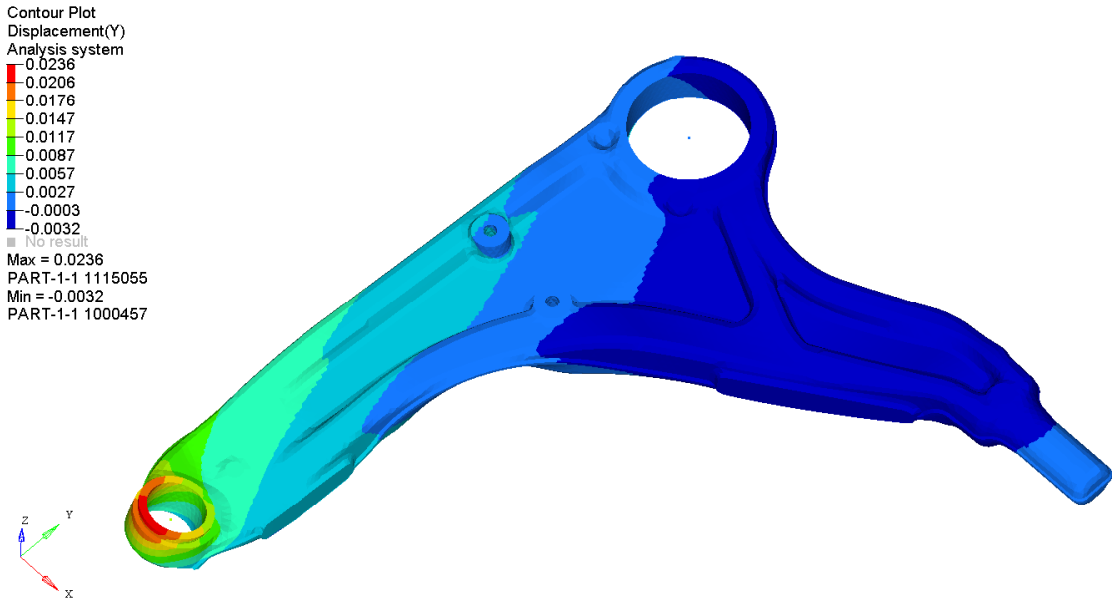

Figure 6: Benchmark lateral deflection [mm] under 1 kN (+y) unit load

3.1.4 Strength Analysis Results

Two types of loading were applied to evaluate the FLCA's strength. Initially, a light overload was applied that may occur over the course of the vehicles normal life. The FLCA would be expected to survive such a load with minimal deformation, such that it can continue functioning without adverse handling or clearance impacts. If the part passed this first stage, the component was subjected to an ultimate loading case, which represents a much heavier overload in which significant deformation is expected. As long as the balljoint (Pt. 6) stays within maximum specified displacement limits, and the plastic equivalent strain is below a threshold value set for the material the part is acceptable.

The setup for the finite element model is very similar to the stiffness model, however instead of direct constraint of the suspension hard points, the RBE3 elements are linked to a linear elastic suspension and chassis model. This flexible model allows the load to be distributed more realistically into the FLCA. The chassis and suspension model is fixed at the locations where the sub-frame bolts to the primary structure of the chassis. In addition to these boundary conditions, the model was run with a non-linear material to capture the plastic deformation. Results for all cases are shown in Table 4 below. All of the load case requirements were passed without issue.

Figure 7 to Figure 12 show the results of the three major areas of interest: permanent deflection after light overload, maximum deflection, and the maximum equivalent plastic strain. Relatively high

deformation was observed under light overloading, but with most of the deformation localized to the region around the balljoint where the cross section narrows, this is an expected behaviour of the design. The contour plots for this case are captured in Figure 7 and Figure 8. For overloading, both maximum deformations were acceptable, and contour plots are shown in Figure 9 and Figure 10. The maximum of 3% for the equivalent plastic strain (PEEQ) is a material specific allowable for A356-T6, but was closely approached in the aft load case. Investigating the model, the peak is located on an inside corner at a mesh induced discontinuity, which suggests that the analysis is conservative because in reality the surface would be relatively smooth. Contour plots of the max PEEQ are shown in Figure 11 and Figure 12.

Table 4: Benchmark Component Strength Results

	Permanent Set		Max Deflection		PEEQ Max	
	Aft Pt 6	Lat Pt 6	Aft Pt 6	Lat Pt 6	Aft Pt 6	Lat Pt 6
	[mm]	[mm]	[mm]	[mm]	[%]	[%]
Benchmark FLCA	0.17	0.42	33.4	4.8	2.74	0.26
Specification Targets					3.00	3.00

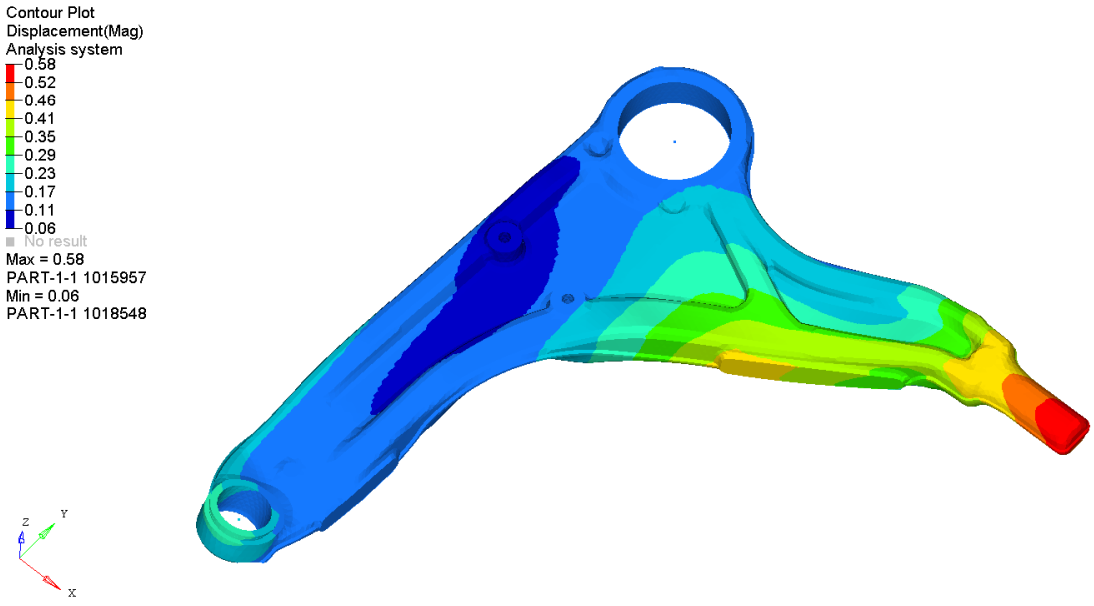

Figure 7: Benchmark aft load permanent set [mm]

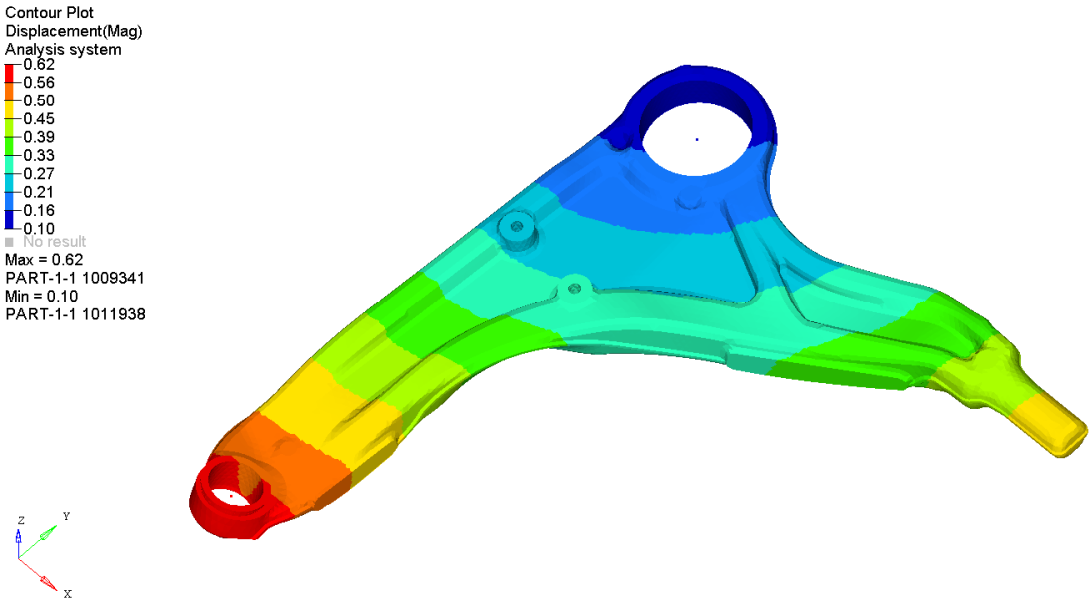

Figure 8: Benchmark lateral load permanent set [mm]

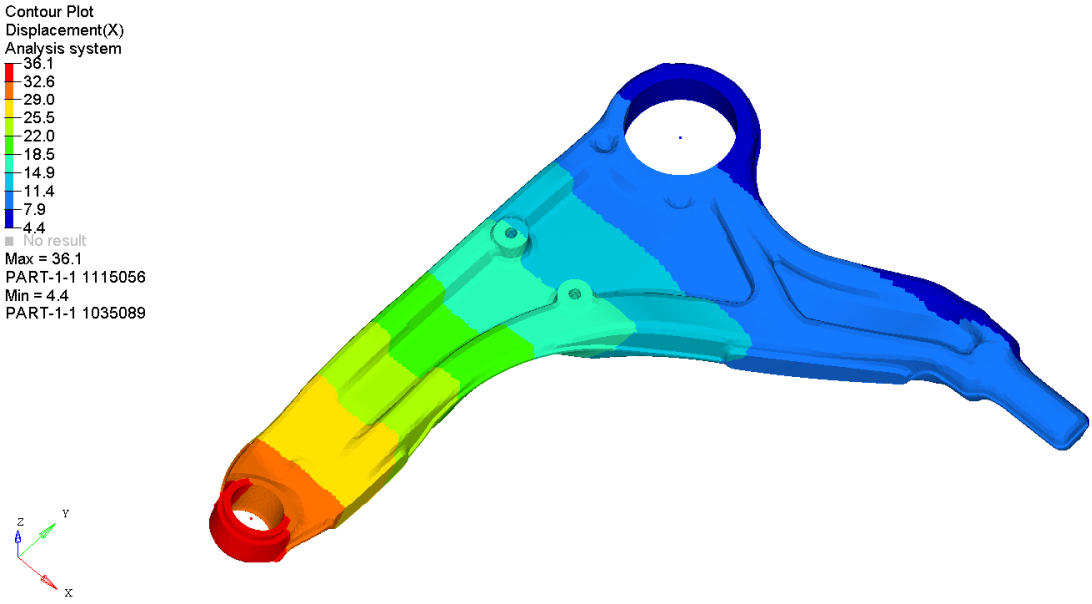

Figure 9: Benchmark aft load max deflection [mm]

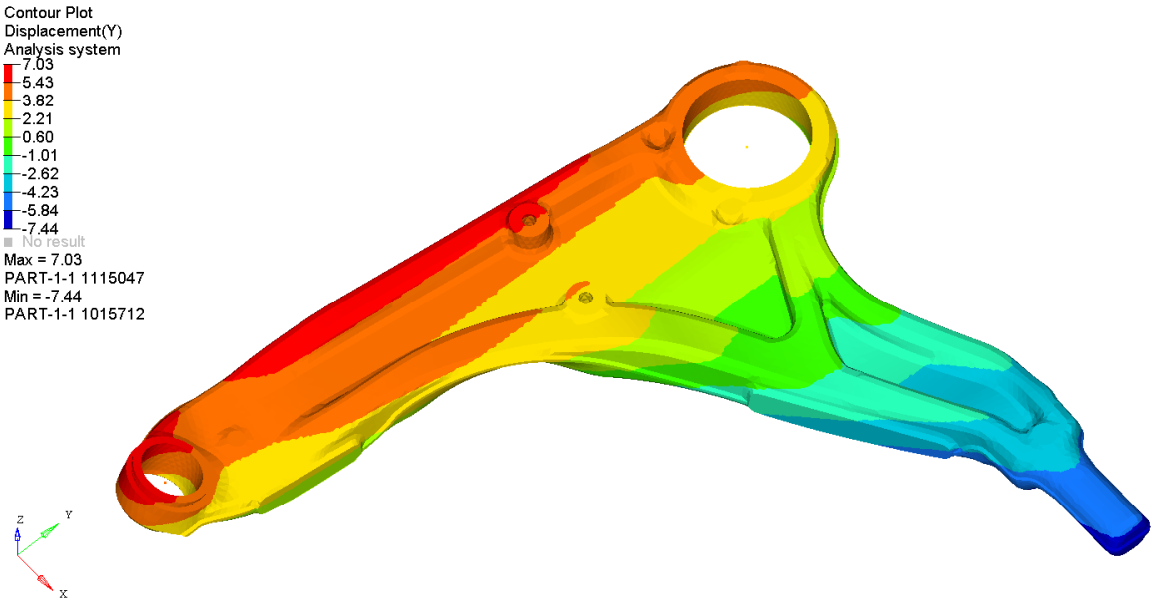

Figure 10: Benchmark lateral load max deflection [mm]

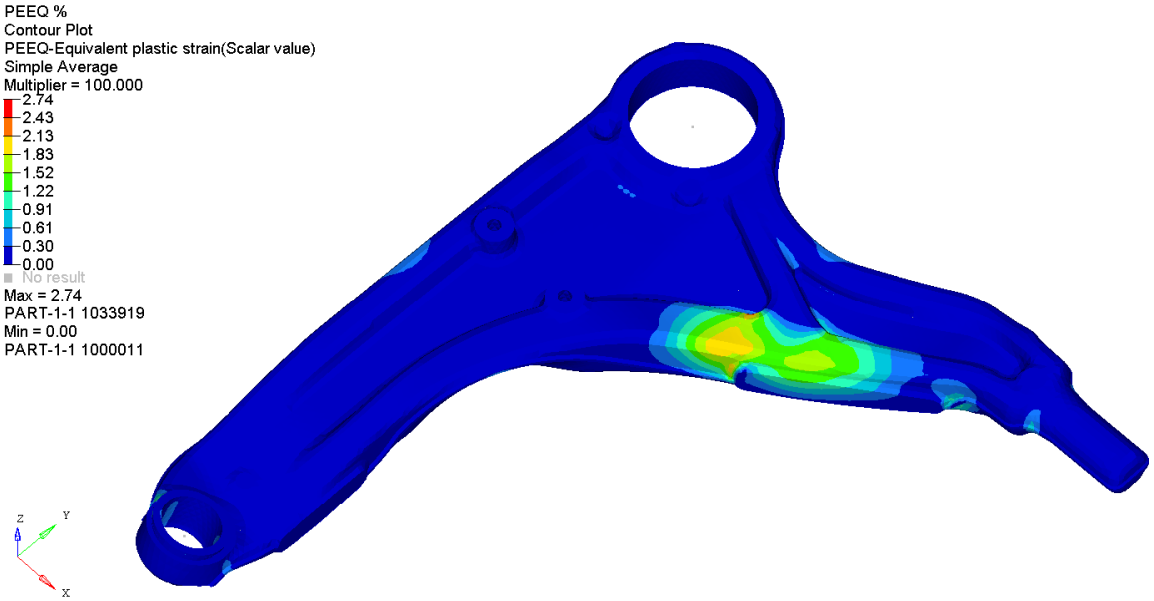

Figure 11: Benchmark aft load equivalent plastic strain [mm/mm]

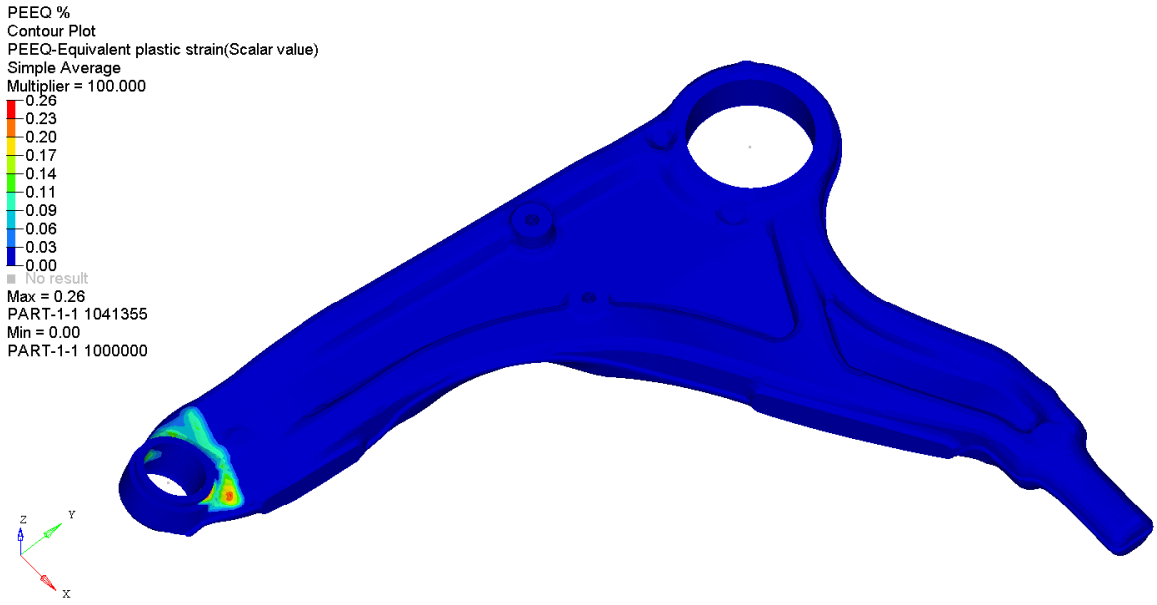

Figure 12: Benchmark lateral load equivalent plastic strain [mm/mm]

3.1.5 Fatigue Analysis Results

For fatigue evaluation, unit load analysis was completed for x, y, and z unit loads at the balljoint and all six force and moment components for each of the bushings. These analysis steps were conducted with inertia relief in order to eliminate rigid body modes. Unit loading stress results were combined with proprietary Ford fatigue loading histories to create a stress and strain history for the component using nCode DesignLife. Strain life fatigue analysis was then conducted on the component within DesignLife using A356-T6 fatigue data from a proprietary Coffin-Manson stress strain curve. The Neuber rule for elastic-plastic correction, and the Smith-Watson-Topper mean stress correction were used to run the fatigue analyses. The model was run with and without a fatigue surface correction factor, however the use of a correction factor may not correlate well to actual fatigue life results for A356-T6. The reason for this is the consistent presence of defects both inside and outside the component in cast specimens, meaning that even the polished samples tested when deriving fatigue data have significant available surface or near-subsurface crack initiation sites [33]. For forged specimens, this characteristic may not hold due to the potential for improved surface quality.

Table 5 shows the results of the fatigue analysis with and without the surface factor for comparison. In both cases, the lowest life detected was on the forward edge of the control arm near the balljoint. Both cases were viable, however as previously discussed no surface factor should be

applied and a polished Ks result is more likely predictive. Figure 13 and Figure 14 show the fatigue life contour plots from this analysis from both sides of the control arm. Both contour plots use a logarithmic scale.

Table 5: Benchmark Component Fatigue Results

	Fatigue Life	
	Polished Ks	Cast Ks
	[Cycles]	[Cycles]
Benchmark FLCA	144776	29100

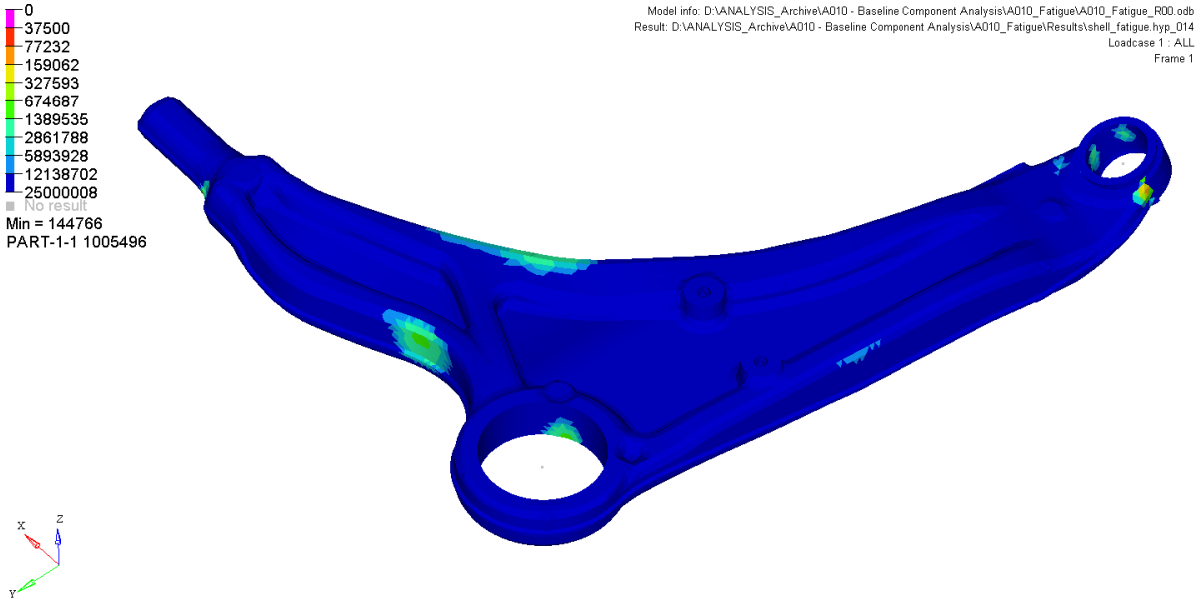

Figure 13: Benchmark fatigue [cycles] inboard view

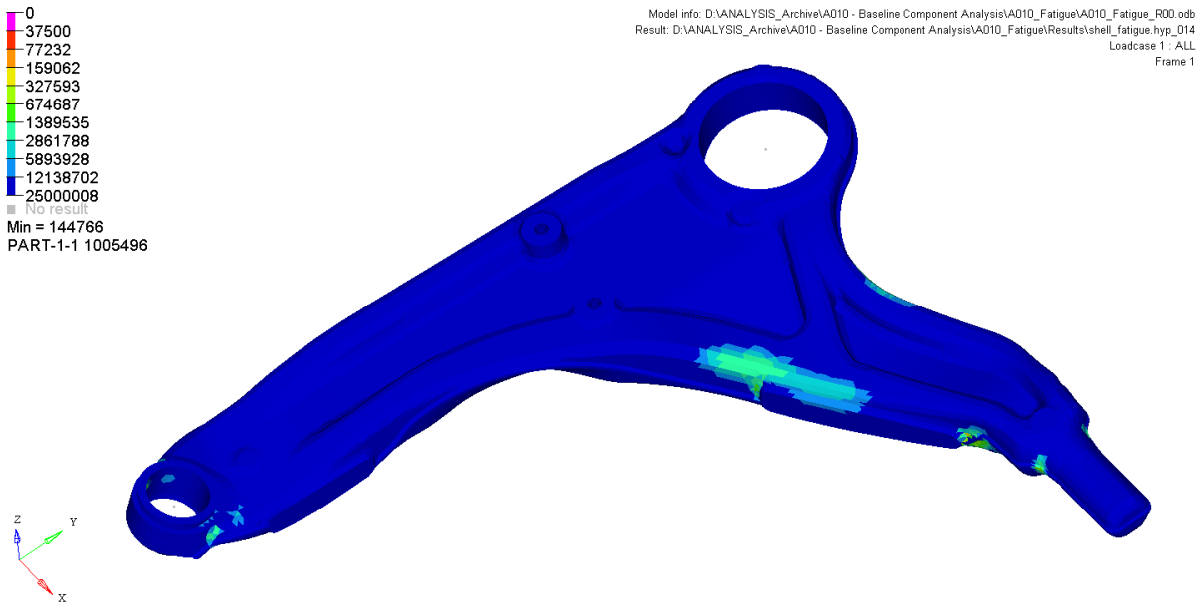

Figure 14: Benchmark fatigue [cycles] outboard view

3.2 General Engineering Specifications

3.2.1 Clearance

In service, the FLCA should not come into contact with any other component of the vehicle in order to avoid damage. This requirement extends to all local components including the brake caliper, knuckle, subframe, stabilizer bar, steering tie rod and boot, brake shield, tire and wheel. Specific clearance guidelines were made available to the project from Ford, however the details are proprietary. The main elements to be accounted for by clearances were compliance, geometric tolerances in the system, and a safety factor derived from experience in vehicle design. In cases of insufficient clearance, it would be necessary to demonstrate functionality via an analysis of deflection and tolerance stackup in the local region to the OEM.

In order to better visualize the critical clearance regions of the model and support optimization tasks, a clearance volume was produced. In the case of this component, the wheel, tie-rod, subframe and knuckle clearances are especially restrictive, as can be seen in Figure 15. To verify acceptable clearance is present, a series of CAD clearance models were extracted for measurement in CATIA v5. The development of this clearance model is further explained in section 4.1.2, as it originated as a core component of the optimization model.

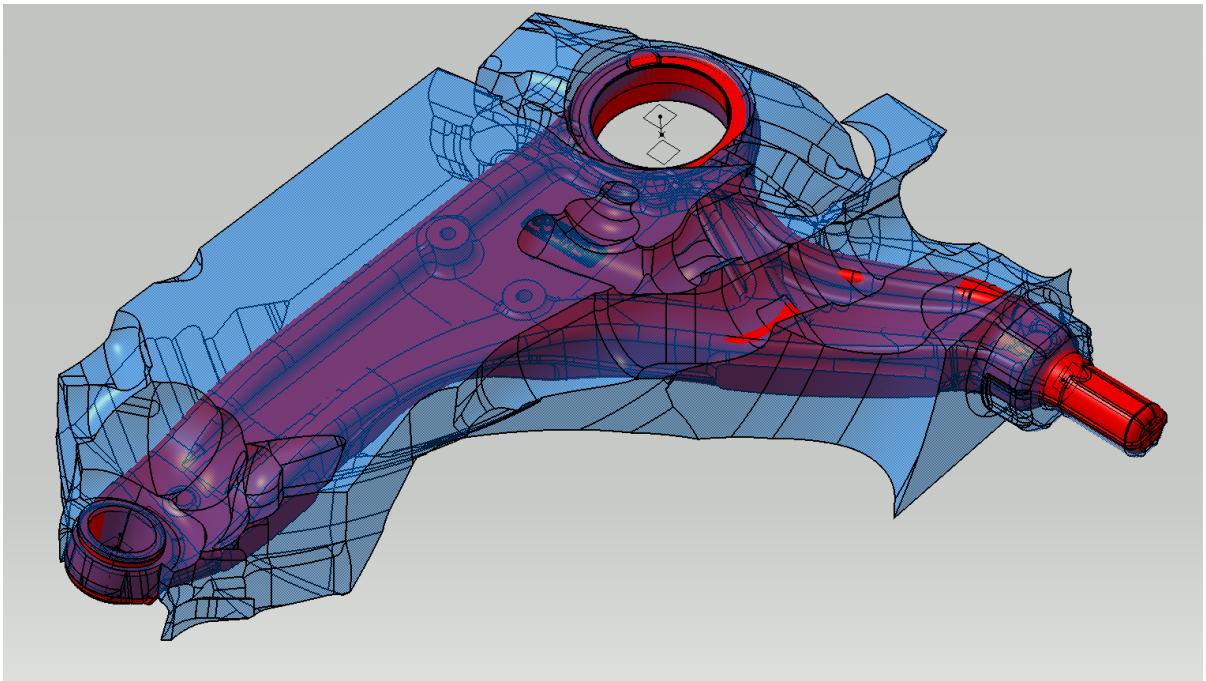

Figure 15: Clearance Volume with Baseline Control Arm

3.2.2 Geometry

Suspension hard point geometry is a set requirement for the structural design of most suspension components. The required positions are shown in Table 6. The local geometry required to accommodate balljoint and bushings must also be preserved to allow their continued use. The use of magnesium is an additional complication for meeting bushing and balljoint specifications, but for this preliminary design stage these elements were not explicitly considered. Possible issues with magnesium include insufficient balljoint pullout strength, maintaining an adequate press fit on the handing bushing, and interface corrosion. The most limiting design implication to come from the preservation of local geometry is the orientation of the balljoint, which is angled inboard towards the bushings and makes ensuring adequate draft angles difficult.

Table 6: Suspension points (rounded to the nearest mm)

Pickup Point	x	y	z
Balljoint [Pt. 6]	1695	-764	333
Handling Bushing [Pt. 3]	1721	-405	346
Ride Bushing [Pt. 4]	1987	-405	355

3.2.3 Quality

Producing a sufficient product quality beyond just passing technical requirements is an additional important part of the OEM specification. The component should give the driver confidence that it will function adequately, as well as not present significant risks in manufacturing. Magnesium components present a number of challenges on these fronts, and although these challenges cannot be formally captured in this study for scope reasons, they should be informally considered. Some of the challenges that should be examined include: crack formation during forging, galvanic corrosion, balljoint cold formability, and balljoint cup strength.

3.3 Structural Design Specifications

3.3.1 Stiffness Requirements

The FLCA serves primarily to fix the wheel in a specific position, and helps maintain the tire in an appropriate orientation. If the FLCA deforms significantly there will be implications for tire life, vehicle stability, and handling [34]. The results of the benchmark analysis are shown in Table 7 for comparison. Any planned design should exhibit values close to these results.

Table 7: Benchmark Stiffness

Requirement	Value	Units
Aft Stiffness	4.33	kN/mm
Lateral Stiffness	81.8	kN/mm

The lateral stiffness result is acceptable, based on an engineering rule of thumb that the stiffness of the control arm should be 5 to 10 times the handling bushing stiffness (~10 kN/mm). Since the handling bushing and the control arm behave as springs in series, there are diminishing returns on total system stiffness as the control arms stiffness gets larger. The system stiffness only increases 8%

from 50 to 100 kN/mm and only 3.5% from 75 to 110 kN/mm. 75 kN/mm was chosen as the target, as it is a reasonable compromise between system stiffness and the ability to reduce mass efficiently, as shown through the optimization model in section 4.3.2. Appendix A shows calculations related to this simplified model of springs in series.

To create the finite element model for stiffness, designs were first meshed using the same process and requirements described in section 3.1.2. The suspension hard points were then connected to the relevant contact points on the mesh using distributed coupling elements (RBE3) to distribute the loads into the arm. Constraints were then applied to the individual hard points as described previously (Table 2). Two linear elastic analysis load steps were created individually, containing a 1 kN load in the relevant direction (positive x for aft, positive y for lateral).

3.3.2 Strength Requirements

In service, it is necessary for the control arm to tolerate occasional high stress loading events. Two types of loading were considered in a manner similar to analysis of the benchmark component (section 3.1.4). The first loads that should be considered are typical overloads possible during service, but that should not adversely affect the function of the control arm. As in the benchmark analysis, some minor local yielding is permissible under these load cases, but should remain below adjustment available in the suspension design. Both aft and lateral cases should be considered, representative of the two primary loading directions.

Ultimate load cases are also required to be met that will likely necessitate the replacement of the FLCA, but cannot result in part failure. Overall deflection must be limited in this scenario to avoid damage to other components. Additionally, failure can be characterized first by the ability of the control arm to support the load, and secondarily by a series of material allowables for equivalent plastic strain (PEEQ), as shown in Table 8. These critical PEEQ values were in most cases taken from the literature, but some also came from initial testing of the material. When the material allowable came from the literature, it was selected initially based on process specific information, but was informed based on other relevant information if available. For this reason, Table 8 shows minimum and maximum values found. It should be noted that the presented values are in many cases from conservative aerospace sources, and in practice more aggressive material allowables might be reasonable.

Table 8: Equivalent Plastic Strain Material Allowables

Material	$PEEQ_{max}$ Allowable [%]	Maximum Elongation [%]	Minimum Elongation [%]
A356.0-T6 Cast Aluminum	3	5 [35]	3 [35]
6061-T6 Forged Aluminum	6	7 [35]	5 [35]
AZ31B Forged Magnesium	6 [35]	19*	4 [35]
AZ80 Forged Magnesium	7 [3]	11 [16]	5 [16]
ZK60 Forged Magnesium	7	7 [35]	4 [35]

*Data from monotonic tensile testing of forged samples

For the setup of the strength model, the stiffness mesh and RBE3 elements were reused. The suspension hard points are then connected directly to a simplified stiffness model of the suspension. This stiffness model was provided by the OEM and generates more realistic deflections and load directions during the analysis. This model is shown for reference in Figure 16. The analysis starts with an initialization step where the skeleton model is allowed to come to static equilibrium. The second step pushes the FLCA to the position the suspension reaches under gross vehicle weight loading. In the third step lateral loads are applied at the tire contact patch, whereas aft loads are applied at the wheel center, and are ramped up to their maximum level by the non-linear solver. To determine permanent deformations, the load can also be ramped down to zero and the arm returned to its base z position in a forth step.

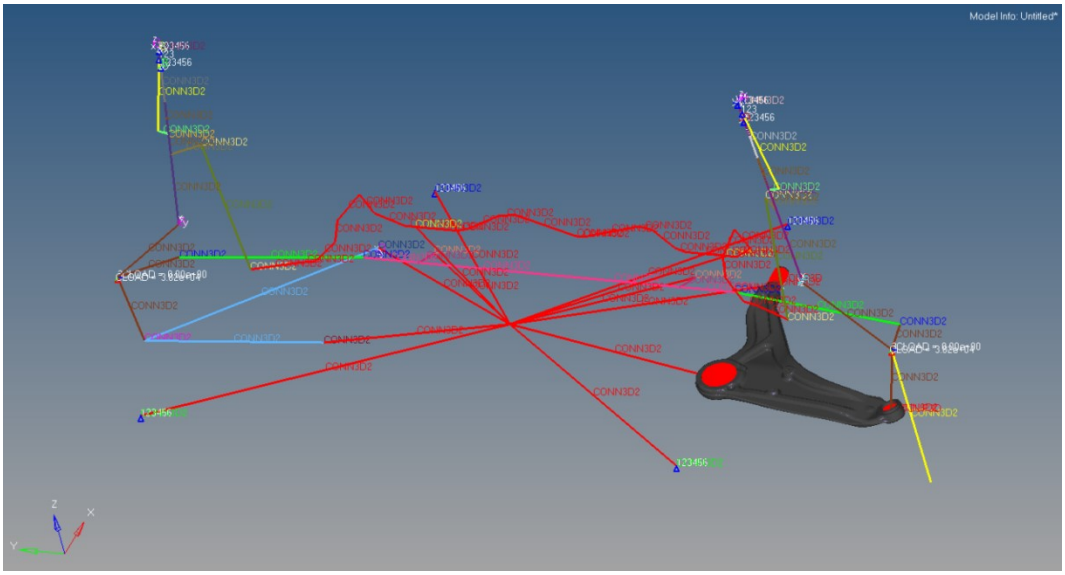

Figure 16: Suspension Skeleton for Strength Load Cases

3.3.3 Fatigue Life

The ability of the FLCA to survive its expected service life is characterized by its predicted fatigue life under a set of OEM-specified fatigue loads. The loads used were simplified representative loads, and for the most part were constant amplitude. To translate the load history into a component stress and strain history, the finite element model of the control arm is first subjected to unit load analyses for all possible load application directions with inertia relief. These component loads are then superimposed in proportion to the fatigue load data to find stress and strain for each of the load cases on the part within nCode DesignLife.,

With the stress strain history in DesignLife, strain life fatigue damage can then be calculated using a Coffin-Manson strain life curve appropriate for the material being evaluated. For the purposes of this project, the Neuber elastic plastic correction factor and Smith Watson Topper mean stress correction were used in the fatigue model. In the case of a cast material, no surface correction should be applied, to account for the consistent presence of material defects throughout fatigue specimens. For a forged material, the surface correction factor should be applied to accurately model the roughness of a forged surface [33]. The FLCA was required to provide similar performance to the baseline component that survived 144,776 fatigue loading cycles.

3.4 Manufacturing Design Specifications

For the initial phase of design, it was decided to use the literature as a reference for geometric requirements, as forging models were still in development. The goal of the manufacturing specifications is to ensure the part can be produced accurately, cost effectively, without defects and with advantageous metal flow. In future design work these specifications should at least be based on future forging tests and analyses, and ideally forgeability would be directly evaluated with a forging simulation. Figure 17 shows the minimum forged I section with critical dimensions as discussed in the following detail sections.

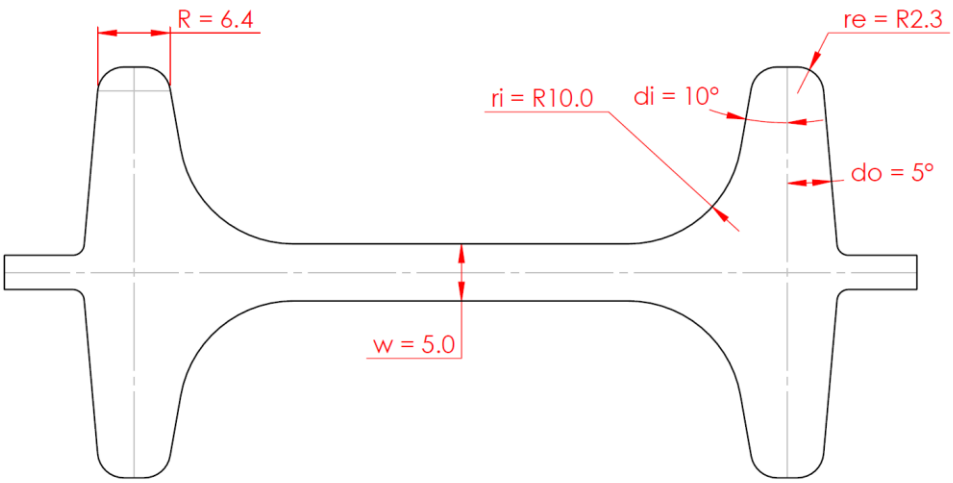

Figure 17: Forged I Section with Specification Variables

3.4.1 Draft Angles

Sufficient draft angles are required to allow the part to fill adequately and clearly extract from the forging die. For the outside draft angles (do) a 5° minimum draft was selected. For the internal pocket draft angles (di) a 10° minimum draft was chosen, as a greater internal angle is required to prevent binding on the die during release [14].

Table 9: Draft Angles

No.	Requirement	Case	Value	Units
M01	Outside Draft Angle (do)	>=	5	deg
M02	Internal Draft Angle (di)	>=	10	deg

3.4.2 Corner and Fillet Radii

The fillet radius has a direct impact on die filling for I section forgings since it directs flow up into the rib. If an insufficient fillet radius is present, the web material may flow directly through to the flash region causing internal defects [16] [14]. The corner radius is less critical than the fillet, however a sharp edge is still difficult to fill. The required values for both of these requirements are shown in Table 10 below.

Table 10: Fillet and Corner Radii

No.	Requirement	Case	Value	Units
M03	Fillet Radius (ri)	>=	10	mm
M04	Corner Radius (re)	>=	2.3	mm

3.4.3 Web Thickness

With a larger part, it becomes more difficult to form thinner sections due to the transition between thick and thin regions, as well as the large forces required [16] [14]. Based on an assumed part surface area for a section of the part, a web thickness of 5 mm was selected for the initial design as shown in Table 11 [13].

Table 11: Web Thickness

No.	Requirement	Case	Value	Units
M05	Web Thickness	>=	5.0	mm

3.4.4 Rib Thickness

Filling the rib section is one of the largest challenges in designing a forging. Due to the shape of the design volume, the rib height is naturally limited and should not be a major constraint. The more critical constraint with this in mind is the minimum allowable thickness of the rib. As the rib gets thinner the material must be extruded up through a smaller gap, making filling more difficult. Based on aerospace industry data, the rib thickness for this geometry was set at 6.35 mm (1/4”) as shown in Table 12 [16].

Table 12: Rib Thickness

No.	Requirement	Case	Value	Units
M06	Rib Thickness	>=	6.35	mm

3.4.5 Barriers to Automation

Since the Ford Fusion is built on a high production global platform [36], production of the FLCA would likely exceed one million parts per year. In order to achieve the required production rate efficiently, some basic requirements were selected as listed below:

1. The design should have provision for ejector pins, in order to allow rapid removal from the production die. Similarly, the design should avoid features that might bind with the die [16].
2. The design should be sufficiently robust after forging to either be handled by a robot manipulator, or dropped into a part chute. Reasonable adaptation can be expected on the automation side to make this feasible [16].
3. After forging, the design should have repeatable reference areas that can be used to efficiently set up the part for machining. Sufficient material should also be present in machined regions of the forging to avoid defects.
4. The rate limiting step in part production should not exceed 1 minute. This is a preliminary guideline, and needs to be verified through a full cost and production analysis compared to the benchmark component.

3.4.6 Surface Finish

Two primary surface finish issues identified so far are corrosion and fatigue. If graphite lubricant is embedded in the final forged part, there is a risk of galvanic corrosion between the graphite particles and the magnesium. Typical aerospace practice indicates that the part should be shot blasted, washed in a mild acid solution, rinsed, and dichromate coated (although other more recent coatings are also available) after forging [16]. Good surface finish also generally improves fatigue durability. Direct requirements for surface finish should be defined to meet the mechanical requirements. In addition, surface cracks should not be present in the final part.

3.4.7 Increased Manufacturing Cost

In order to ensure the component is economically viable, the cost per unit weight reduction versus the baseline component should be considered. Automotive OEM's are required to meet certain fuel economy standards, and as such are willing to compromise part cost in order to achieve lower part mass. The equivalency value of 1 USD/kg saved is conservative, and this should be established based on further analysis, research, and consultation with project partners [2].

Chapter 4
Topology Optimization

Topology optimization was used to generate an optimal distribution of material based on meeting the target stiffness constraints. This model was developed in three phases. First the available region in which material could be placed was defined using a CAD model of surrounding components. The model was then improved by assessing its response to changes in analysis technique, model composition and design constraints. Finally, the model was put through several design studies with varying materials, design objectives and manufacturing constraints to generate designs for consideration. Of these designs, a promising concept was selected and extracted for use as a design reference. This concept was then used to create a CAD model from which further improvements were made manually at the preliminary design stage.

4.1 Design Volume

To obtain an appropriate optimization model, a design volume was defined. This region corresponded to all the areas in which material could be placed without violating the clearance specifications (section 3.2.1). Initially a complete assembly model of the front suspension was not available for use, so the reference control arm was filled in to form a conservative initial design volume. This volume was manipulated to give insight on the model until more detail was available. Once a complete suspension assembly model was available, a series of increasingly accurate design volumes were produced as a basis for the optimization.

4.1.1 Initial Clearance Models

Testing of the optimization model started with filling in the cast baseline geometry between the ribs and any other regions of complexity with material while preserving the outside perimeter of the part. The topology optimization model was created in Altair Optistruct (Hyperworks 13) and was based on a fairly coarse mesh, linked using RBE2 elements to suspension hard points that had been constrained as described in Table 2 (3.1.3). The optimization was driven entirely by an estimated aft stiffness requirement, as it was found to be impossible to meet the lateral stiffness load case due to the limited section available and magnesium's 36% lower elastic modulus.

The baseline model resulted in almost the entire section being filled with material to meet the stiffness target. Since this was not an efficient use of material, a number of experiments were run

which expanded the model section in both width and height. It was found that expanding the width of the arm section resulted in the most efficient removal of material, as would be expected for a simple beam in bending. An example contour plot of a 15mm width expanded design that meets the stiffness criterion is shown in Figure 18.

Although the edge growth model gave an initial idea of what parameters might drive the optimization, it was clear that a higher fidelity model would be necessary to challenge the baseline design. Other limitations with this original simplified model, such as the analysis setup, also needed to be updated to better match the ABAQUS model.

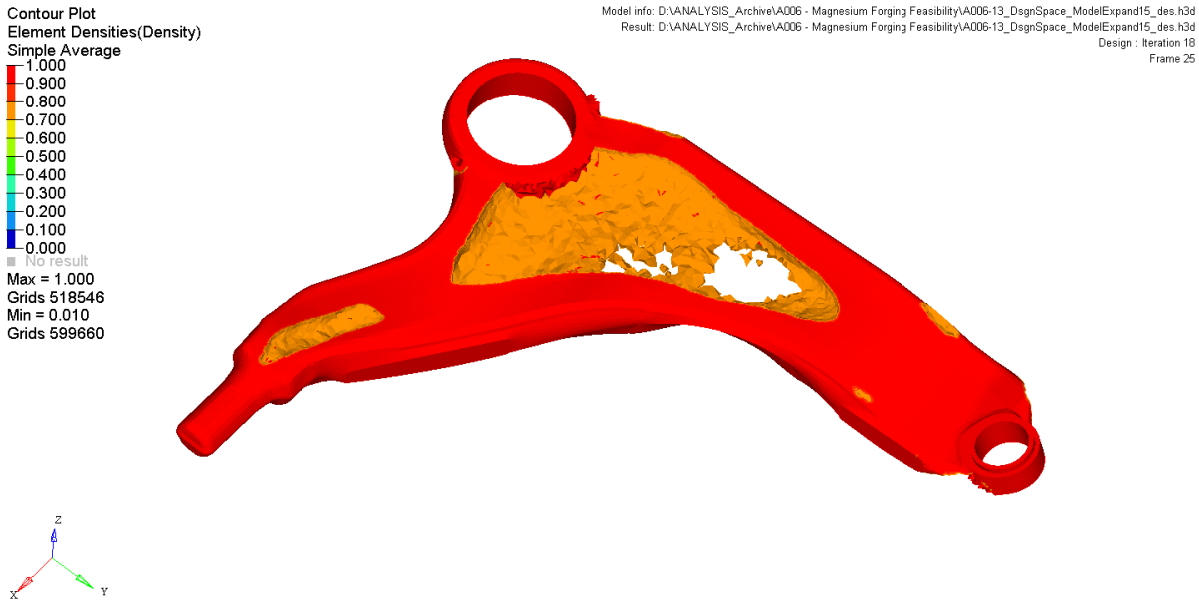

Figure 18: 15mm Edge Growth Topology Optimization

4.1.2 High Fidelity Clearance Model

When accurate CAD data became available, a precise design volume could be created to overcome the limitations of the previous model. After determining the relevant clearance requirements, CAD geometry was extracted from the suspension kinematic CAD model at critical points. For example, the geometry of the subframe was extracted in full vehicle jounce and rebound to determine the closest pass to the area material might be placed. All of the components relevant to clearance were mapped this way as surfaces or offset surfaces. Defining a large box shape around the possible design space, the interferences with these surfaces were methodically cut away until the blue design space shown in Figure 19 remained.

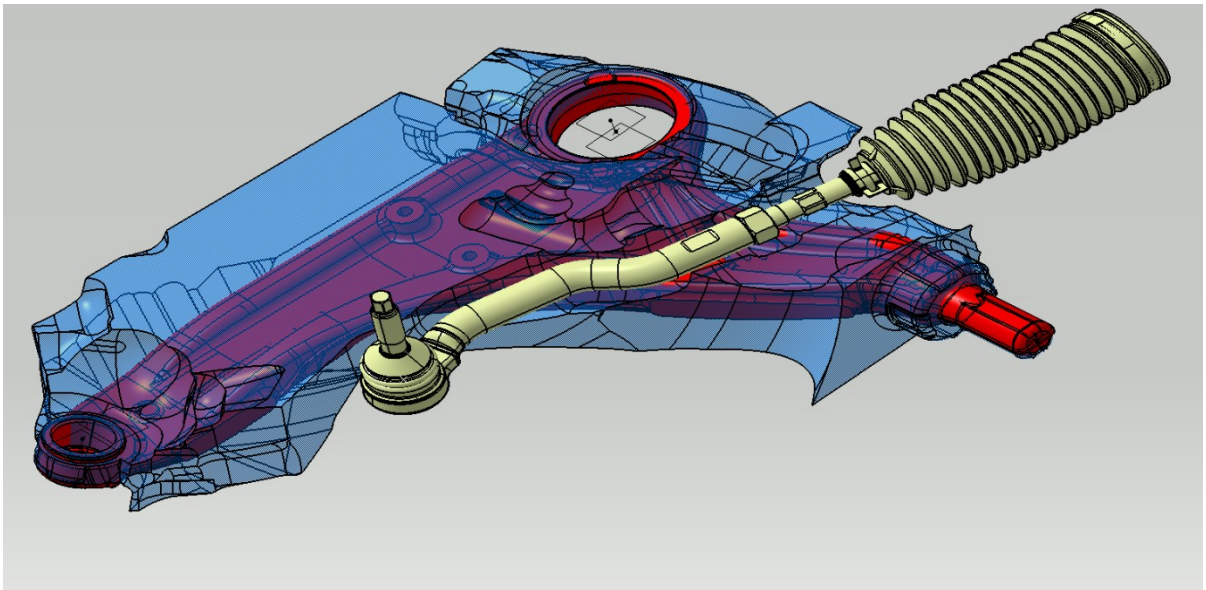

Figure 19: High Fidelity Clearance Model with Benchmark FLCA and Tie Rod

When overlaid with the benchmark design, it became clear that some regions did not follow the first tier of clearance requirements, and were instead likely being evaluated with more complex tolerance based, or compliant models. For this reason, clearance offsets were reduced in the region of the tie rod, as more detailed data was unavailable on the exact requirements. Overall the most limiting parts for the design space, as defined by their proximity to the benchmark arm, are the steering tie rod, subframe window and knuckle bolt.

The modelling of this high fidelity design space took substantial time. While this accuracy gave a level of confidence in the design results appropriate for experimentation, the use of this kind of modelling in industry would severely limit its applications. Using the right balance of high fidelity modelling in critical regions and low fidelity modelling in non-critical regions would be necessary to implement design space creation as an industry workflow.

4.2 Model Development Studies

With a reliable high fidelity design space model, it was possible to establish an accurate topology optimization model. The model was created to mirror the accepted Abaqus model, and the real behavior of the part by extension. Initial studies were run with the intention of assessing the models stability and reliability for predicting reasonable designs. Attention was also paid to the computing

performance effects of changes. The goal of this was to end up with an efficient model that produced a high fidelity concept design.

4.2.1 Baseline Model

The design space was meshed with 3D tetra elements, aiming for a 2mm average size. This size was chosen because the smallest minimum member size constraint value is three times the average mesh size [24]. Since the minimum web thickness was initially estimated at 6mm, this was considered adequate. It was also important that the element size not vary significantly through the thickness of the part, as all elements might need to form the outer edge of the part. As a result, the model for the 2mm mesh has 495 394 elements, as shown below in Figure 20. Non-design space (pink) was also defined as a single element layer around the handling bushing, the contacted post of the ride bushing, and the modelled balljoint cup.

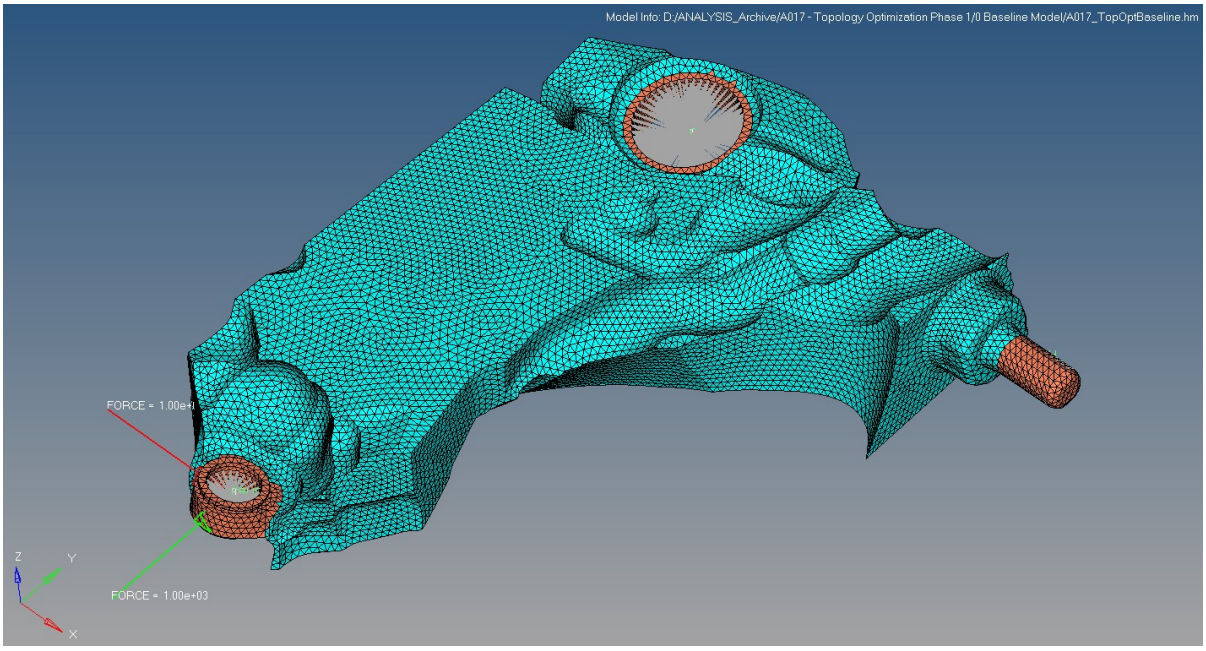

Figure 20: Baseline Topology Optimization Mesh (2mm)

The model was set up with the same boundary conditions as a stiffness analysis (3.3.1). In Optistruct, it was also necessary to place a very stiff CBUSH (configurable bushing) element in between the RBE3 elements and the hard point constraints to avoid an error. Through experimentation, the stiffness of this bushing element was set high enough to not significantly effect the final stiffness results. The design objective was set to minimize mass, while constraints were

applied on the maximum x and y deflections allowed. These deflections were set to correspond to the stiffness specifications. Split draw was selected as a topology optimization constraint, with its axis pointing in the global z direction. This constraint disallowed designs that would not allow dies to part from both sides of the geometry. Minimum member size was specified as 13mm, due primarily to a misunderstanding of the parameters requirements (see section 4.2.4). The model was run using a linear elastic load step with an elastic magnesium material model. The model details for comparison are shown in Table 13.

Table 13: Baseline Topology Optimization Model Parameters

Parameter	Value/Details
Element Order	1st Order 3D Tetra
Mesh Size	2mm average size
Boundary Conditions	RBE3 elements to fixed CBUSH, constrained CBUSH
Material	Elastic Magnesium
Manufacturing Constraints	13mm Minimum Member Size, Split Draw
Load Cases	Stiffness Only

The mass history plot of the baseline analysis is shown in Figure 21, and an iso-plot of element density for the converged design is shown in Figure 22. The optimized mass was 1666g, and although somewhat bulky, the material distribution looked reasonable for the load case. The model was also run without manufacturing constraints for comparison. There was not a significant difference in mass distribution, but the material was not more spread out and there were some undercuts. The converged mass was also significantly lower at 1383g. This led to some suspicion that the minimum member size might be too large. Overall, the model seemed reasonable, so studies of its robustness were continued.

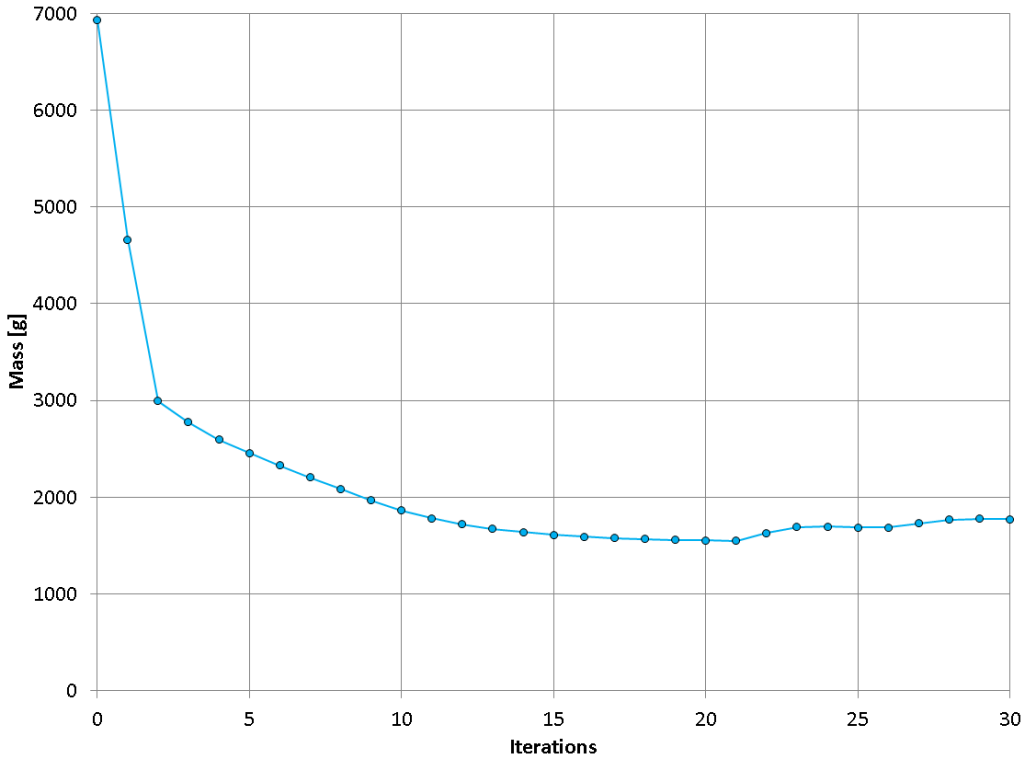

Figure 21: Baseline Topology Optimization Mass History

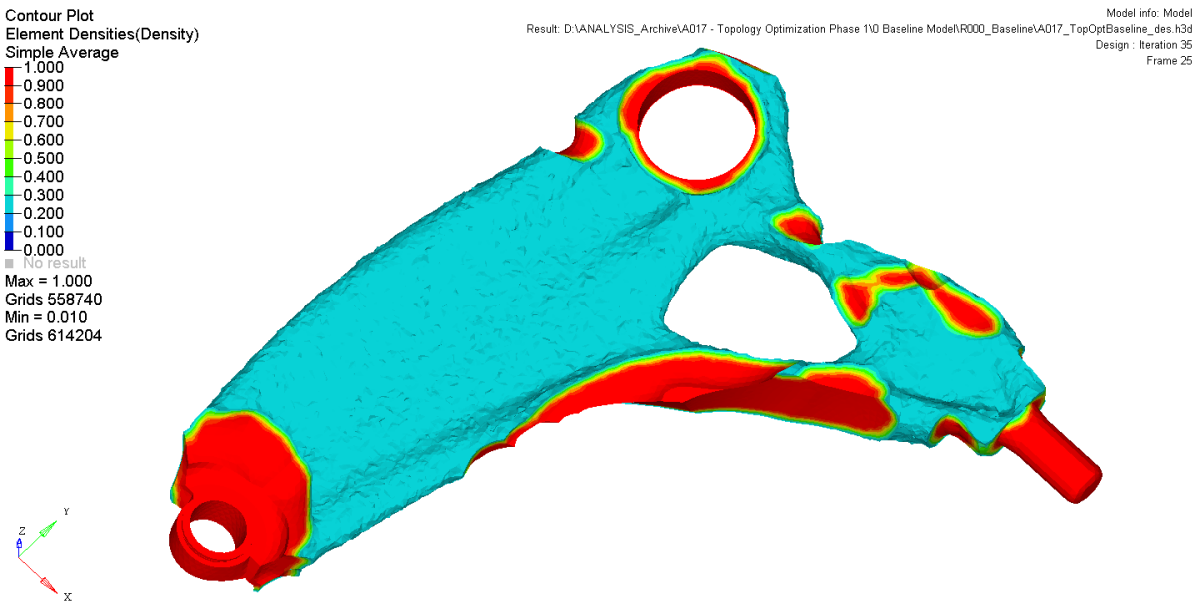

Figure 22: Baseline Topology Optimization Element Contour Plot

4.2.2 Element Order and Mesh Refinement

For an accurate model, it was expected that changes in element order and further refinement of the mesh would not have an effect on the model results. In prior work, 2nd order elements had been used to model most optimization volumes by default. Due to a significant reduction in run time, it was recommended by Altair Engineering to switch to 1st order elements [37]. With the associated effect on minimum member size constraint bounds, it was also desirable to see what the implications of a higher density mesh were. To compare the 1st and 2nd order models, the same mesh was used with the relevant element type. For the refinement study, a 1.4mm average size mesh was meshed created with a total of 1 574 455 1st order elements. Table 14 shows a summary of the model parameters with highlighted changes.

Table 14: Refinement/Order Model Parameters

Parameter	Value/Details
Element Order	1st Order vs. 2nd Order 3D Tetra
Mesh Size	2mm vs. 1.4mm average size
Boundary Conditions	RBE3 elements to fixed CBUSH, constrained CBUSH
Material	Elastic Magnesium
Manufacturing Constraints	13mm Minimum Member Size, Split Draw
Load Cases	Stiffness Only

The comparison contour plot of the 1st and 2nd order model is shown in Figure 24, while the mesh density model comparison is shown in Figure 25. Figure 23 shows the mass history of both models compared to the baseline optimization. Overall, both models were very close to the baseline optimization, giving confidence in the simple model. The 2nd order model ended up slightly heavier, but this was expected due to the more accurate and conservative stiffness of 2nd order tetrahedral elements [32]. Run time for the three simulations varied wildly, with the baseline running in 22 minutes, the refined model running in 3 hours and 8 minutes, and the 2nd order model running in 18 hours and 2 minutes. This is understandable due to the massively increased number of degrees of freedom in the 2nd order model and the more modest increase in the refined model. Both first order models were small enough to run entirely in RAM on the analysis computer (32 GB), which was a clear speed advantage going forward.

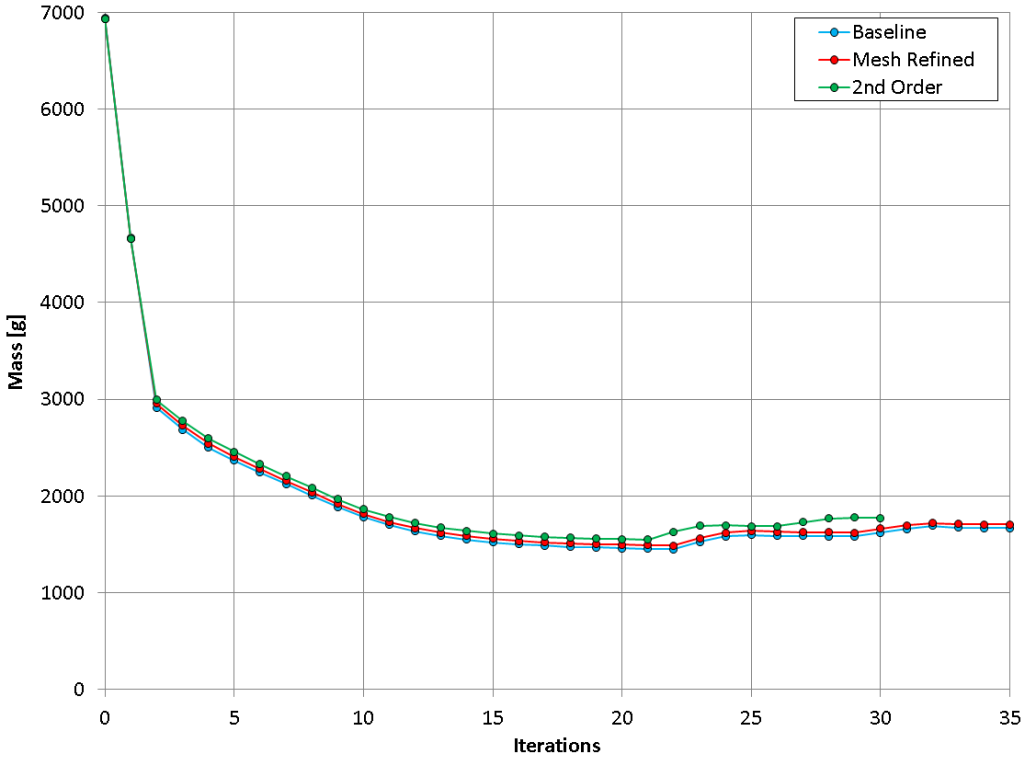

Figure 23: Refinement/Order Study Mass History

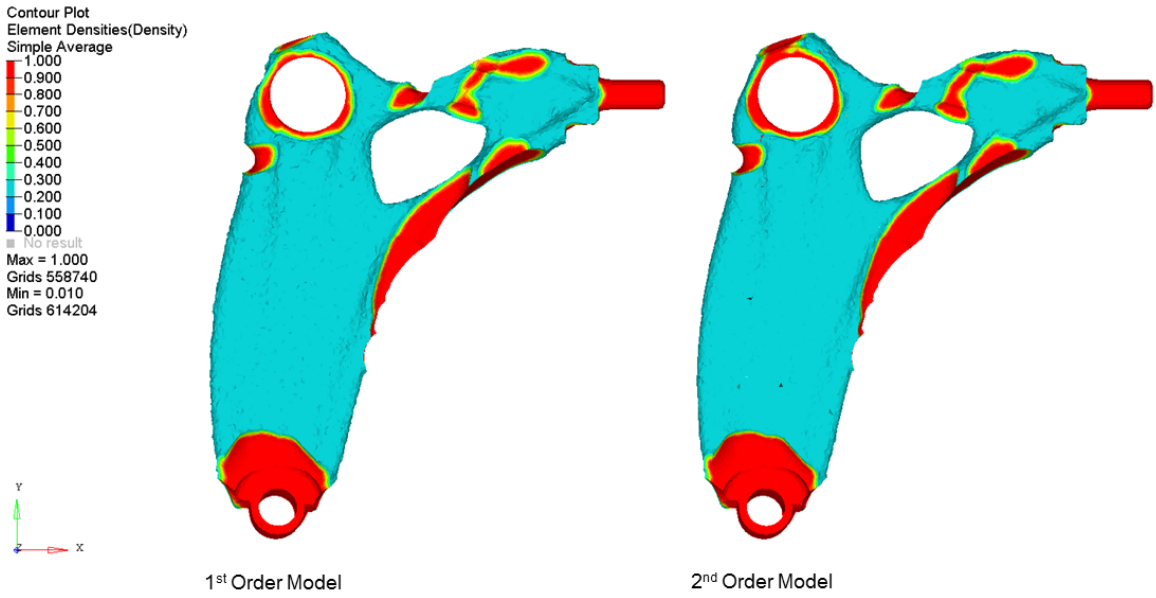

Figure 24: Element Order Topology Optimization Comparison

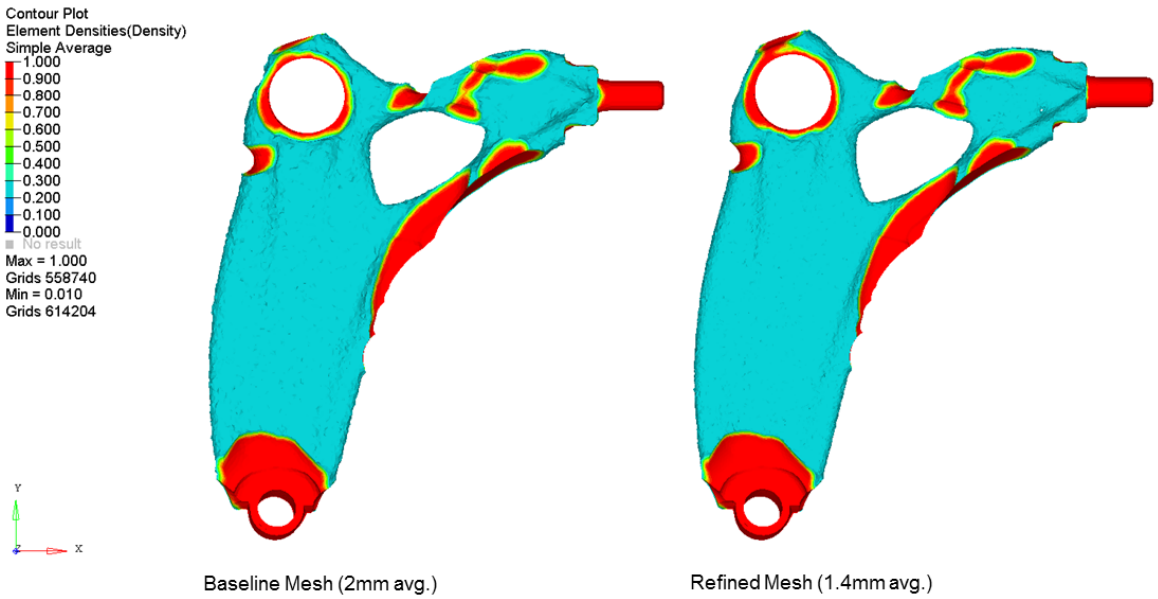

Figure 25: Mesh Density Topology Optimization Comparison

4.2.3 Boundary Conditions

In earlier simulations, RBE2 elements had been used to simplify the optimization model. To understand the effect this would have on topology results, the baseline model was run with RBE2[1] elements and constrained hard points. Table 15 shows the model details with the highlighted changes.

Table 15: Boundary Condition Comparison Model Parameters

Parameter	Value/Details
Element Order	1st Order
Mesh Size	2mm average size
Boundary Conditions	RBE 2 vs. RBE3 elements to fixed CBUSH, constrained CBUSH
Material	Elastic Magnesium
Manufacturing Constraints	13mm Minimum Member Size, Split Draw
Load Cases	Stiffness Only

[1] RBE2 elements are composed of a rigid beam element connecting two nodes, and therefore transfer all loads from the independent node to the dependent node without any change. RBE3 elements average the displacement of all dependent nodes to determine the displacement of the independent node, therefore allowing the boundary on which the dependent nodes are located to flex [41]

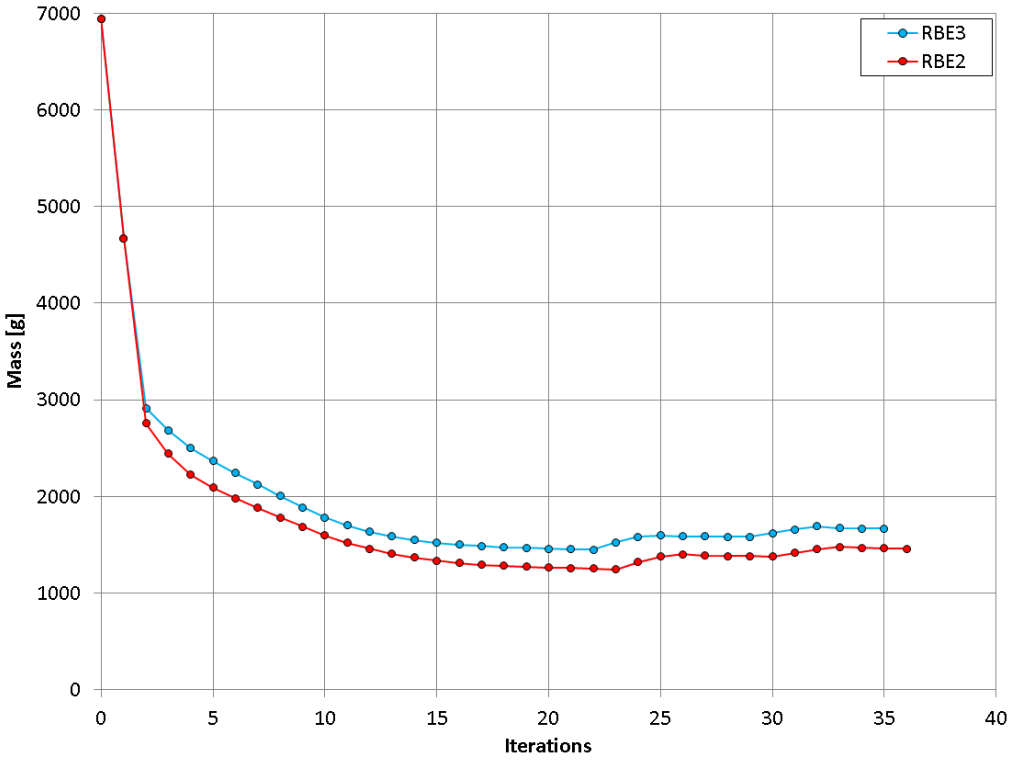

Figure 26: Boundary Condition Study Mass History

The converged mass of the RBE2 model is 12% lower than the baseline model with RBE3 constraints, and this is a consistent trend through the optimization as shown in Figure 26. Figure 27 shows a significant difference in material distribution, especially around the handling bushing. Due to the definition of RBE2 elements as simple rigid beams, the constrained surfaces are unable to deform naturally. This leads to increased part stiffness to weight ratio, as the region is rigid and barely any material is required to support the bushing. Using RBE3 elements allows the bushing bore to deform, providing a more realistic model. It may be relevant in future models to add the steel bushing core to the bore in order to more accurately determine material requirements in this area [31].

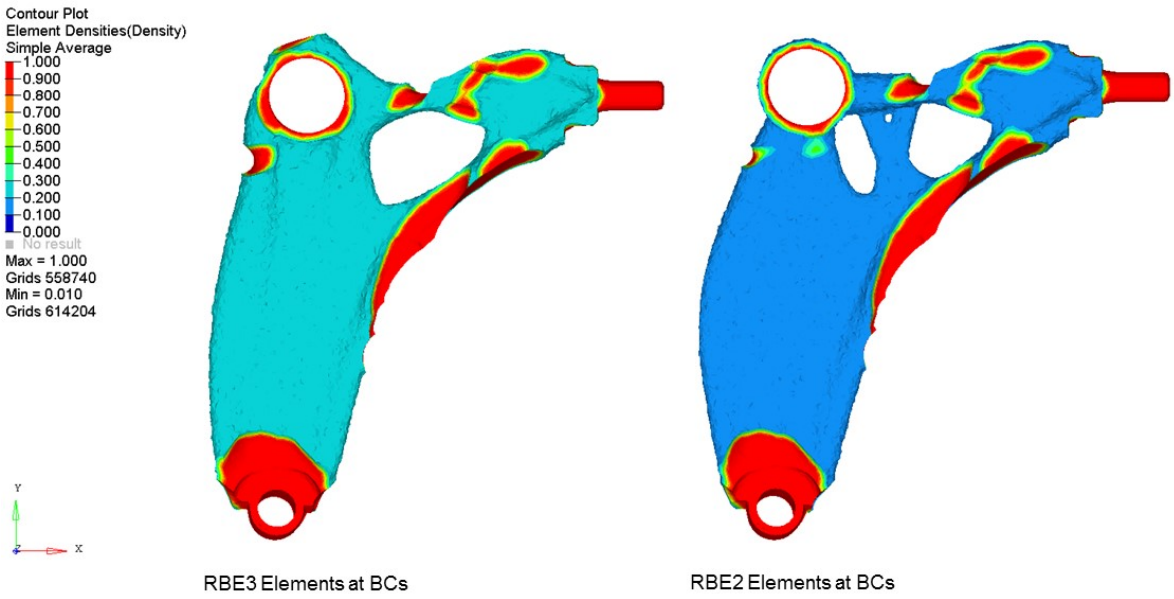

Figure 27: Boundary Condition Topology Optimization Comparison

4.2.4 Minimum Member Size Constraint

One of the available methods with which to capture the limitations of the forging process is through the minimum member size constraint. With this constraint in place structural members produced below the specified constraint value are penalized by reduced stiffness. While this may not completely eliminate thin sections, the simulation will avoid creating them in most cases.

In order to evaluate the effectiveness of this parameter, a study was conducted with a range of acceptable minimum member sizes. The accepted minimum member size in Optistruct is three times the average element size. Element size is calculated by taking the cube root of the average element volume [37]. For the standard mesh used, this allowed minimum member sizes down to 6mm, while the refined mesh allowed 4.2mm. It was decided to run parameter values of 13, 9, 6.3 and 4.5 millimeters, as these values corresponded to possible forged web thicknesses found in the literature [16] [13]. The parameters used in the study are shown in Table 16, with variations highlighted.

Table 16: Minimum Member Size Comparison Model Parameters

Parameter	Value/Details
Element Order	1st Order 3D Tetra
Mesh Size	2mm average (1.4mm average for 4.5mm min member size)
Boundary Conditions	RBE3 elements to fixed CBUSH, constrained CBUSH
Material	Elastic Magnesium
Manufacturing Constraints	13, 9, 6.3, 4.5mm Minimum Member Size, Split Draw
Load Cases	Stiffness Only

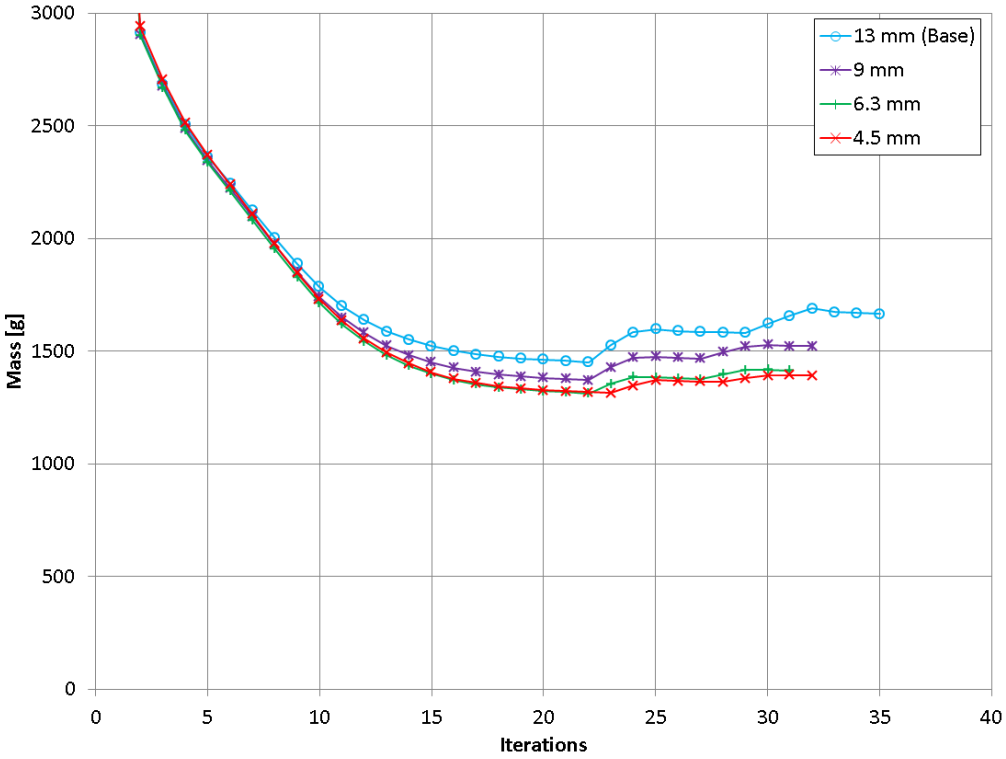

Figure 28: Minimum Member Size Study Mass History

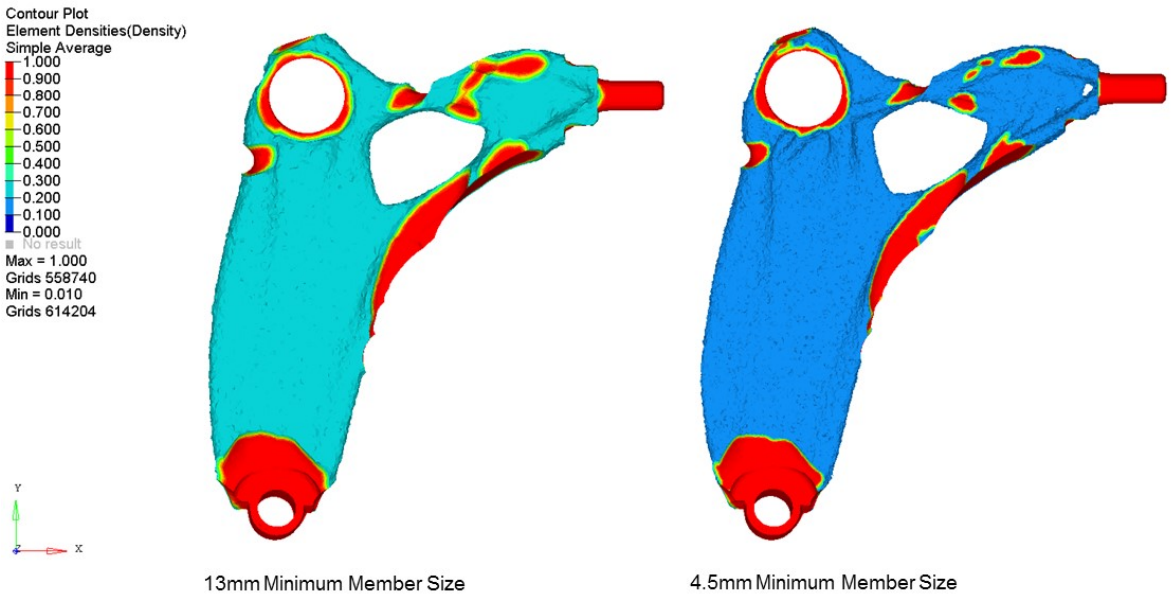

Figure 29: Minimum Member Size Study Topology Optimization Comparison

Figure 28 shows the mass history of the simulations conducted. As the minimum member size was reduced from the baseline value of 13mm, there was a significant decrease in mass. This decrease had diminishing returns as the parameter dropped to below 6.3mm, but at 4.5mm saved a total of 275g off the baseline of 1666g. Overall the mass converged to the results of the simulation unbounded by manufacturing constraints. The topological differences between the 13mm and 4.5mm simulations can be clearly seen in Figure 29. With a lower minimum member size, the simulation is able to form efficient reinforcing ribs that closely mirror what can be achieved in a forging design.

4.2.5 Added Load Cases

For a topology optimization to produce a structurally efficient design, it is necessary to build in all significant load cases. If this is not done the optimization is unable to capture anything to do with the load cases that are not present, and passing these requirements will not be guaranteed [37]. Prior to the study, two load cases were used in the optimization: lateral stiffness and aft stiffness. It was decided to search for other load cases that might cause issues within the OEM fatigue data. Maximum and minimum loads were derived from this data, producing 24 possible critical load cases. Figure 30 shows the load cases producing maximum stress at each simulated element. Through this analysis, six fatigue load cases were identified as possibly critical for stress.

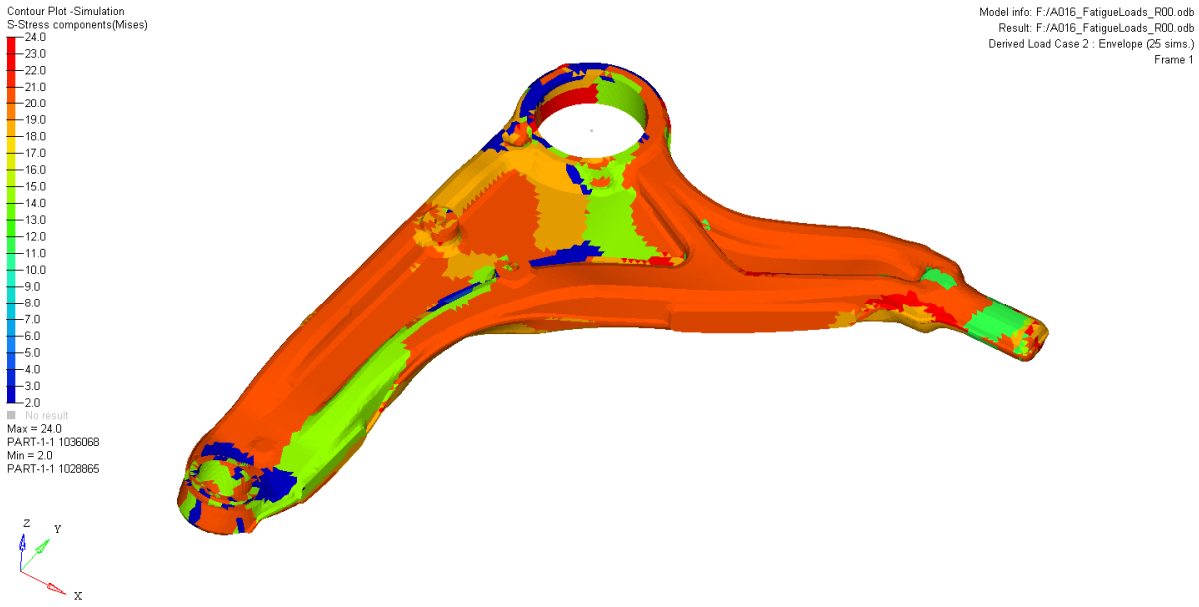

Figure 30: Critical Fatigue Load Cases for Individual Elements

In order to try to capture the effect of the critical fatigue load cases, they were added to the topology optimization. To add the load cases, the point loads and moments were applied at the suspension hard points and the load step was set up with inertia relief to suppress rigid body modes. The optimization was set up with a 100 MPa stress constraint based on tests with the baseline component and these load cases. Table 17 shows the simulation parameters used with changes from the baseline highlighted.

Table 17: Additional Load Case Study Parameters

Parameter	Value/Details
Element Order	1st Order 3D Tetra
Mesh Size	2mm average size
Boundary Conditions	RBE3 elements to fixed CBUSH, constrained CBUSH
Material	Elastic Magnesium
Manufacturing Constraints	6mm Minimum Member Size, Split Draw, Stress (100 MPa)
Load Cases	Stiffness and Critical Strength Load Cases

Running the model, it was clear that no significant changes to the part topology were created in this simulation. Figure 31 shows a plot of Von Mises stresses for the critical load case, with all elements with stress below 1 MPa removed. This plot shows that most regions of the part were below the 100

MPa constraint, with certain sharp edges generating higher stresses. Due to the nature of the optimization, surface elements are not removed [24]. The stress constraint would be more effective if the critical points were not driven by the geometry of the design space. An additional reason why the stress constraints had a minimal effect was because the largest loads were in the same direction as the stiffness loads. Since material was already well distributed to meet the stiffness requirements, in this design the additional loads were mostly accommodated. Lastly, the loads that were not in the directions of the stiffness loads were relatively small, and did not generate stresses in excess of the constraint. Overall the conclusion of this study was that the model should remain driven by only the two stiffness requirements.

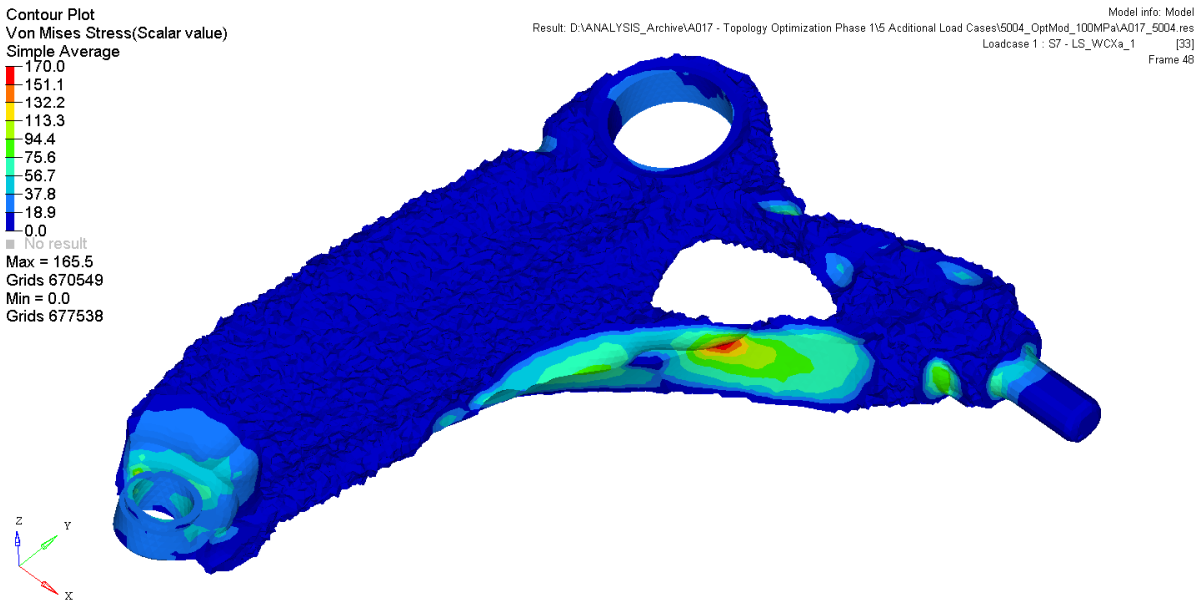

Figure 31: Von Mises Contour of Critical Load Case

4.3 Design Studies

With the robustness of the topology optimization model established, the primary objective of creating an optimal material distribution for the magnesium FLCA could be realized. Studies were planned to evaluate the results achievable with different materials, the effect of the lateral stiffness constraint on outcomes, and what effect different manufacturing constraints might have on the realized topology. These studies were to be part of the project conceptual design phase, helping to generate usable design concepts for the final part.

4.3.1 Material Changes

Steel and aluminum are already commonly used for control arms in the form of castings, forgings and sheet metal parts. In order to determine which material would be optimal for a forging, topology optimizations were run with a new set of baseline parameters established in the first set of studies, and the different materials as shown in Table 18.

Table 18: Material Study Parameters

Parameter	Value/Details
Element Order	1st Order 3D Tetra
Mesh Size	1.4mm average size
Boundary Conditions	RBE3 elements to fixed CBUSH, constrained CBUSH
Material	Elastic Magnesium, Aluminum and Steel
Manufacturing Constraints	4.5mm Minimum Member Size, Split Draw
Load Cases	Stiffness Only

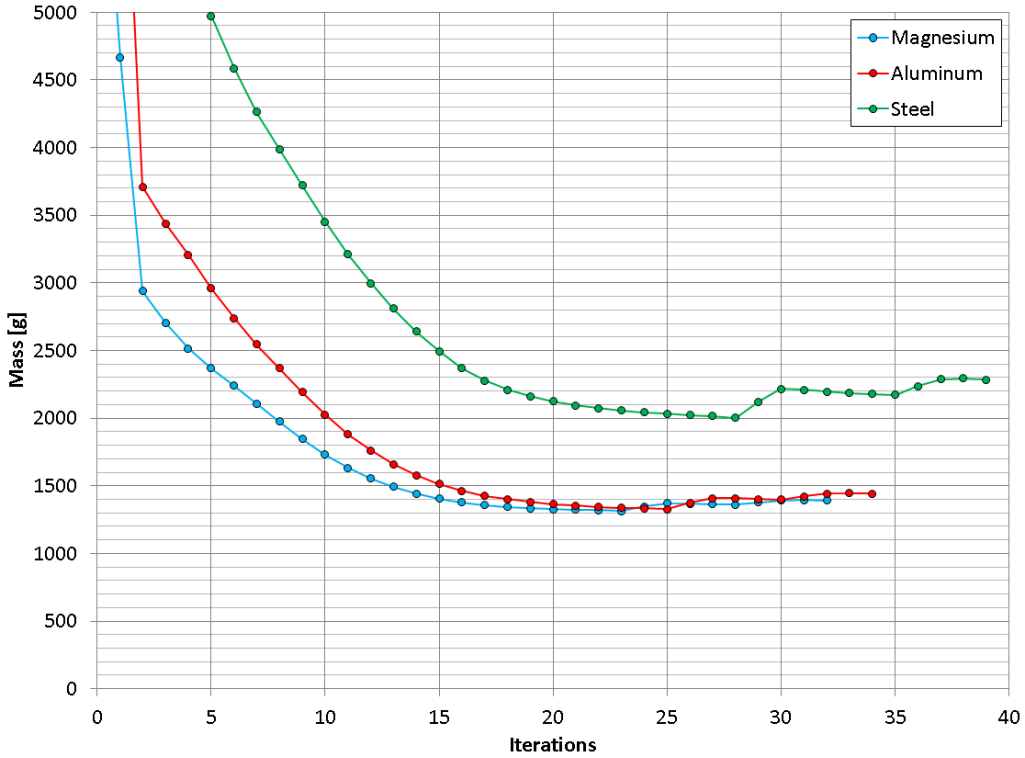

Figure 32: Material Study Mass Histories

Figure 34 above shows the mass history of the three materials in the same optimization model. All three materials actually beat the baseline design in terms of mass; however, they only consider the stiffness load cases. While magnesium and aluminum are quite competitive, the forged steel design is less so in this optimization, as it struggles to use the efficient edges of the design space without adding heavy web material. The use of thinner steel sheet and tube based designs would necessitate a finer mesh or different optimization strategy but has been shown to be effective at challenging aluminum's specific stiffness and strength, especially in more restrictive spaces [28].

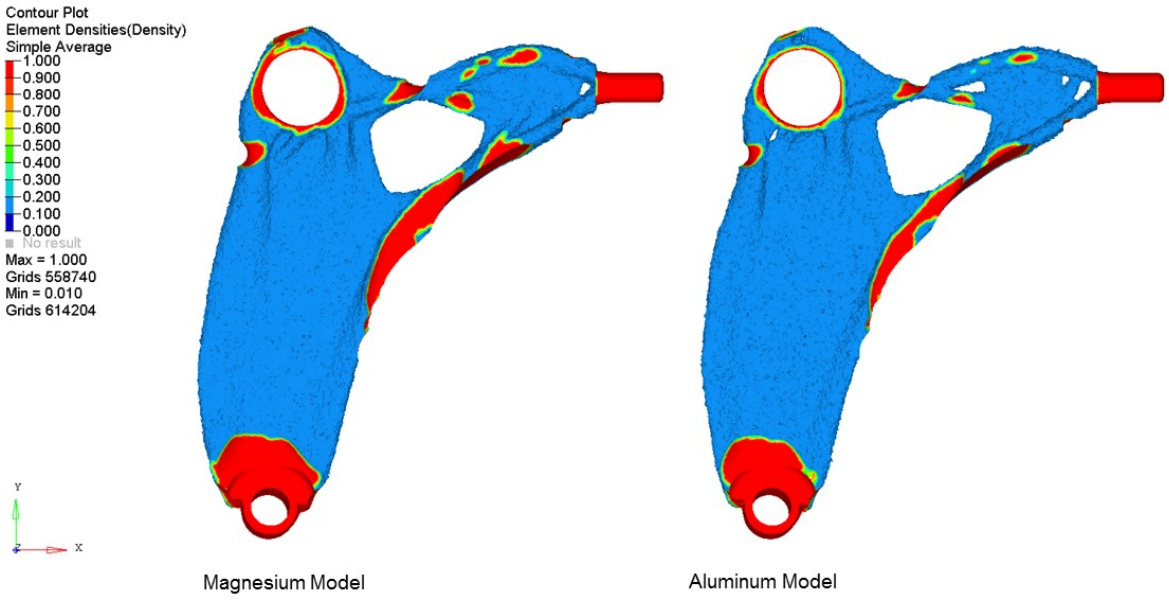

Figure 33: Magnesium vs. Aluminum Topology Results

Figure 33 shows fairly similar topologies generated by aluminum and magnesium. The aluminum model is unable to spread to fill the design space as efficiently as the magnesium, and leverages the manufacturing constraints to allow more holes in the design volume. The tie rod cut-out requires more magnesium to fill, as it is a relatively restricted area, giving the aluminum a local advantage in a critical region. Overall the two designs are very competitive for mass. The stiffness constraints may not be the critical design constraint; given strength and fatigue cases need to be explicitly considered.

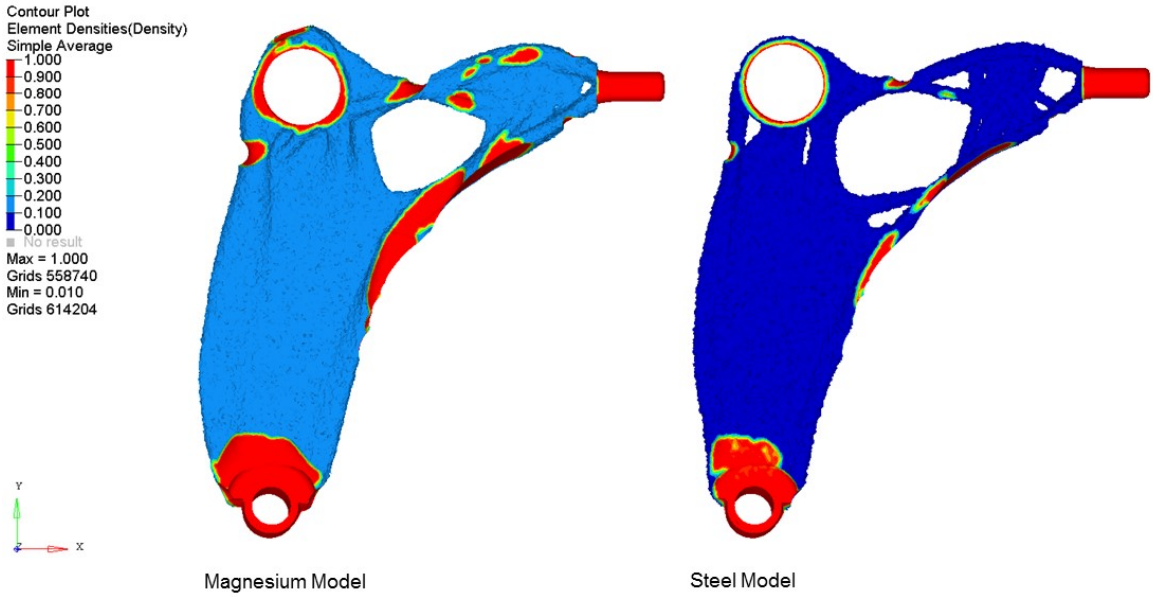

Figure 34: Magnesium vs. Steel Topology Results

The comparison of steel and magnesium optimized designs shown in Figure 34 provides much greater contrast. The steel design uses a number of small internal stiffening members to allow for more internal holes, and has a comparatively restricted distribution of its ribs. Additionally, it is very clear that to support the bushing structure a comparatively large amount of magnesium may be required.

4.3.2 Lateral Stiffness Sensitivity

In order to inform the final selection of a viable lateral stiffness constraint, a study of the effects of changing lateral stiffness constraints was performed on both aluminum and magnesium. Magnesium is at least even with, and at worst only 94% as stiff per unit mass as aluminum under tension-compression loading as shown in Appendix B. Due to diminishing returns with increasing lateral stiffness, as discussed in section 3.3.1, it was decided to set the specification target lower to reflect the opportunity for light weight design more effectively. Table 19 shows the model parameters used for this analysis with study variations highlighted.

Table 19: Lateral Stiffness Sensitivity Model Parameters

Parameter	Value/Details
Element Order	1st Order 3D Tetra
Mesh Size	2mm average size
Boundary Conditions	RBE3 elements to fixed CBUSH, constrained CBUSH
Material	Elastic Magnesium
Manufacturing Constraints	6.3mm Minimum Member Size, Split Draw, varied Lateral Stiffness constraint
Load Cases	Stiffness Only

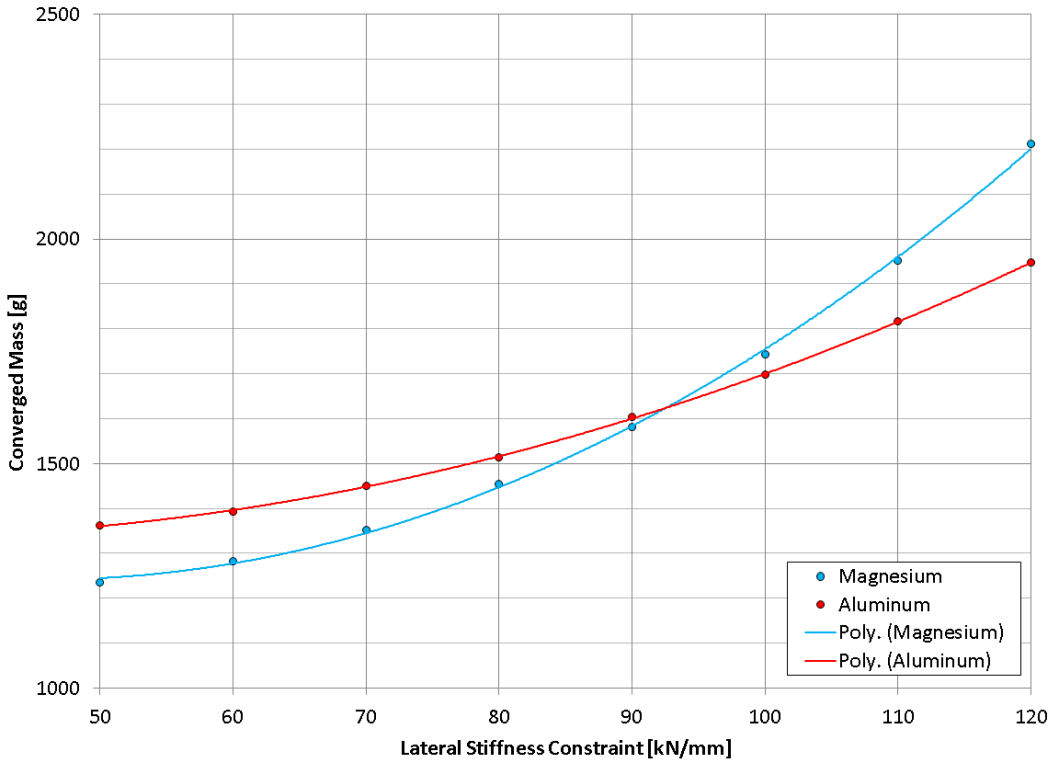

Figure 35: Lateral Stiffness vs. Topology Optimization Converged Mass

Figure 35 shows the variation in converged mass with changing lateral stiffness constraint. Initial studies with RBE2 elements linking to the suspension hard points showed superior magnesium performance in the whole domain, whereas this study with RBE3 elements shows a clear crossover point in terms of mass efficiency around the 90 kN/mm point. While the aluminum model does not change much over 90 kN/mm, the magnesium model shifts from an efficient I-beam section to filling

the tensile load path directly as shown in Figure 36. In order to produce a magnesium part with a better stiffness to weight ratio, it is necessary to drop the lateral stiffness constraint to below 90kN/mm so that the aft stiffness is the optimization driver.

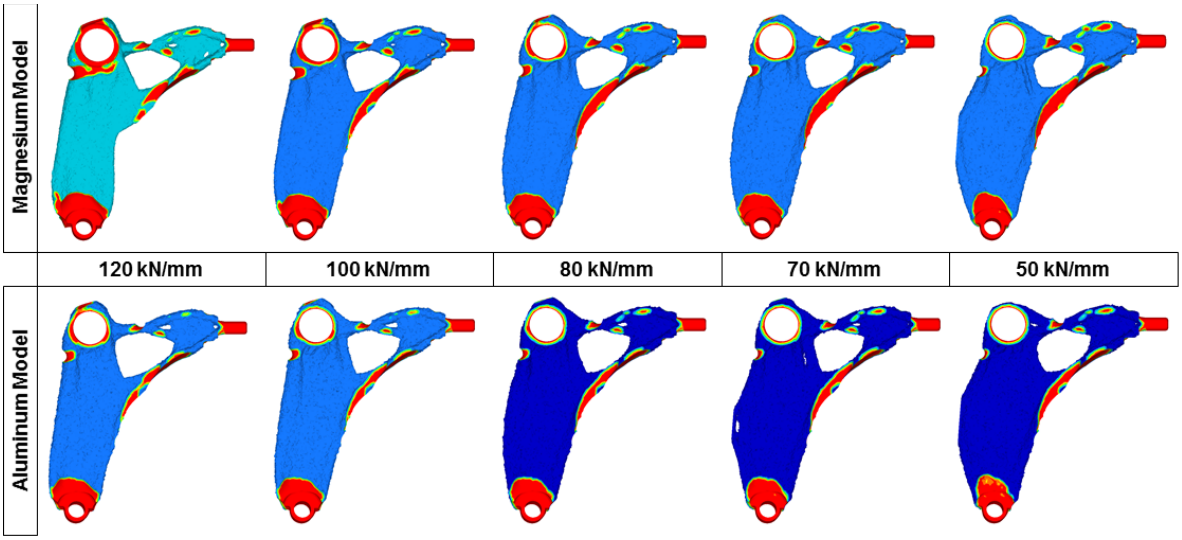

Figure 36: Topology Optimization Changes with Material and Lateral Stiffness

4.3.3 Maximum Member Size Constraint

Several manufacturing constraints are available within Optistruct beyond those previously explored. Maximum member size uses a similar penalization effect to the minimum member size constraint, with a recommended minimum size of 6 times the average element size [24]. In general, it is used to put a limit on how thick a member can be, for example in the case of a casting where a relatively uniform wall thickness is needed to avoid defects. It was decided to explore the effects of this constraint given that it might generate different design possibilities, and had the potential to create more uniform rib sizes. Table 20 shows the model parameters used for this study, with changing parameters highlighted.

Table 20: Maximum Member Size Constraint Study Parameters

Parameter	Value/Details
Element Order	1st Order 3D Tetra
Mesh Size	1.4mm average size
Boundary Conditions	RBE3 elements to fixed CBUSH, constrained CBUSH
Material	Elastic Magnesium
Manufacturing Constraints	10, 15, 20, 25, and 30 mm Maximum Member Size, 4.5mm Minimum Member Size, Split Draw
Load Cases	Stiffness Only

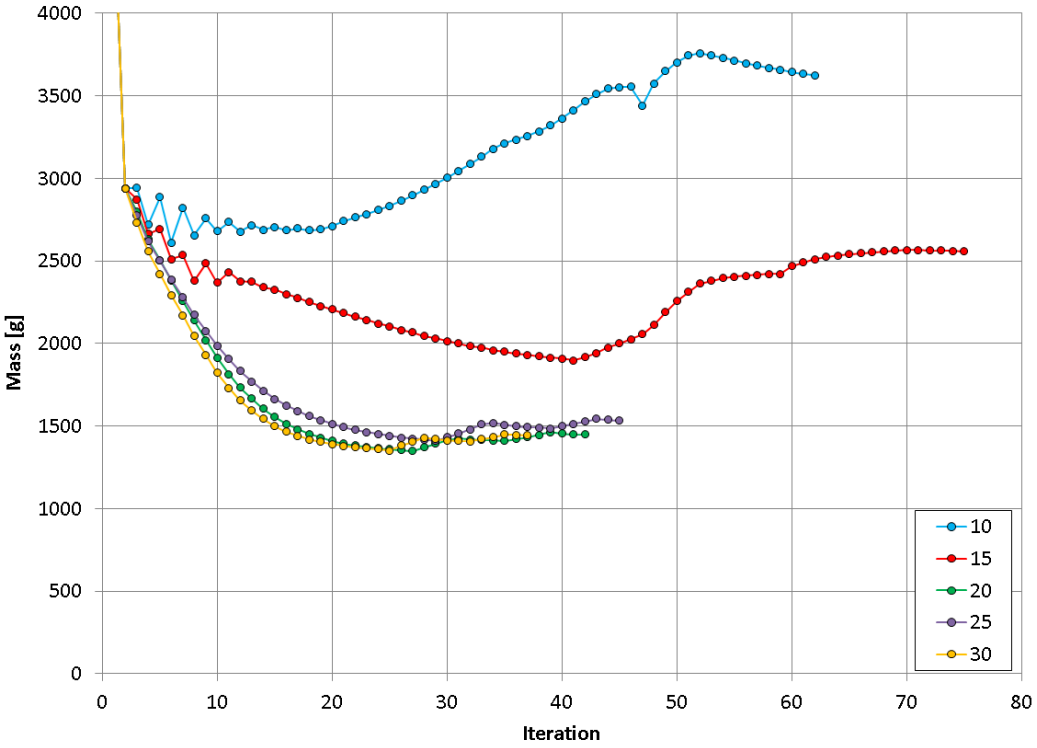

Figure 37: Maximum Member Size Study Mass History

As can be seen in Figure 37, the simulation was not always very stable. With low maximum member size, it was very difficult for the design to effectively support the lateral stiffness constraint. The lack of connectivity in the final topology for a 10mm max member size value contributed to a very full design space, as observed in Figure 38. Further instabilities were reached past a 20mm maximum member size, likely due to the recommendation not to go past half the model thickness

with this parameter [24]. Overall, the distributions produced were not particularly easy to manufacture, but the higher values gave some insight as to where thicker doubled up wall sections might be useful on the final part to avoid excessively tall ribs.

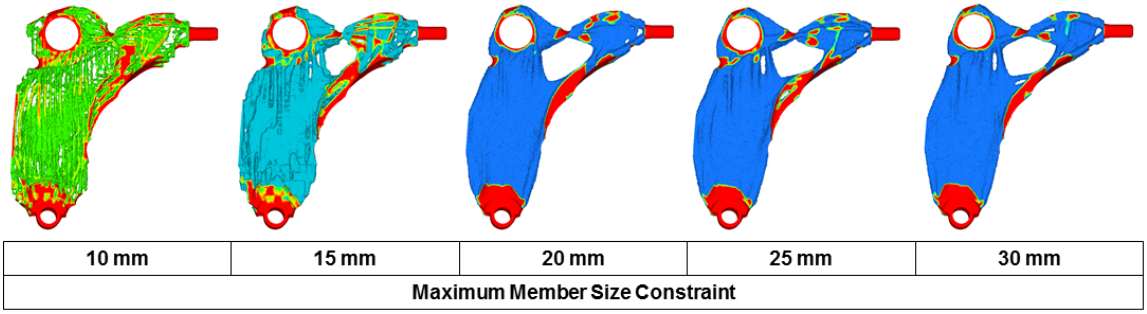

Figure 38: Topology Changes with Maximum Member Size Constraint

4.3.4 Alternative Manufacturing Constraints

Continuing to explore possible manufacturing constraints, it was decided to run exploratory studies with the extrusion constraint, and the no-hole constraint with split draw. The extrusion constraint study was intended to discover where direct load paths existed in the part, without the complication of a web. Studies with the no hole constraint were designed to discover the effect on topology of disallowing holes to form in the web. The intention of this was to possibly skip the added difficulty of hot shearing internal features on the part. Table 21 shows the study parameters, with changes highlighted.

Table 21: Alternative Manufacturing Constraint Study Model Parameters

Parameter	Value/Details
Element Order	1st Order 3D Tetra
Mesh Size	1.4mm average size
Boundary Conditions	RBE3 elements to fixed CBUSH, constrained CBUSH
Material	Elastic Magnesium
Manufacturing Constraints	4.5mm Minimum Member Size. Extrusion and Split Draw with No Hole Constraint
Load Cases	Stiffness Only

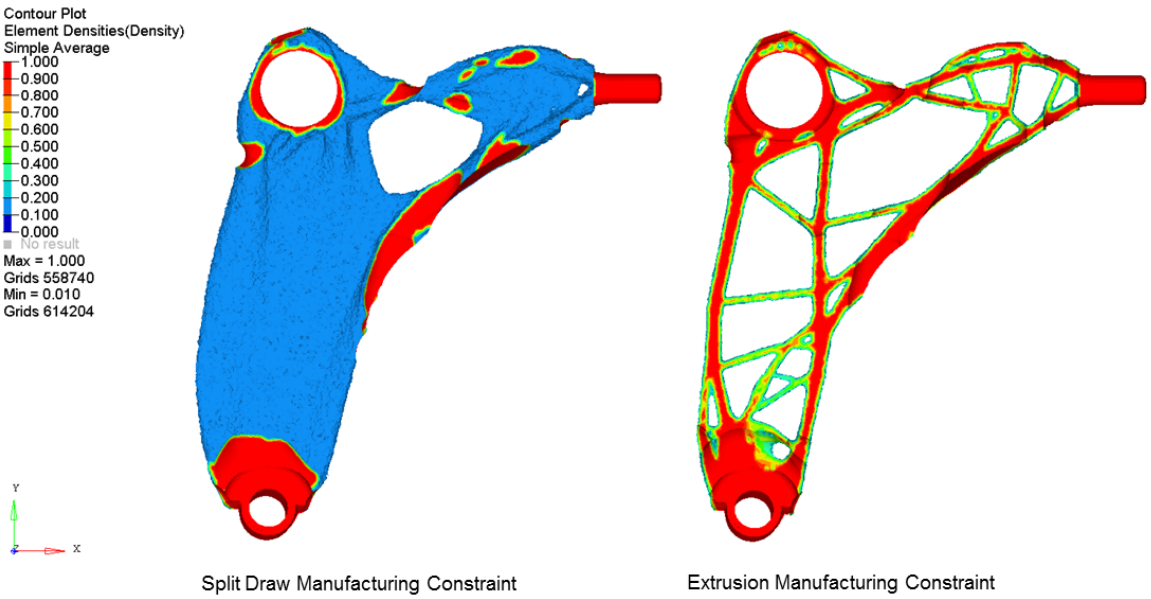

Figure 39: Extrusion Constraint Topology Comparison

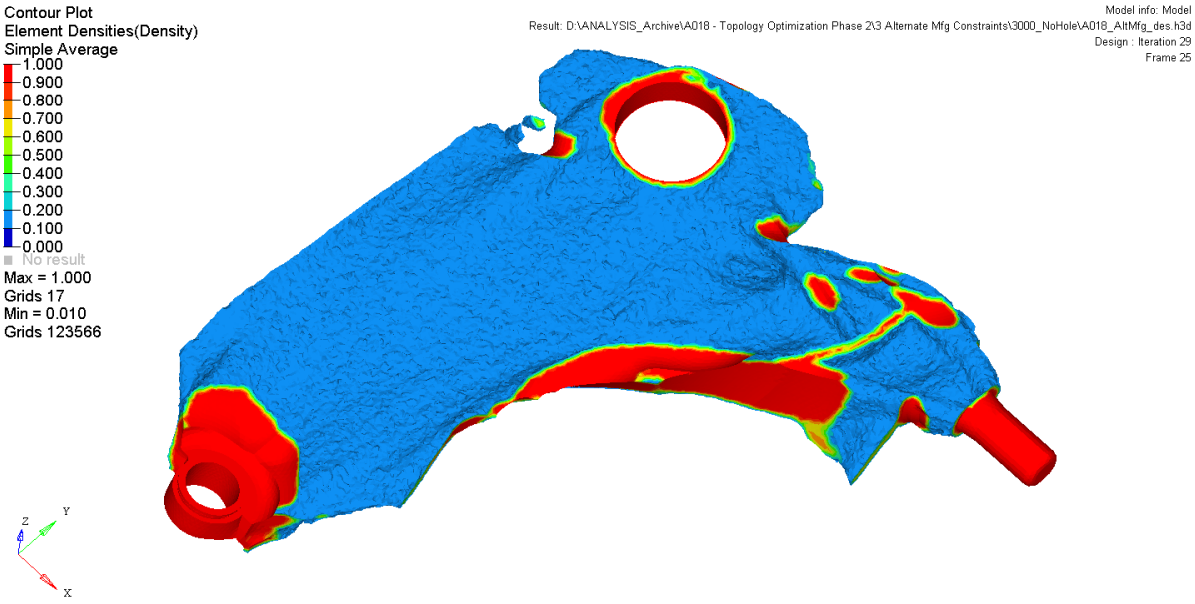

Figure 40: No-hole Constraint Topology

Figure 39 shows the extrusion topology compared to the baseline topology. Although the result is a well-defined set of material traces, it is difficult to draw direct conclusions since the extrusion constraint forces use of the entire height of the design volume. With the ability to adjust height, or a shorter design volume, this may have been more useful, but the current design is limited by the need

for very tall thin members. The results of the no-hole optimization are shown in Figure 40. Again, the findings of this optimization were interesting, but not directly usable as the constraint forced the use of material sufficient to fully cover the part from a top view. It is clear that web distortion and localized ribbing can be efficiently used in the region of the ride bushing post, whereas the rest of the part is viable as a more traditional I section. While neither of these optimization results were directly usable, they both gave useful insights. If it were of interest to implement either design strategy a more specific design volume would need to be constructed based on the initial results shown here.

4.4 Preliminary Design

With a number of viable design concepts, it was necessary to select one and move forward with it as a preliminary design. It was decided to move forward with the simple split draw model with a 4.5mm minimum member size as developed in section 4.2.4. This model was a good approximation of expected forging capabilities in terms of meeting the geometrical specifications, and also made direct use of typical industry forging practices such as the hot trimming of holes. At this point it was necessary to extract the model from the topology optimization, and check the extracted design for initial compliance to the specifications.

4.4.1 Model Extraction

Using the OSSmooth module within Optistruct, a model was extracted for analysis from the topology optimization contours. The contour model cannot be used directly, as it has many elements with intermediate stiffness and density. OSSmooth identifies the shape of the exterior contour, creates a surface mesh, and has the ability to fill the mesh and retain boundary conditions. Due to element quality issues, the model was remeshed in order to run at all in Abaqus. Element quality was not referenced as a critical factor, since it was very difficult to control without generation of errors. Since these analysis trials were to be focused on getting an approximation of performance, this was deemed to be reasonable. Figure 41 shows the final extracted mesh with boundary conditions. The optimized mass at this point was 1813g, which was significantly heavier than the converged topology optimization value. With the filling in of partial density elements, this compensation was expected, but further design interpretation was expected to reduce this value in the final design.

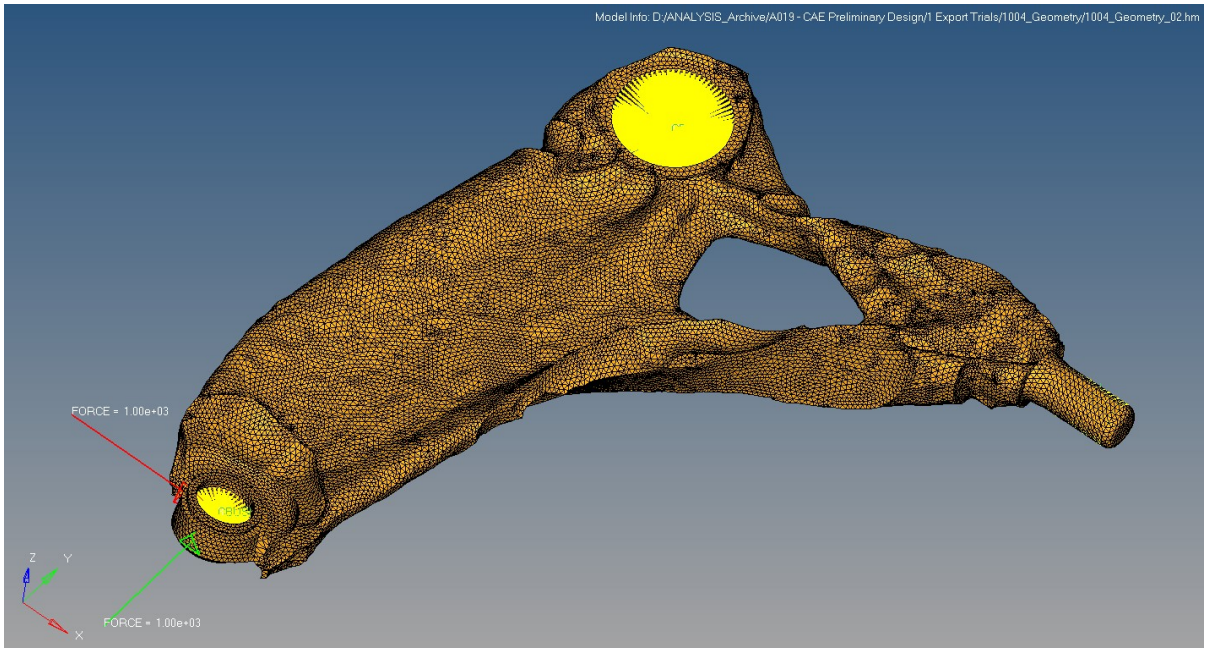

Figure 41: Extracted Optimized Topology

4.4.2 Initial Design Verification

Before proceeding with the interpretation of the design in the form of a CAD model, it was analyzed to judge compliance with the engineering specifications and detect any potential issues for implementation. Stiffness and strength analysis were conducted, but fatigue analysis was not.

Using Abaqus, the stiffness of the component was analyzed as required by the stiffness specifications described in section 3.3.1. Table 22 shows the results of these simulations. In both lateral and aft stiffness, the preliminary design passed with a substantial margin over the benchmark. This was somewhat expected due to the excess mass of the part, but no major issues were identified with the design, as the excess prediction is roughly proportional to the mass increase.

Table 22: Extracted Model Stiffness Results

	Stiffness (RBE3)	
	Aft Pt 6	Lat Pt 6
	[kN/mm]	[kN/mm]
Extracted Model	5.79	95.1
Benchmark Design	4.33	81.8

Strength analysis produced a more mixed set of results than seen in the stiffness trials as shown in Table 23 below. Permanent set produced under the aft load cases was high enough to warrant concern, generated by a global buckling effect at the tie rod cut-out. The overloading analysis in the aft direction also failed to solve, meaning the part was unable to adequately sustain the full load. This failure also seemed to be driven by the transition around the tie rod cut-out, generating a large local stress concentration as shown in Figure 42. However, despite significant stress concentrations around the balljoint region, the lateral strength performance was similar to the benchmark. With additional refinement of these regions and smoother transitions, they should not present a major design obstacle.

Table 23: Extracted Model Strength Results

	Permanent Set		Max Deflection		PEEQ Max	
	Aft Pt 6	Lat Pt 6	Aft Pt 6	Lat Pt 6	Aft Pt 6	Lat Pt 6
	[mm]	[mm]	[mm]	[mm]	[%]	[%]
Extracted Model	1.56	0.58	FAIL	4.7	FAIL	1.13
Benchmark/Targets	0.17	0.42	33.4	4.8	6.00	6.00

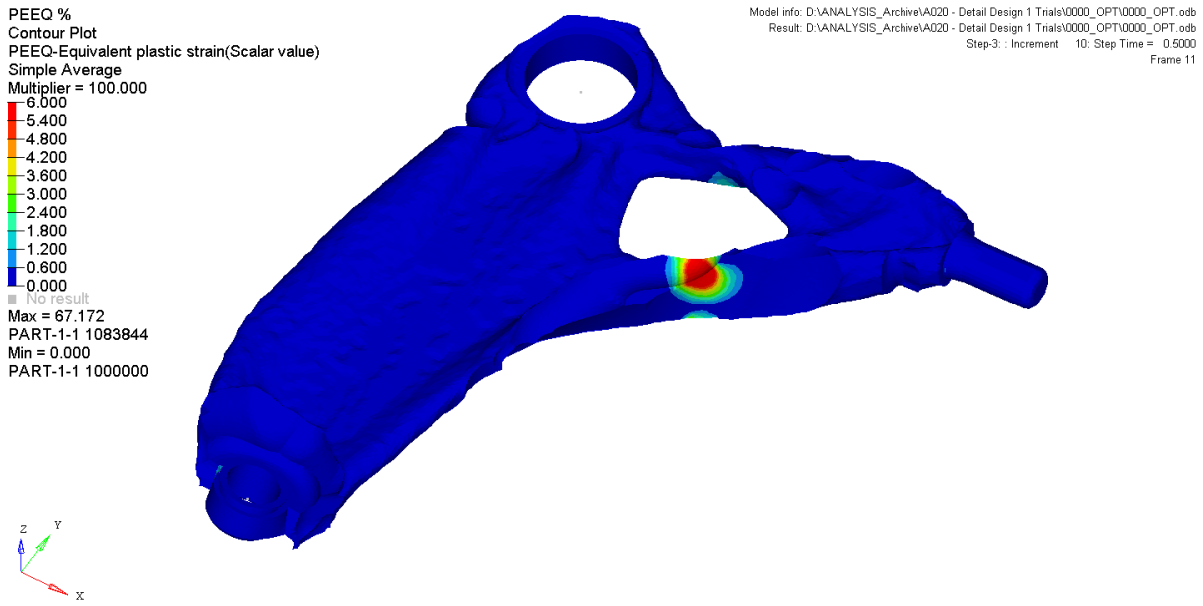

Figure 42: Terminal Step of Strength Loading on Extracted Geometry

In order to further explore the failure of the part under aft strength loading, it was decided to run a trial with a linearly ramped displacement, and measure the reaction force. The resultant load displacement curve is shown in Figure 43 below. Clearly, the load displacement curve does not peak

close to the benchmark result. Generally, this ramped displacement analysis is conservative as it does not use as small of a simulation step time when the maximum load is reached, and therefore does not necessarily capture the peak load. As a tool to understand the behavior of the part under load to compare design changes, this was determined to be a useful first step to try to quickly reach a design capable of achieving equivalent strength.

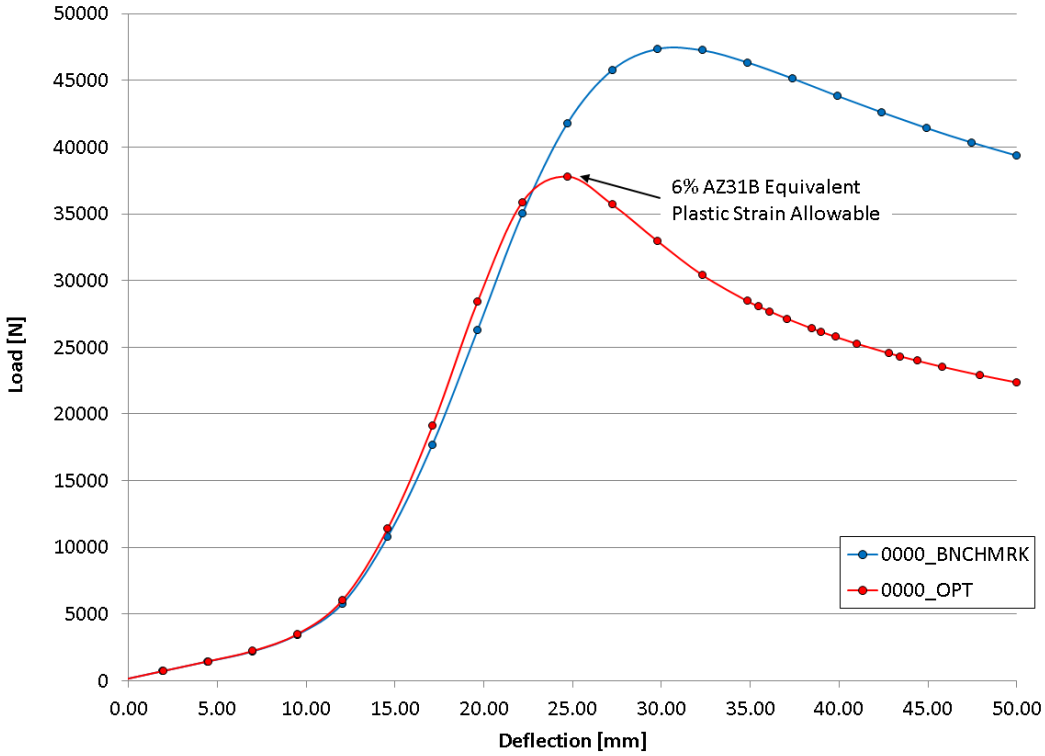

Figure 43: Extracted Optimization Load Displacement Curve

Chapter 5
Detail Design and Verification

5.1 Detail Design Process

With the completion of the project's first stage of optimization trials, it was necessary to turn the optimization output into a viable design for production. Using CATIA v5 the FLCA was modelled, referencing the engineering specification and optimization results. With the initial model a series of verification trials were conducted, resulting in design iterations that eventually met most of the engineering specifications.

5.1.1 CAD Model

Figure 44 shows the D010_R11 CAD model rendered to represent the appearance of a forged and machined part. The model was constructed from a bulk enclosed volume, deriving its external features by comparison to the optimization model. Internal material was removed with Boolean operations on the top and bottom. Further trims were then added to create features such as the tie rod nest and wheel cut-out. Overall the process was subtractive from the initial volume, and this worked fairly well for a complex part, including reasonable compatibility with draft generation tools.

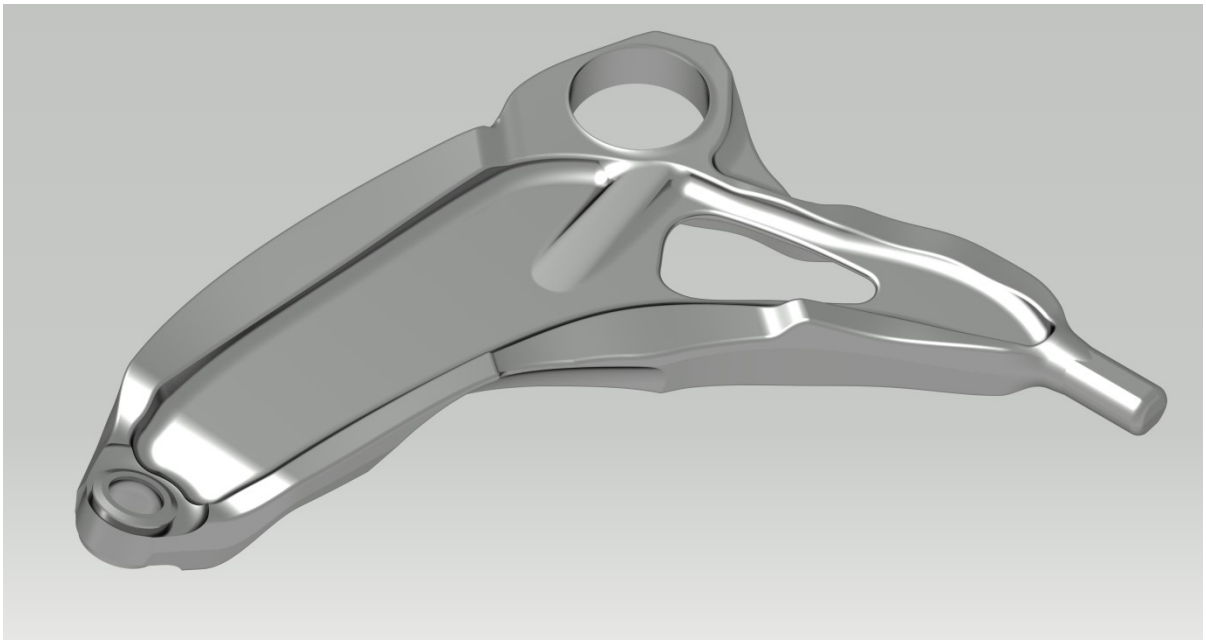

Figure 44: D010_R11 Control Arm (Machined)

Two views of the designed forging are shown in Figure 45 below. The forging weighs 1713g, with material saving pockets inside the areas to be machined. The component is intended to be forged in at least two steps. One set of steps would be used to form the bulk geometry of the part, where a secondary operation would have to be used to hot trim the flash and the hole in the part.

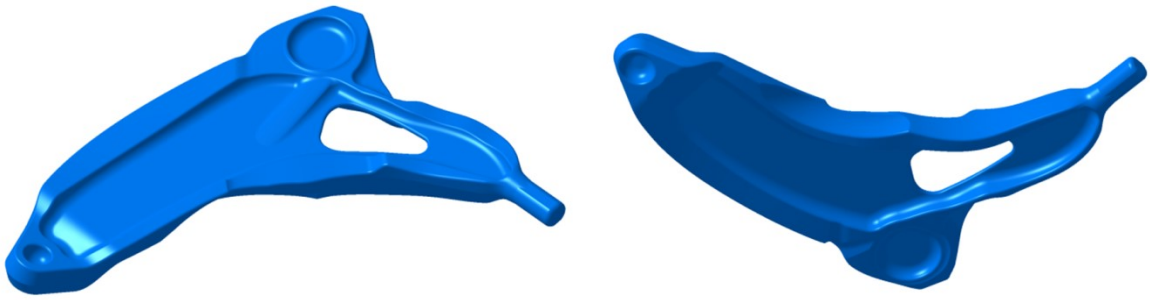

Figure 45: Forging CAD Model (Hot Trimmed)

Machining is required in order to produce the accurate surfaces needed for the press fit handling bushing and the balljoint used in the OEM design. Figure 46 shows the part after machining operations, with machined surfaces highlighted in green and forged surfaces in blue. The handling bushing bore is machined in one operation with a tapered lead-in derived from the OEM benchmark part. To machine the area around the integral balljoint, operations are required on both sides of the part. An additional operation was used to profile the steep drafts required around the balljoint cup forging so that reasonable clearance would be present to the brake shield, although the control arm design typically dictates the shape of the brake shield. Although more machining than the OEM benchmark would be required, this is somewhat offset by magnesium's high machinability and affinity for high speed machining [13].

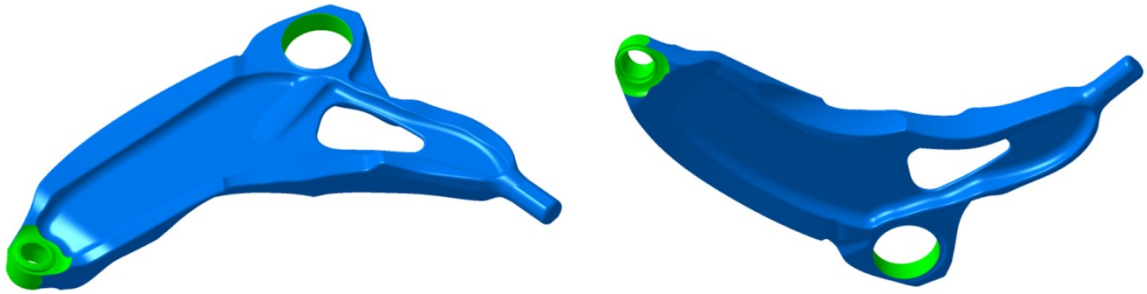

Figure 46: Machined CAD Model

5.1.2 Clearance Checking

In order to retain the efficiency of the optimized structure, it was necessary to push material up against the limits of the design space. Figure 47 shows the end effect of the design process compared to the design space. It can be observed that there are some violations of design space clearance by small amounts in this comparison. To ensure the FLCA had sufficient clearance to other components it was inserted into a series of clearance assemblies generated to accurately represent the limits of suspension travel.

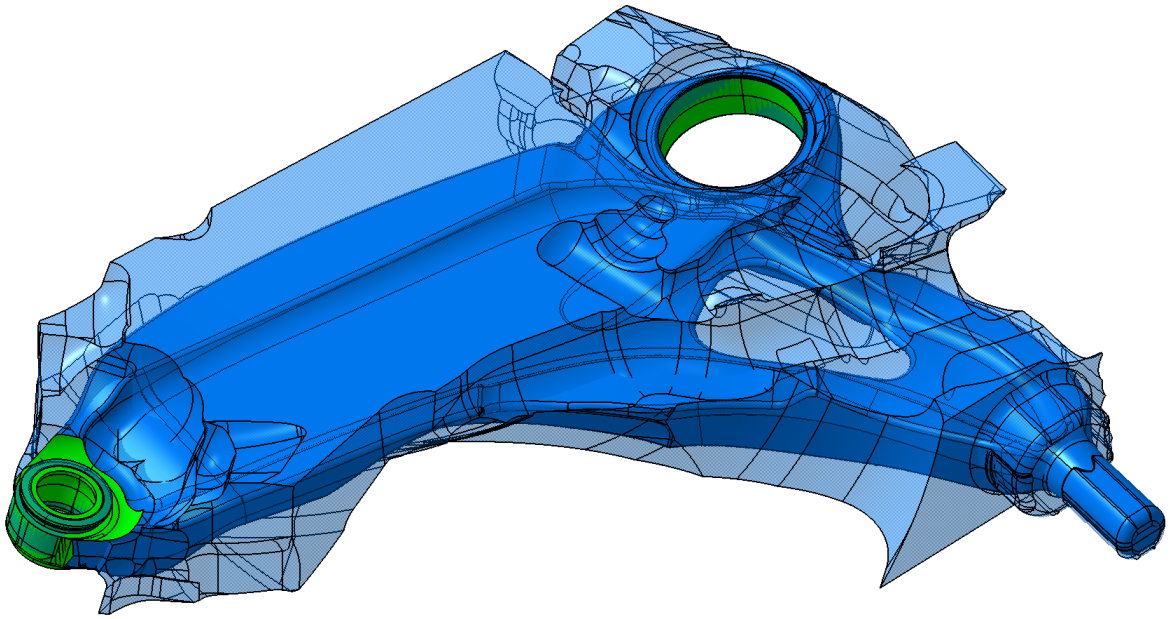

Figure 47: R11 Design Compared to Design Space

Figure 48 shows the critical position for the steering tie rod. Because of the depth at which the tie rod cuts this critical region, it was necessary to flow material around the tie rod without creating too much of a stress concentration. Although the stress concentration was minimized, it was still a factor in analysis results detailed later in this chapter. The minimum tie rod clearance to the benchmark component was matched with this design detail.

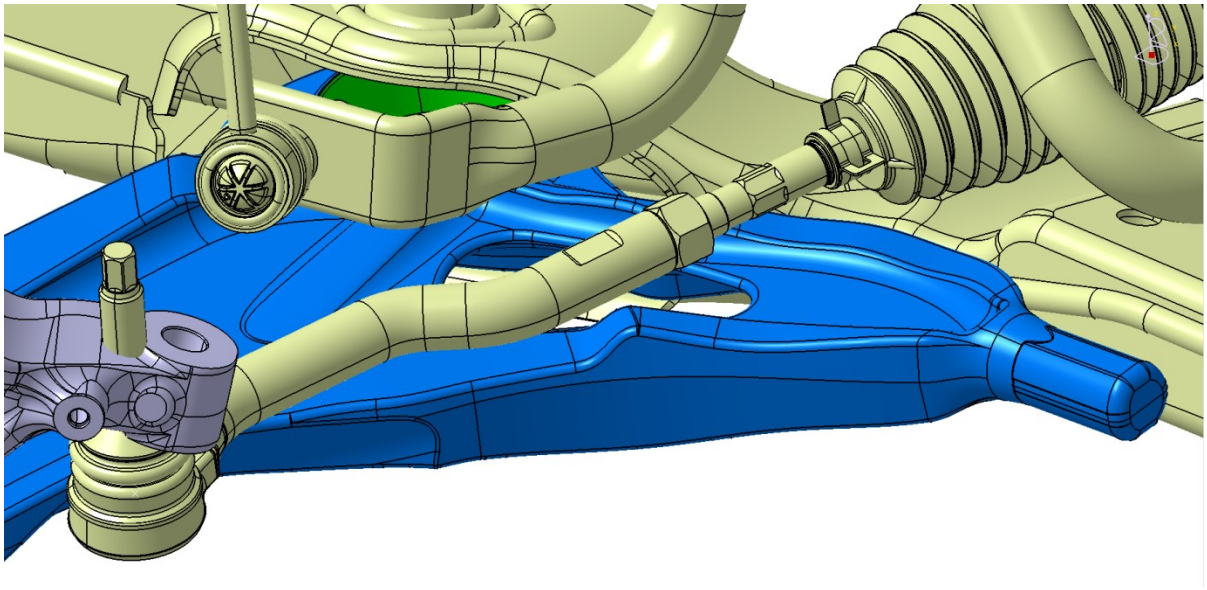

Figure 48: Clearance to Tie Rod, Closest Step

Figure 49 and Figure 50 show the clearance model at its upper and lower most positions respectively. In both of these cases the control arm was initially very close to the subframe flanges. Profiled cuts were added to the front edge of the part, created by offsetting from the subframe geometry. This technique allowed the design to match the benchmark OEM component for clearance in these regions.

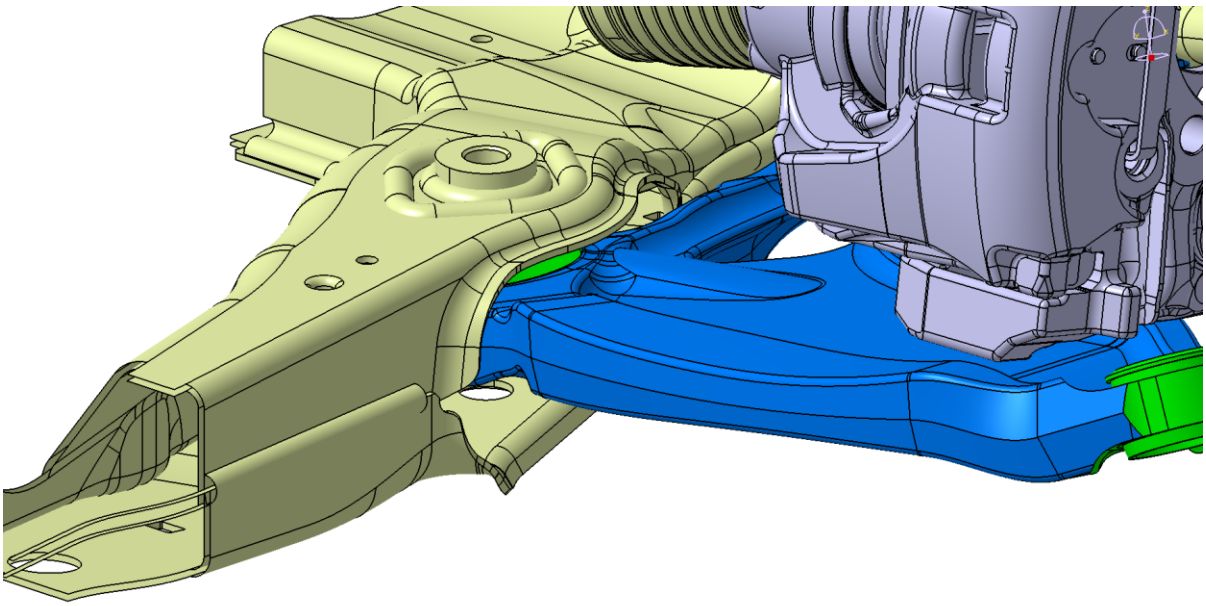

Figure 49: Clearance to Upper Subframe, Closest Step

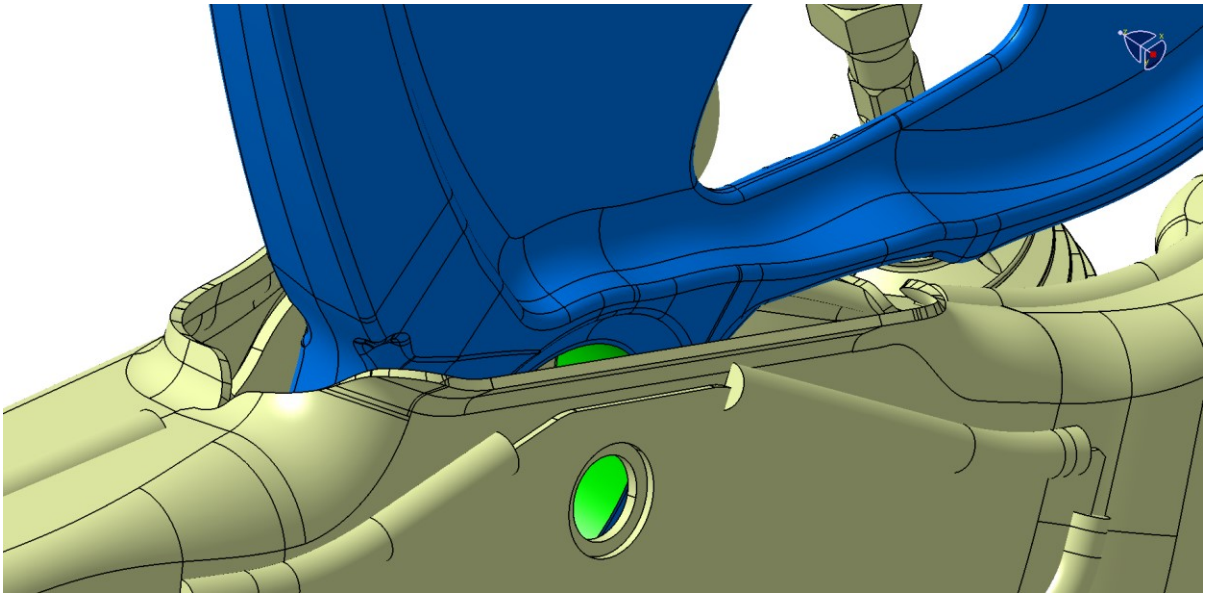

Figure 50: Clearance to Lower Subframe, Closest Step

Not all of the potential clearance issues could be addressed adequately in the first stage of design. Figure 51 below shows regions where clearance difficulties eventually passed the specification in green circles, and where they did not in yellow circles. On the inboard side of the control arm there were difficulties making the vertical portion of the rib pass clearance. Any movement away from the

subframe is parallel to the clearance surface for this part, so some height may need to be removed from the rib. Two outboard clearance issues remained unaddressed after the first design stage, since they were relatively minor and would have required major rework or the addition of abnormal trimming surfaces. On the top side, the knuckle bolt minimally violated the overall clearance requirement, while on the bottom side, the wheel weight clearance zone barely touched the FLCA. In the long run these clearances will need to be addressed, but they were avoided in the initial stages to speed up identification of more critical structural issues.

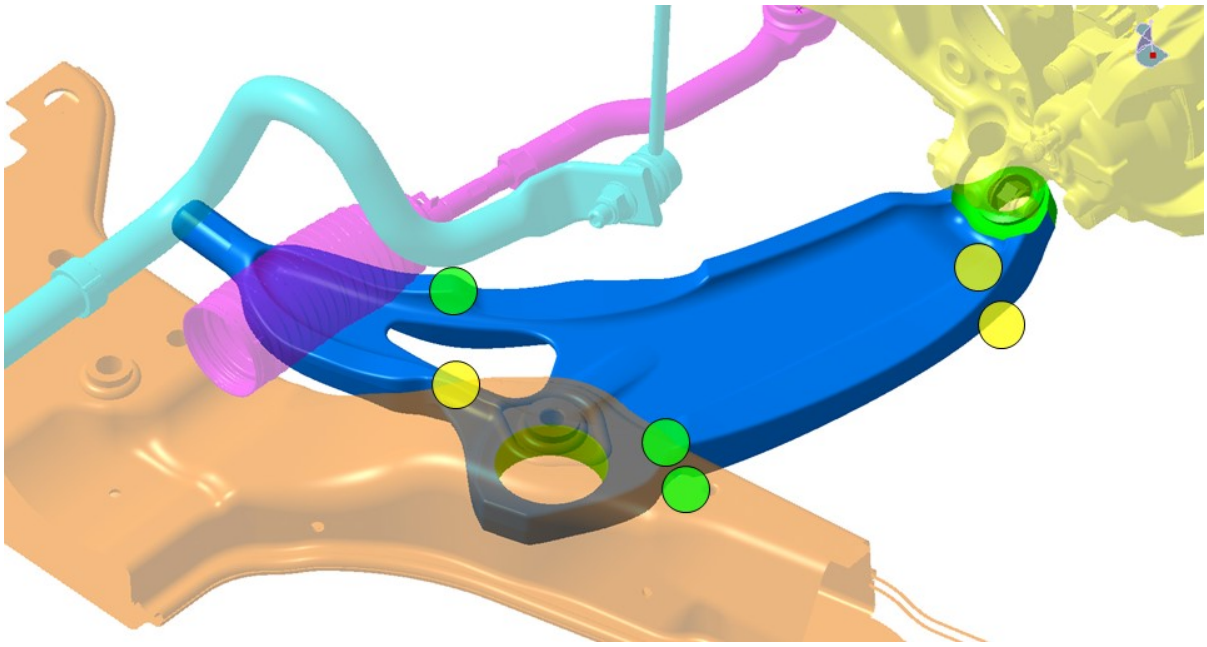

Figure 51: Identified Clearance Issues

5.1.3 Design Iterations

Table 24 shows the development of the design in order to meet the structural requirements. The mass increased from the starting 1447g to 1558g in the R11 design due to the need for a thicker rib in the region around the tie rod cut-out.

Table 24: D010 Design Iteration Record

Design Iteration	Mass	Notes
D010_PD_Control Arm_04	1447	First complete model, poor strength performance
D010_PD_Control Arm_05	1468	Thickened rear edge rib
D010_PD_Control Arm_06	1485	Clearance modifications, inboard edge continuity
D010_PD_Control Arm_07	1485	Modified AZ80 model for T6 heat treatment

D010_PD_Control Arm_08	1542	More rear edge rib width, height, tighter to wheel
D010_PD_Control Arm_09	1522	Fully smoothed tie rod cut-out
D010_PD_Control Arm_10	1542	More rear edge and inboard rib width
D010_PD_Control Arm_11	1558	Thickened rib rear edge, short height addition

Upon analysis of the initial design, it was found to be able to support only a little more than half of the benchmark strength loading. Due to the criticality of this problem, it was decided to pursue a development strategy based on load deflection analysis. Design changes would be made, and the model analyzed for load deflection behaviour to quickly evaluate the effect of those changes. Meshes were recycled as often as possible but this form of manual optimization was very time consuming. After changes to the geometry, and the adoption of a stronger AZ80A-T6 material, the design was close to the benchmark performance (0008_R11). Figure 52 shows the history of changes to load deflection as the design was iterated. Some steps in the optimization were more productive than others, but in general the manual optimization strategy was inefficient, as no strategies for improving strength were enough on their own. Local shape optimization should be investigated in the future to speed up this process.

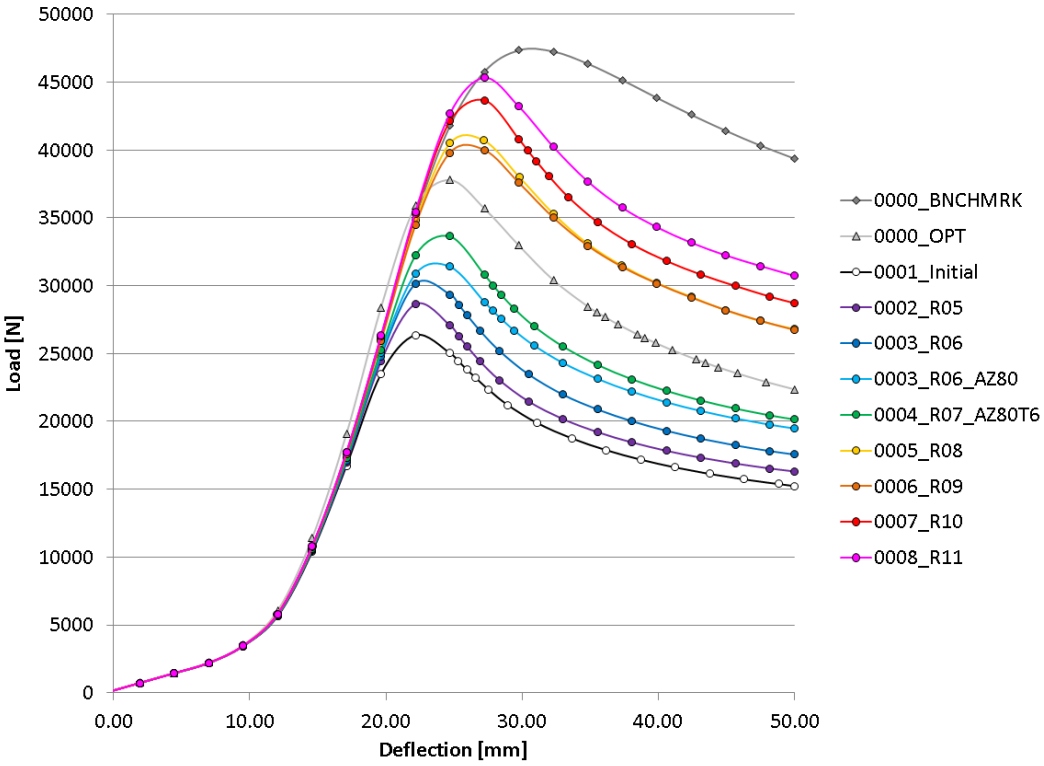

Figure 52: Load Displacement Development Curves

5.2 Design Verification

Once the design had achieved aft strength performance in the load displacement analysis, the R11 model was run through all required load cases for verification of the specifications. Stiffness and strength load cases were analyzed with the developed material data, while fatigue analysis was run using available test data for AZ80.

5.2.1 Stiffness Verification

Stiffness analysis was conducted in accordance with the specification requirements described in section 3.3.1. Table 25 shows that in both lateral and aft load cases the benchmark stiffness was very closely approximated. It has been observed that extracted optimization results are usually stiffer than the targets, and that stiffness is often lost in interpretation through the simplification of structural forms. Both stiffness values were relatively close to the benchmark, indicating that the design optimization and interpretation processes offset each other to create a successful design. This is not likely to be a consistently repeatable pattern, but was very useful in this case.

Table 25: D010_R11 Stiffness Analysis Results

	Stiffness (RBE3)	
	Aft Pt 6	Lat Pt 6
	[kN/mm]	[kN/mm]
D010_ Control Arm_11	4.37	79.8
Benchmark FLCA	4.33	81.8

Figure 53 shows the deflection under aft loading, with the design exhibiting very consistent and symmetrical bending deflection as would be ideally expected. In Figure 54, the lateral load case shows some localized deformation around the balljoint, but for the most part the ribs around the balljoint seem to stabilize it more effectively than the benchmark design. The load is also not evenly split between the front and rear facing edges of the control arm, with the front edge taking the majority of the deflection. The front edge may need to be balanced more efficiently with the rear edge, although the rear edge has already been built up as a result of strength requirements. It is possible the front edge can be refined to carry the majority of the lateral deflection, with less consideration towards bending strength, as this design shows.

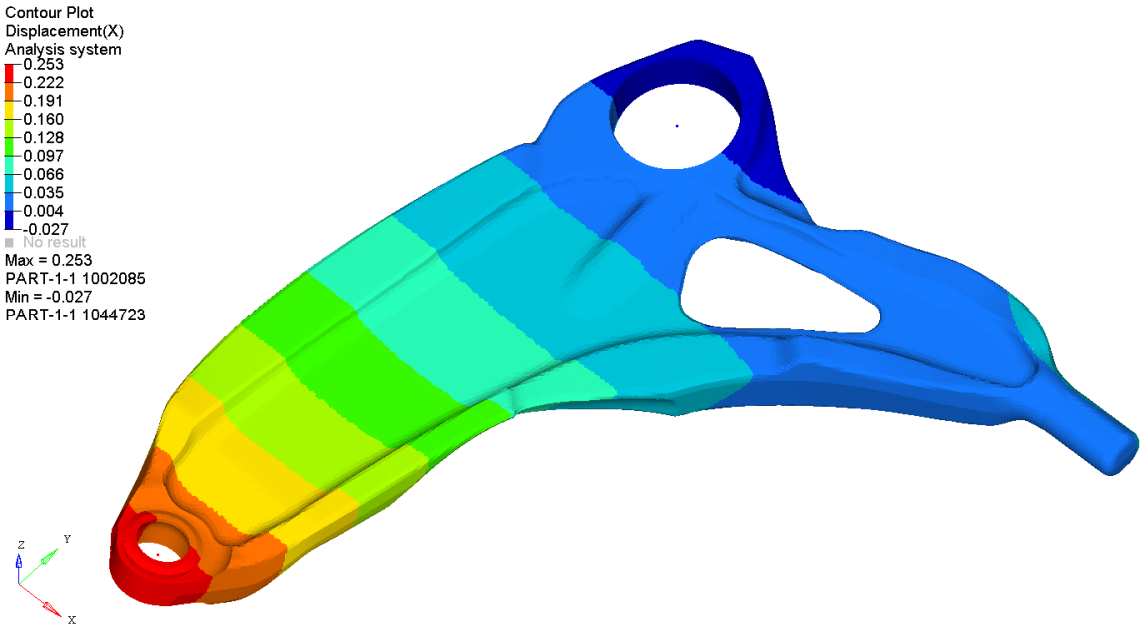

Figure 53: D010_R11 Aft Stiffness Contour Plot

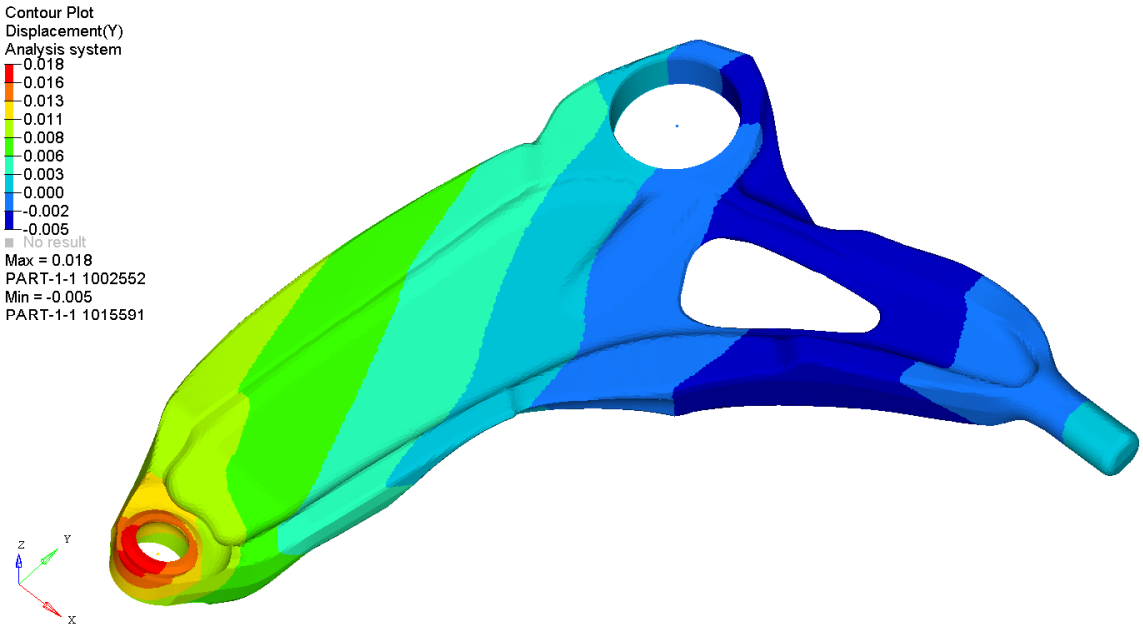

Figure 54: D010_R11 Lateral Stiffness Contour Plot

5.2.2 Strength Verification

In the development of the strength model, three material models were explored as shown in Figure 55. The AZ31B model was based off of monotonic tensile testing conducted using forged magnesium

specimens. Due to higher yield and ultimate properties, AZ80 data derived in a similar fashion was initially used to help enhance strength. With additional research it was found that heat treatment further improved the yield strength of AZ80, but did not have much of an effect on ultimate strength compared to the existing model [38]. In order to account for this shift, the AZ80 model was bumped linearly to increase the yield without an effect on the ultimate properties.

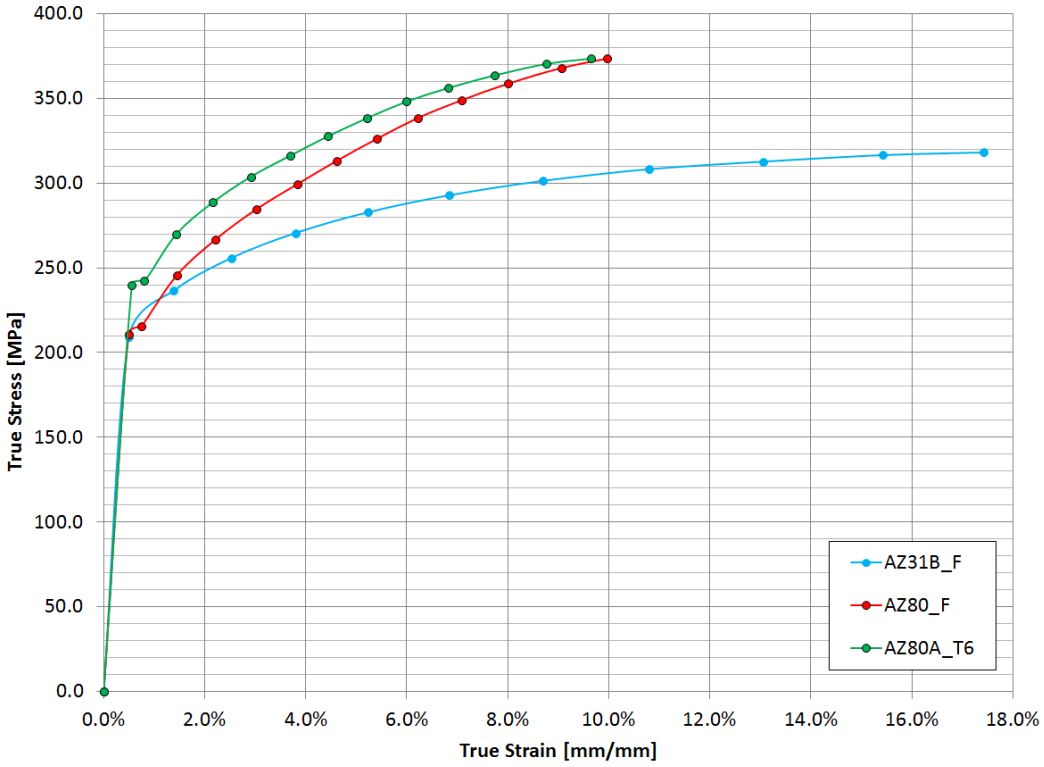

Figure 55: Comparison of Magnesium Material Models

Table 28 shows the results of strength analysis on the R11 model with the procedures described in section 3.3.2. The component passed all analysis trials with similar performance to the benchmark.

Table 26: D010_R11 Strength Analysis Results (with AZ80A-T6 Properties)

	Permanent Set		Max Deflection		PEEQ Max	
	Aft Pt 6	Lat Pt 6	Aft Pt 6	Lat Pt 6	Aft Pt 6	Lat Pt 6
	[mm]	[mm]	[mm]	[mm]	[%]	[%]
D010_ Control Arm_11	0.12	0.59	29.9	4.8	4.41	0.44
Benchmark/Targets	0.17	0.42	33.4	4.8	7.00	7.00

Figure 56 and Figure 57 show the aft and lateral permanent set contour plots respectively. Both cases performed similarly to the benchmark with minimal balljoint deflection for the aft load case, and moderate local deformation around the balljoint under lateral loading.

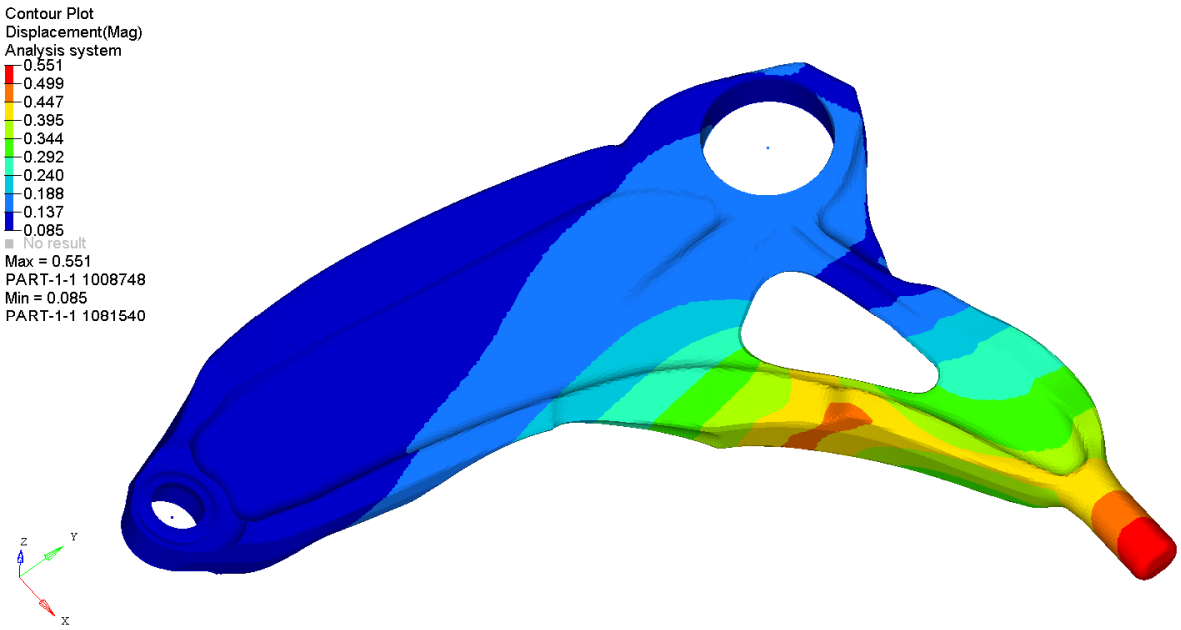

Figure 56: D010_R11 Aft Permanent Set

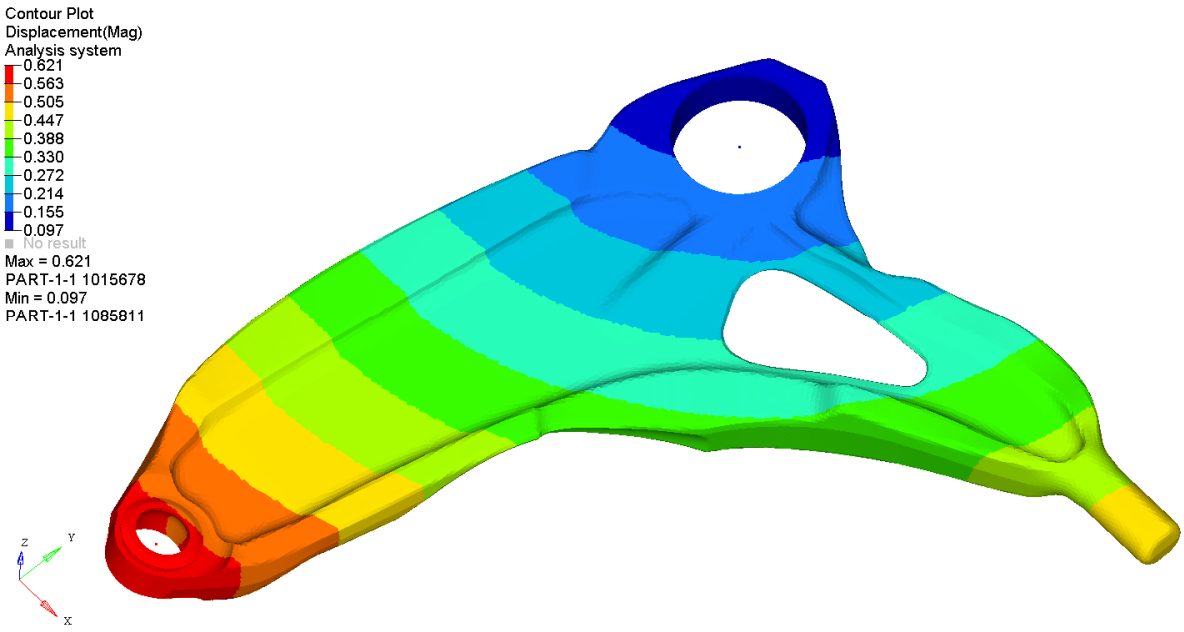

Figure 57: D010_R11 Lateral Permanent Set

In Figure 58 and Figure 59, contour plots of the aft and lateral max deflections are shown. Both values are reasonably similar to the benchmark analysis. Deflection instabilities were not found with the design prior to its ultimate load.

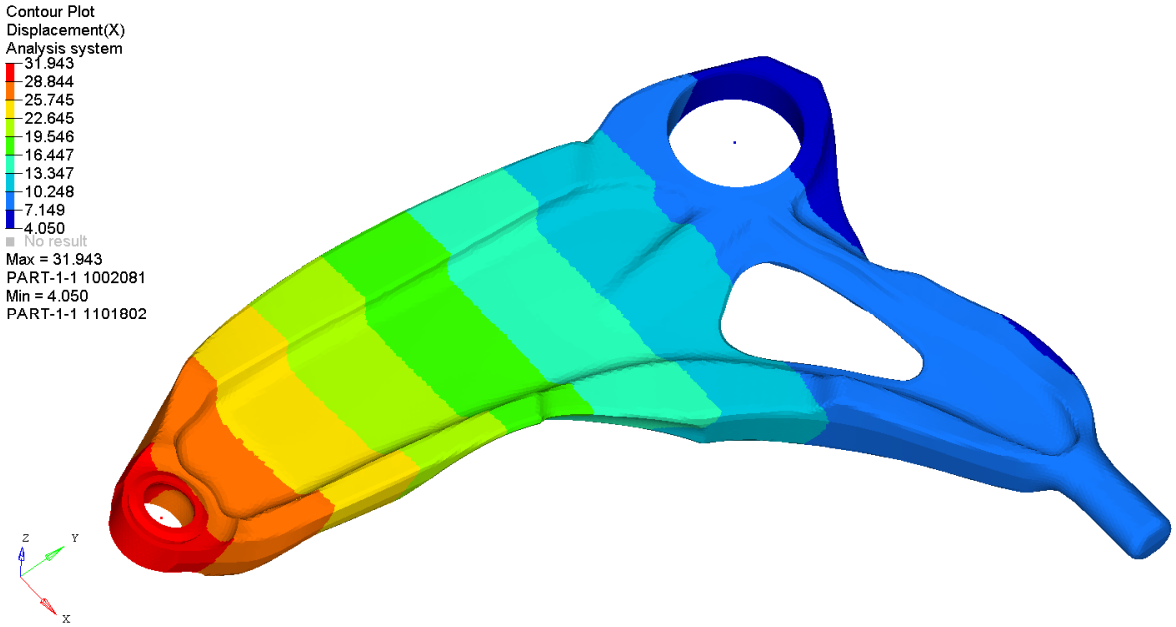

Figure 58: D010_R11 Aft Max Deflection

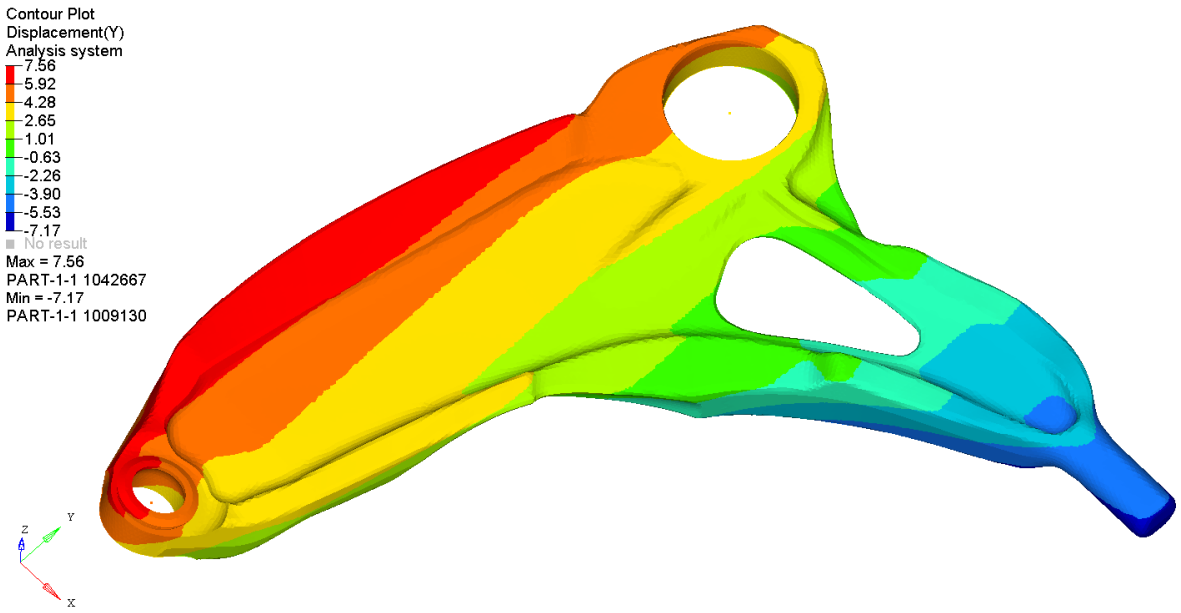

Figure 59: D010_R11 Lateral Max Deflection

Contour plots of equivalent plastic strain are shown in Figure 60 and Figure 61. For aft loading, plastic strain initially develops on the inboard reinforcing web, but is then overtaken by the tie rod cut-out stress concentration. The lateral case generates only minimal plastic strain around the balljoint cup.

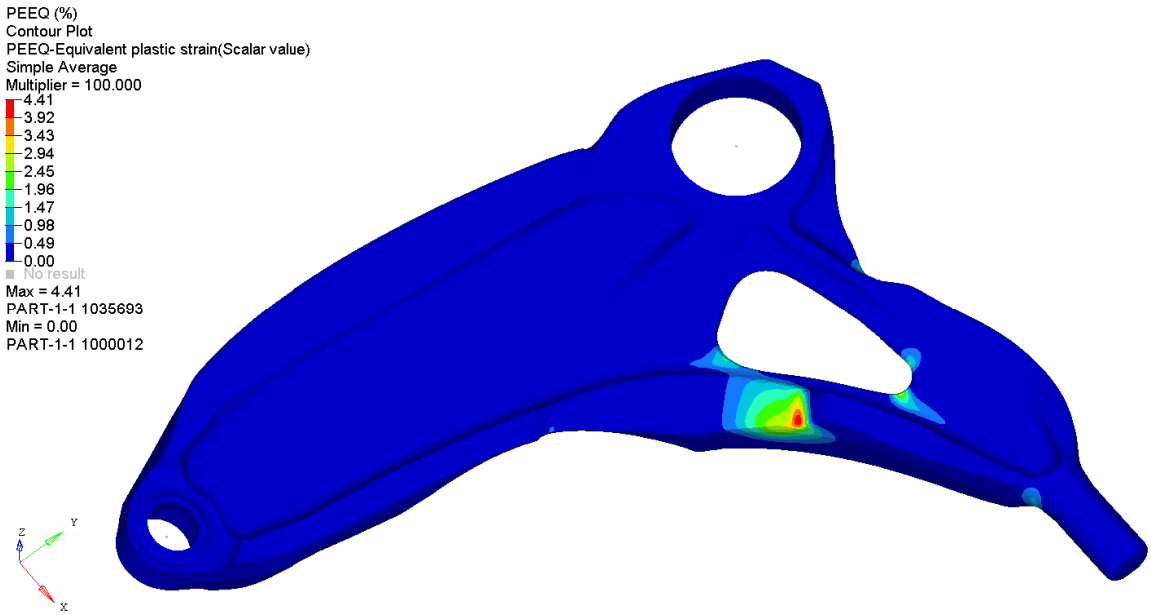

Figure 60: D010_R11 Aft PEEQ

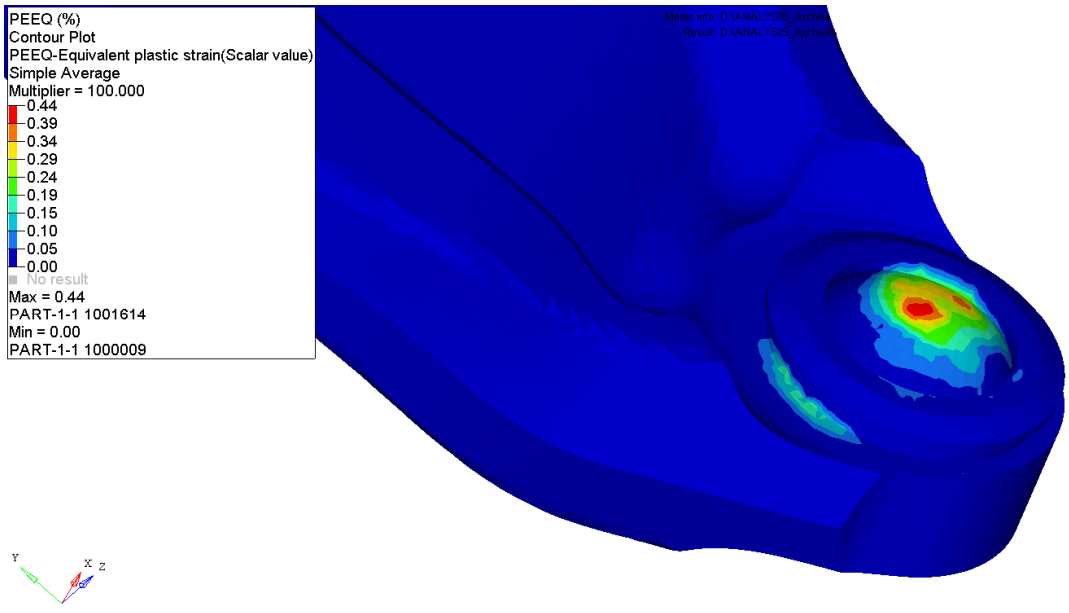

Figure 61: D010_R11 Lateral PEEQ

5.2.3 Fatigue Verification

Using nCode DesignLife v12.0, and the process described in section 3.3.3, the fatigue life of the R11 design was determined. Table 27 shows the final minimum fatigue cycles. The part failed by a significant margin, even though no surface correction factor was applied during the analysis.

Table 27: D010_R11 Fatigue Analysis Results

	Fatigue Life Ks = Polished [Cycles]
D010_ Control Arm_11	2623
Benchmark Design	144776

Figure 62 and Figure 63 show fatigue plots of the part from both an outboard and inboard view. The main hot spots for low fatigue life are at the tie rod cut-out, and also the external reinforcing web on the inboard side. One element on the inside of the hole through the part also failed, suggesting a bead around the hole may be beneficial to reduce local stresses. Overall the failure locations are primarily regions of high stress concentrations, and should mean local modifications with low mass penalties will result in a survivable part. As part of this project, local fatigue strengthening using cold spray coatings is being evaluated. This may also be used to improve the situation.

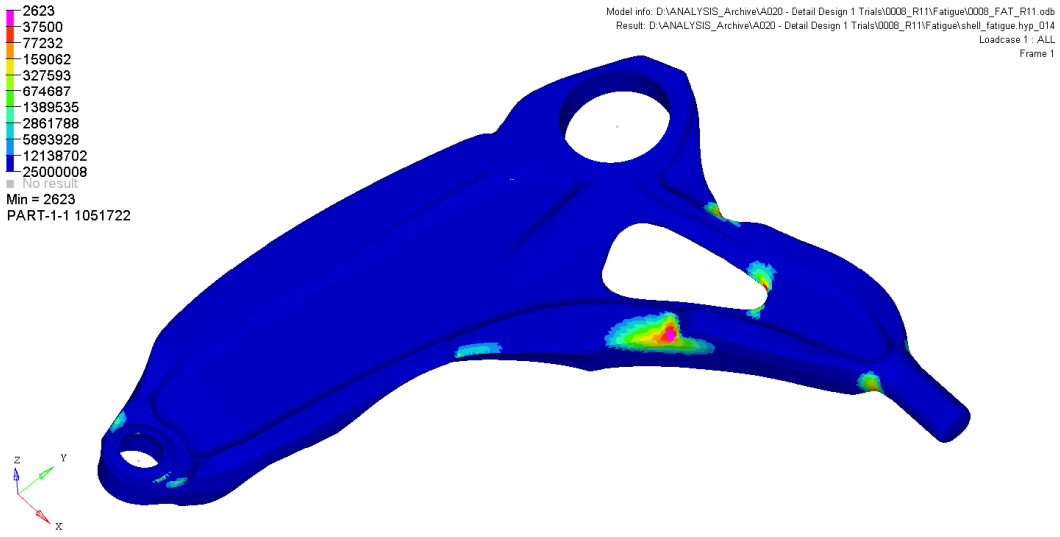

Figure 62: D010_R11 Fatigue Life Outboard View

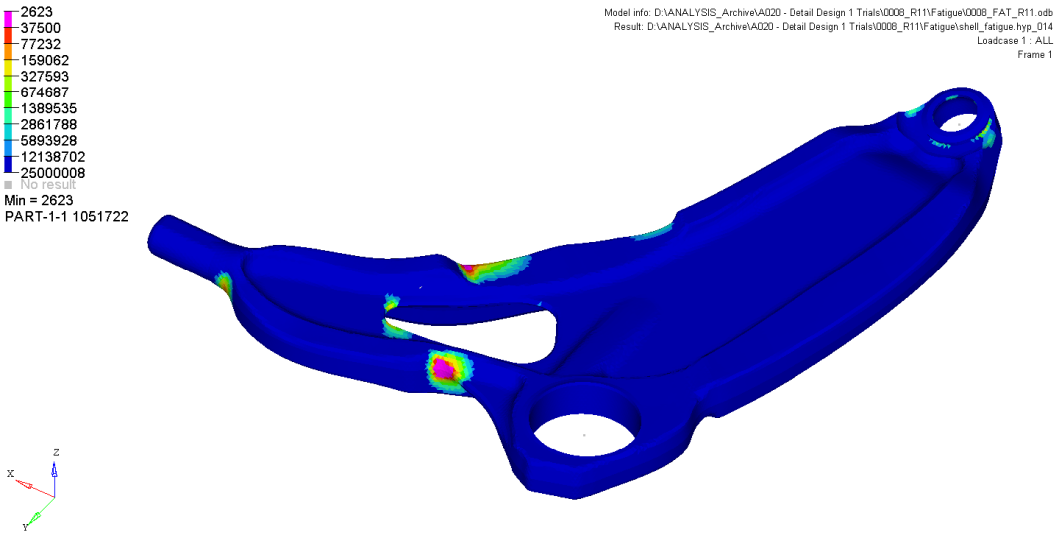

Figure 63: D010_R11 Fatigue Life Inboard View

5.2.4 Geometric Manufacturing Verification

During the design phase, adherence to the geometric design specifications was integrated into CAD modelling. Table shows the final design parameters compared to the specifications. Overall most of the specifications were met exactly. Minor issues with the stability of the CAD model in generating some of the fillets led to placeholders being used until the structural specifications had been fully verified. Additionally, some of the ribs near transitions need to be made slightly larger to meet the requirements.

Table 28: D010_R11 Forging Geometry Verification

Geometric Verification: D010_Control Arm_11		
Specification	Min. Model Value	Target
Outside Draft Angle [M01]	5°	> 5°
Internal Draft Angle [M02]	10°	> 10°
Fillet Radius [M03]	10 mm	> 10 mm
Corner Radius [M04]	2.5 mm*	> 2.3 mm
Web Thickness [M05]	5.0 mm	> 5.0 mm
Rib Thickness [M06]	6.1 mm	> 6.35 mm

*Issues with CAD model stability, must be fixed prior to release (lower radii present)

Figure 64 shows the regions that need to be refined to meet dimensional requirements. Regions with ribs that do not yet meet the minimum thickness requirement are highlighted in red, and the area with

an external radius problem is highlighted in yellow. With further experience creating CAD models of this kind, these difficulties should be less common. The problems are usually caused by local topological complexity that would make manufacturing difficult as well, or feature layering that does not triage regions of complexity well.

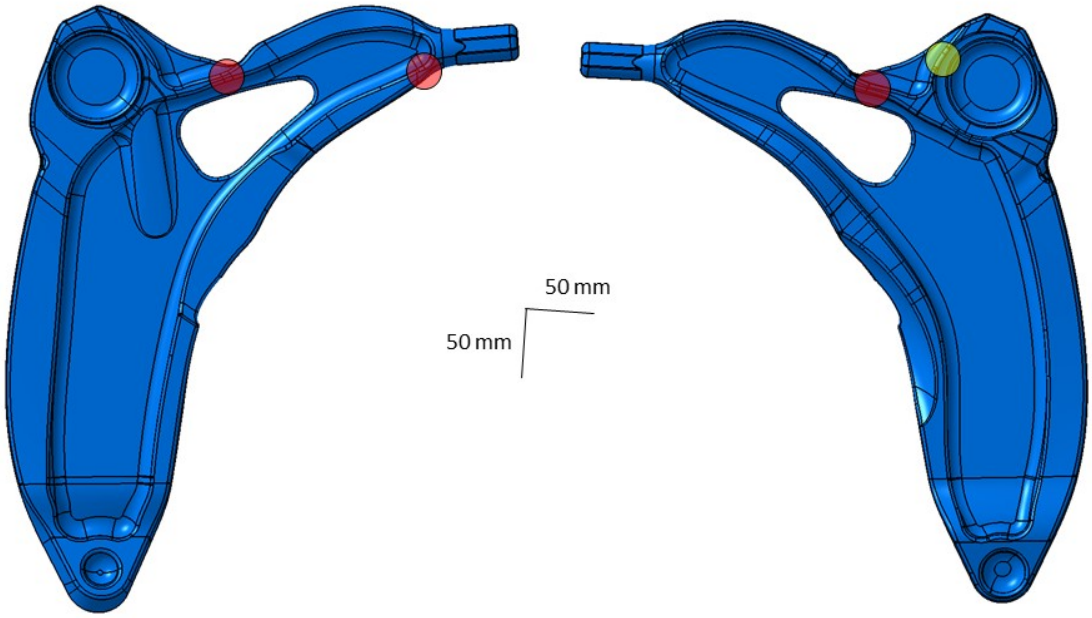

Figure 64: D010_R11 Outstanding Manufacturing Geometry Issues

5.2.5 Manufacturability Verification

At the level of design reached during the initial design, manufacturing-specific features were mostly omitted. Forged impressions inside the balljoint and handling bushing were added to speed up machining and reduced material usage, but beyond that none of the other manufacturability specifications could be verified. Knockout pin pads to help eject the part from the forging die are planned as shown in Figure 65, but the detail design and analysis work required to implement them has not yet been completed. It is also planned to use these features as machining references; however, provisioning for a reference normal to the forging plane may be more difficult due to forging draft limitations. Due to the dimensional tolerances achievable with forging, it may be possible to use drafted surfaces to accurately reference instead [16].

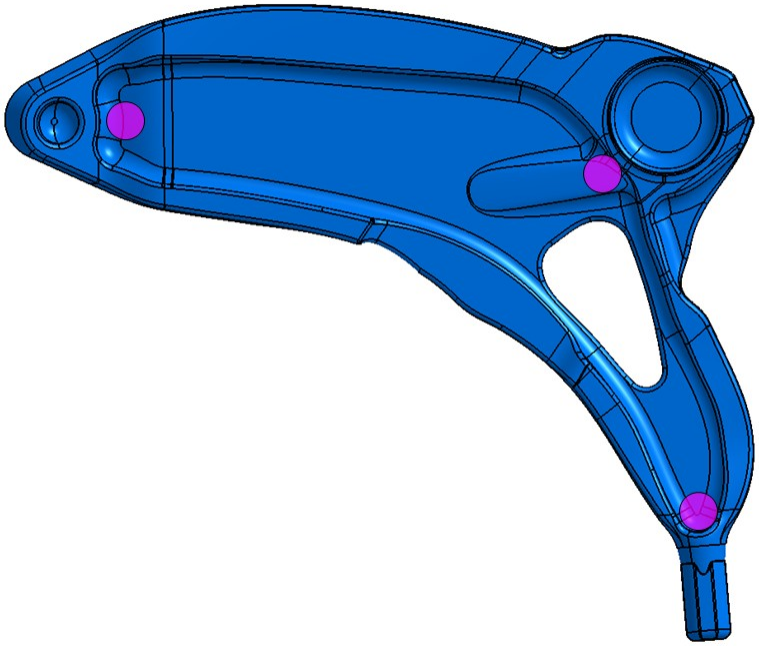

Figure 65: Planned Knock-Out Pin Locations

5.2.6 Unverified Specifications

Several specifications were not verified in this initial stage of design and simulation. In its current state, the R11 design is unable to challenge the benchmark in terms of fatigue performance. This seems to be a local geometry problem rather than a material or overall design issue though. The assessment of quality and surface finish issues was not covered directly, although forging trials conducted outside of this project have given useful insight on how to account for these challenges. The robustness of the part at forging temperature was also not considered, although this is a problem that might be better suited to solving on the automation side. Lastly, the combination of manufacturing cycle time and the related total cost requirements were not analyzed, but effort was expended to design a forging with minimal wasted material. In the future these requirements will need to directly feed into the design processes to achieve a design that can be implemented practically.

Chapter 6
Conclusions

Over the course of this project, a forged magnesium control arm was designed to replace an in-service cast aluminum part. Optimization techniques were used to inform this design, and the end result of the work to date is a control arm that is close to equivalence with the benchmark component, with concrete plans in place to overcome remaining shortcomings without the addition of significant mass.

With the initial establishment of specifications, it was clear that while the specifications for mechanical performance were generally considered, it would be helpful to delve further into more detailed requirements including the design of interface components such as the balljoint. The manufacturing specifications were established effectively as a good starting point, and ongoing research into magnesium forging will doubtless better inform these specifications as more information becomes available.

The optimization process revealed that a much lighter than baseline control arm was possible through the use of forged magnesium. Significant insight was gained through the development of this model regarding the construction of an efficient optimization model, and different configurations that might be viable for the final design. It was found that magnesium maintains a mass advantage over steel and aluminum only if a tensile/compressive stiffness requirement isn't the dominant requirement. If magnesium is restricted by over-constraint of a design space, or sufficient space is not present, it will be very difficult to challenge incumbent materials. This factor also depends on how thin other materials can be formed. Stiffness was very well predicted by the topology optimization process, however strength and fatigue were not. This was understandable, as the strength and fatigue requirements were not explicitly present in the optimization process.

Translation of the optimization results into a detailed design resulted in the verification of all structural design requirements except fatigue. An iterative manual optimization process was required for the component to achieve similar strength to the benchmark, and it is expected a similar process will be needed for fatigue performance. The use of a stronger material than currently available was required, presenting a challenge for groups involved in developing better forged mechanical properties.

In the end, a preliminary design with a mass of 1558g was designed, presenting a 39% mass savings opportunity. With further optimization, additional mass savings may yet be realized while

still achieving equivalent performance. This work suggests forged magnesium is a potentially valuable tool for automotive lightweighting efforts, even under significant structural loading.

Chapter 7
Recommendations

The following are recommendations for future work based on the author's experiences with this project. The recommendations are grouped by their relevant subtopic.

Optimization Practices

1. It requires a significant time investment to generate a high fidelity design space for optimization. It is therefore pertinent for the analyst to generate a general design space model and only refine areas that prove to be critical to the optimization. The development of a software solution to create design spaces from kinematic models directly would also be helpful, as many analysts do not typically work with CAD modelling on a regular basis.
2. If a requirement is not captured in the optimization process, it seems unlikely that the optimized result will actually prove effective in meeting that requirement. For this reason, future optimization trials should be conducted in at least two stages, starting with a topology optimization process and following with a shape optimization process to reduce stress concentrations.

Design

1. It may be important to capture the effects of trimmed flash in the design. Definitely this will be useful for the creation of forging die designs, and secondarily it will be useful for capturing stress concentrations that may cause fatigue issues. This was observed to some extent in the baseline component fatigue analysis, but was not critical.
2. The group should consider creating an aluminum forged benchmark to challenge the magnesium design. There is a strong possibility that an aluminum design with the aggressive web thicknesses permitted by industry will present a serious challenge to the refined magnesium design. Aluminum is a more accepted material in the automotive industry, and has generally better corrosion performance than magnesium. Cost and performance wise, it may be a more representative and difficult component to try to beat.
3. More effective design task integration is desirable now that other research group elements are generating findings that can be used in design. It would be valuable for all parties to have design reviews on a regular basis so that the requirements are understood and research efforts

can be directed to create better materials and processes for the component, while design efforts can be directed at leveraging novel findings.

Materials and Manufacturing

1. It was structurally advantageous to use AZ80 due to its higher specific strength over AZ31B to improve strength loading performance. If the strength of AZ31B cannot be further improved to meet the requirements, it will not produce the greatest mass savings for this part. It should be determined if the other advantages of AZ31B merit its continued investigation for the program.
2. Strength being critical in this part, the provision for maximum yield and ultimate strengths should be the driving factor in design of the forged material. Various heat treatments are cited in the literature for improved properties, and seem worthwhile to investigate.
3. In trials of the baseline component, fatigue surface factor was found to have a significant effect on the final result. For this reason, an accurate correction factor should be determined for the forged magnesium design.

References

[1] L. Cheah, C. Evans, A. Bandivadekar and J. Heywood, "Factor of Two: Halving the Fuel Consumption of New US Automobiles by 2035," MIT Laboratory for Energy and Environment, Cambridge, MA, 2007.

[2] L. Deptula and A. Noah, *Estimating the Cost Impact of Lightweighting Automotive Closures,* SAE Technical Paper, 2015.

[3] A. A. Luo and A. K. Sachdev, "Applications of magnesium alloys in automotive engineering," in *Advances in wrought magnesium alloys*, Philadelphia, PA, Woodhead Publishing, 2012, pp. 393-426.

[4] B. A. Behrens, I. Pfeiffer and J. Knigge, "Forging technology for magnesium alloys," in *Advances in wrought magnesium alloys*, Philadelphia, PA, Woodhead Publishing, 2012, pp. 376-389.

[5] M. P. Bendsøe and O. Sigmund, Topology Optimization: Theory, Methods and Applications, Heidelberg, DE: Springer-Verlag, 2003.

[6] D. Poerschke, "The Effects of Forging on the Microstructure and Tensile Properties of Magnesium Alloys AZ31 and ZK60," Case Western Reserve University, Cleveland, OH, 2008.

[7] S. R. Agnew, "Deformation mechanisms of magnesium alloys," in *Advances in wrought magnesium alloys*, Philadelphia, PA, Woodhead Publishing, 2012, pp. 63-104.

[8] M. R. Barnett, "Twinning and its role in wrought magnesium alloys," in *Advances in wrought magnesium alloys*, Philadelphia, PA, Woodhead Publishing, 2012, pp. 105-143.

[9] M. O. Pekguleryuz, "Current developments in wrought magnesium alloys," in *Advances in wrought magnesium alloys*, Philadelphia, PA, Woodhead Publishing, 2012, pp. 3-62.

[10] M. K. Kulekci, "Magnesium and its alloys applications in automotive industry," *International Journal of Advanced Manufacturing Technology,* no. 39, pp. 851-865, 2008.

[11] R. S. Beals, Z.-K. Liu, W. J. Jones, P. Mallick, D. Emadi, D. Schwam and B. R. Powell, "USAMP Magnesium Powertrain Cast Components: Fundamental Research Summary," *Journal of the Minerals, Metals & Materials Society,* pp. 43-48, 2007.

[12] D. A. Jones, Principles and Prevention of Corrosion, Upper Saddle River, NJ: Prentice Hall, 1996.

[13] Magnesium Elektron, Designing with Elektron Magnesium Alloys, Manchester, UK:

Magnesium Elektron, 2012.

[14] S. Kalpakjian and S. R. Schmid, Manufacturing Processes for Engineering Materials (5th Edition), Upper Saddle River, NJ: Pearson Education, 2008.

[15] Global Security, "B-36 Peacemaker," 2016. [Online]. Available: http://www.globalsecurity.org/wmd/systems/b-36.htm. [Accessed 16 07 2016].

[16] T. Altan, F. Boulger, J. Becker, N. Akgerman and H. Henning, Forging Equipment, Materials, and Practices, Springfield, VA: National Technical Information Service, 1973.

[17] A. Gontarz, Z. Pater and K. Drozdowski, "Hammer Forging Process of Lever Drop Forging from AZ31 Magnesium Alloy," *Metlurgija,* vol. 52, no. 3, pp. 359-362, 2013.

[18] Q. Wang, Z.-m. Zhang, X. Zhang and J.-m. Yu, "Precision forging technologies for magnesium alloy bracket and wheel," *Transactions of Nonferrous Metals Society of China,* no. 18, pp. 205-208, 2008.

[19] V. Vazquez and T. Altan, "Die design for flashless forging of complex parts," *Journal of Materials Processing Technology,* vol. 98, pp. 81-89, 2000.

[20] Y. Shao, B. Lu, H. Ou, F. Ren and J. Chen, "Evolutionary forging preform design optimization using strain-based criteria," *International Journal of Advanced Manufacturing Technology,* vol. 71, pp. 69-80, 2014.

[21] T. Pepelnjak, R. Werkhoven, D. Kobold and K. Kuzman, "Analysis of Warm Magnesium Forging in Digital Environment," *Journal of Technology of Plasticity,* vol. 35, no. 1-2, pp. 13-23, 2010.

[22] D. Kobold, G. Gantar and T. Pepelnjak, "Finite element analysis of magnesium AZ80 wrought alloy anisotropic behaviour during warm forging," *Mechanika,* vol. 18, no. 3, pp. 251-258, 2012.

[23] M. P. Bendsøe and N. Kikuchi, "Generating optimal topologies in structural design using a homogenization method," *Computer Methods in Applied Mechanics and Engineering,* vol. 71, pp. 197-224, 1988.

[24] Altair Engineering, "HyperWorks Online Help," Altair Engineering, Troy, MI, 2016.

[25] M. P. Bendsøe, "Optimal shape design as a material distribution problem," *Structural Optimization,* vol. 1, pp. 193-202, 1989.

[26] M. Zhou, R. Fleury, Y. Shyy, H. Thomas and J. Brennan, "Progress in topology optimization with manufacturing constraints," Altair Engineering, Irvine, CA, 2002.

[27] E. A. Nelson, *Draw Direction Constraints in Topology Optimization - A Practical Example,* SAE Technical Paper, 2003.

[28] H. Fuchs and R. Salmon, *Lightweight MacPherson Strut Suspension Front Lower Control Arm Design Development,* SAE Technical Paper, 2011.

[29] T. Binder and P. Hougardy, "Optimization of Castings and Forgings at Audi AG," *Simulation,* vol. 2, 2003.

[30] Y. Ogata, S. Suzuki and M. Hiraoka, *Development of Topology Optimization Method for Reduction of Transmission Housing Weight,* SAE Technical Paper, 2005.

[31] J. Prsa, Interviewee, *Lead Structures Engineer, Multimatic Technical Centre.* [Interview]. 25 June 2015.

[32] Dassault Systèmes, "Abaqus Analysis Users Guide," Dassault Simulia, Paris, 2013.

[33] M. Zoroufi, Manufacturing Process Effects on Fatigue Design and Optimization of Automotive Components - An Analytical and Experimental Study, Toledo: University of Toledo, 2004.

[34] K. Reif and K.-H. Dietsche et al, Bosch Automotive Handbook (8th Edition), Plochingen, DE: Robert Bosch GmbH, 2011.

[35] R. C. Rice, J. L. Jackson, J. Bakuckas and S. Thompson, Metallic Materials Properties Development and Standardization (MMPDS), Washington: US DOT, FAA, Office of Aviation Research, 2003.

[36] A. Luft, "85 Percent of Ford Vehicles are Built on 9 Global Platforms: Interesting Insights," 21 September 2013. [Online]. Available: http://motrolix.com/2013/09/85-percent-of-ford-vehicles-globally-built-on-9-global-platforms-interesting-insights/. [Accessed 2 July 2016].

[37] R. Myher and D. Kirby, Interviewees, *Altair Canada Engineering.* [Interview]. 20 January 2016.

[38] Matweb, "Magnesium AZ80A-T6, Forged," 2016. [Online]. Available: http://www.matweb.com/search/DataSheet.aspx?MatGUID=ea14a88a576a45f08ff009fb5749df15&ckck=1. [Accessed July 2016].

[39] R. G. Budynas and J. K. Nisbett, Shigley's Mechanical Design (Ninth Edition), New York,

NY: McGraw-Hill, 2008.

[40] Predictive Engineering, "NX Nastran Connection Elements," 2014. [Online]. Available: http://www.predictiveengineering.com/support-and-training/whitepapers/FEA/small-connection-elements-rbe2-rbe3-and-cbush. [Accessed 9 September 2014].

Appendix A
Simplified Lateral Stiffness Model

In order to determine the relationship between the control arm stiffness and the total stiffness, a simplified model was constructed using two springs in series as shown in Figure 66. The relationship determined is shown in Figure 67. Overall, there are significant diminishing returns in overall stiffness as control arm stiffness becomes much greater than bushing stiffness, and this indicates only a few percentage points of stiffness difference that may be easily compensated for by increased bushing stiffness.

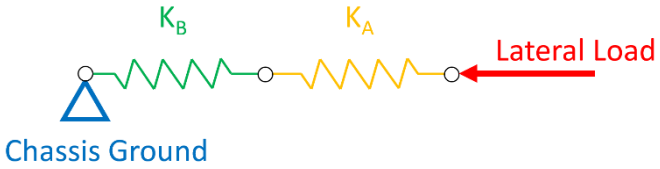

Figure 66: Lateral Stiffness Model

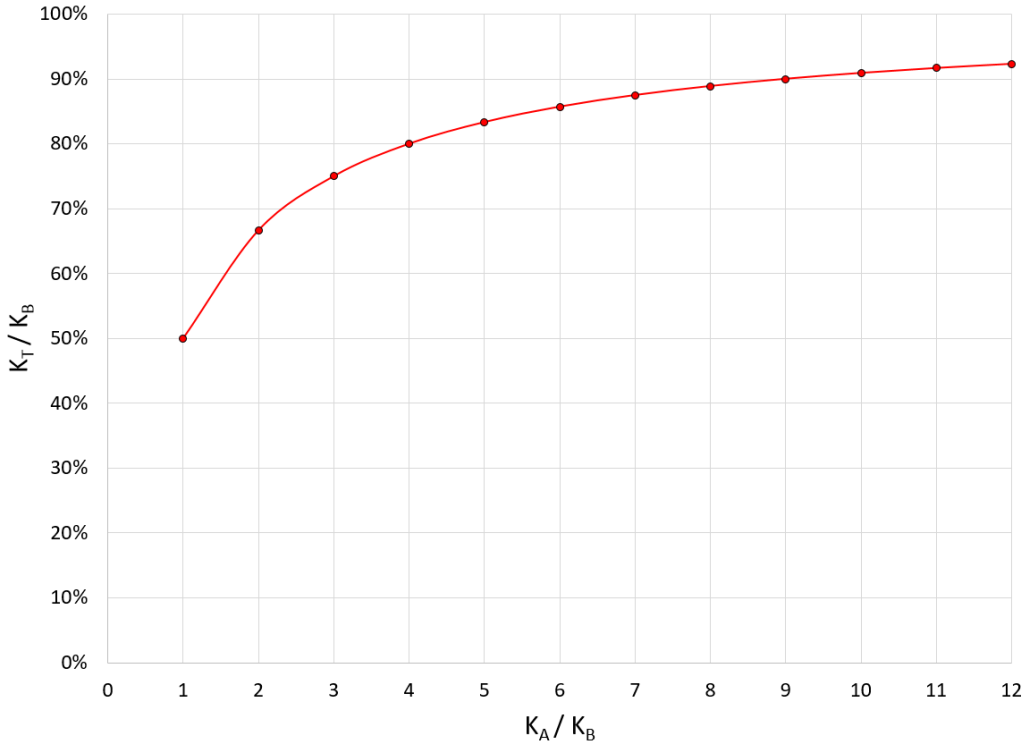

Figure 67: Lateral Stiffness Relationship Between Bushing and Control Arm

Appendix B
Specific Stiffness Comparison

Stiffness in Tension/Compression

$$where, u = \frac{PL}{AE}$$

$$and, AL\rho = m$$

$$\therefore u = \frac{\rho PL^2}{mE}$$

$$for\ equivalent\ performance: \frac{\rho_{al}}{m_{al}E_{al}} = \frac{\rho_{mg}}{m_{mg}E_{mg}}$$

$$\frac{2.66\ [\frac{g}{cm^3}]}{m_{al} \cdot 71.7\ [GPa]} = \frac{1.76\ [\frac{g}{cm^3}]}{m_{mg} \cdot 44.8\ [GPa]}$$

$\therefore$ *In elastic tensile or compressive loading* $m_{mg} = 1.06 \cdot m_{al}$ *for an equivalent structure*, using typical properties. [39]

Both aluminum and steel have about 6% higher specific stiffness under tensile compressive loading than magnesium. If a part is driven primarily by a tension/compression stiffness load case it will not be feasible to use magnesium.

Stiffness in Bending of an Equal Width Cantilever Beam

$$where, y_{max} = \frac{-Fl^3}{3EI}\ for\ a\ cantilever\ beam\ in\ bending$$

It is our goal to find the equal mass rectangular beam with an equal length and base that deflects the same amount at the tip.

$$knowing, I = \frac{bh^3}{12}\ and\ m = bhl\rho$$

$$simplifying\ and\ setting\ equality, E_1I_1 = E_2I_2$$

$$I = \frac{m^3}{b^2l^3\rho^3}, where\ b\ and\ l\ can\ be\ eliminated\ as\ constants$$

$$substituting, \frac{E_1{m_1}^3}{{\rho_1}^3} = \frac{E_2{m_2}^3}{{\rho_2}^3}$$

$$m_1 = \sqrt[3]{\frac{{\rho_1}^3 E_2}{{\rho_2}^3 E_1}}$$

$$\therefore \textit{In elastic bending of an equal base cantilever beam}, m_{mg} = 0.77 m_{al}$$

$$\textit{for an equivalent structure, using typical properties}$$ [39].

In the case of bending, magnesium clearly expresses superior stiffness compared to aluminum, resulting in 23% mass savings. With steel, this difference increases to a mass savings potential of 62%. If sufficient space is available and the load can be efficiently transferred, magnesium is certainly a viable mass saving material.